R-06-89

Mechanical and thermo-mechanical discrete fracture near-field analyses based on preliminary data from the Forsmark, Simpevarp and Laxemar sites

Billy Fälth, Harald Hökmark
Clay Technology AB

January 2007

Svensk Kärnbränslehantering AB
Swedish Nuclear Fuel
and Waste Management Co
Box 5864
SE-102 40 Stockholm Sweden
Tel 08-459 84 00
+46 8 459 84 00
Fax 08-661 57 19
+46 8 661 57 19

ISSN 1402-3091
SKB Rapport R-06-89

Mechanical and thermo-mechanical discrete fracture near-field analyses based on preliminary data from the Forsmark, Simpevarp and Laxemar sites

Billy Fälth, Harald Hökmark
Clay Technology AB

January 2007

Keywords: Thermo-mechanical calculation, 3DEC, Glaciation, Fracture shear displacement, Fracture normal stress, Rock stress, Spalling.

Abstract

This report addresses mechanical processes in the rock due to construction, thermal load and glaciation in a KBS-3 repository for spent nuclear fuel. The models which were used were based on preliminary data from the Forsmark, Simpevarp and Laxemar site investigations and on the current repository design premises. The following items were considered:

- Fracture shear displacements.
- Fracture normal stresses.
- Rock stresses close to openings.
- Thermal stresses between the repository and the ground surface.

The work was carried out using *3DEC*, which is a numerical three-dimensional program based on the distinct element method. Both thermo-mechanical near-field models and a thermo-mechanical large-scale model were analyzed. The near-field models included a portion of a deposition tunnel, three deposition holes and six fractures. Different in situ stress states and fracture shear strengths were tried. The influence of pore pressure was also explored. In the large-scale model, no fractures were present (elastic conditions) and only thermal stresses were calculated.

The near-field models were used for the study of fracture shear displacements, fracture normal stresses and of rock stresses close to openings. The large-scale model was used to evaluate the effects of the mechanical near-field model boundary conditions and to study the development of thermal stresses between the repository horizon and the ground surface.

Sammanfattning

Rapporten behandlar mekaniska processer i berget på grund av utgrävning, termisk last och glaciation i ett KBS-3 förvar för använt kärnbränsle. Modellerna som användes var baserade på preliminära data från platsundersökningarna i Forsmark, Simpevarp och Laxemar och på rådande designkriterier. Följande studerades:

- Skjuvrörelser i sprickor.
- Normalspänningar i sprickor.
- Bergspänningar nära öppningar.
- Termospänningar mellan förvaret och markytan.

Arbetet utfördes med hjälp av *3DEC*, som är ett tredimensionellt beräkningsprogram baserat på distinkta elementmetoden. Både termomekaniska närfältsmodeller och en termomekanisk storskalig modell analyserades. Närfältsmodellerna innefattade ett avsnitt av en deponeringstunnel, tre deponeringshål och sex sprickor. Olika insitu- spänningstillstånd och spricksskjuvhållfastheter testades. Inverkan av portryck undersöktes också. Den storskaliga modellen innehöll inga sprickor (elastiska förhållanden) och endast termospänningar beräknades.

Närfältsmodellerna användes för att studera skjuvrörelser och normalspänningar i sprickor samt bergspänningar nära öppningar. Den storskaliga modellen användes för att utvärdera effekterna av de mekaniska randvillkoren i närfältsmodellerna samt för att studera hur termospänningar mellan förvarsnivån och markytan utvecklas.

Contents

1 Introduction 7

2 Objectives 9

3 Loads and time perspectives 11
3.1 General 11
3.2 Transition from initial state to state at the time of closure 11
3.3 Thermal pulse, 0 years to 20,000 years 12
3.3.1 General 12
3.3.2 Fuel initial power and power decay 12
3.4 Ice load 13

4 Description of models 15
4.1 General 15
4.2 Geometric outlines of the thermo-mechanical near-field 3DEC model 15
4.3 Near-field model fracture geometry 16
4.4 Near-field model boundary conditions 17
4.4.1 Thermal 17
4.4.2 Mechanical 18
4.5 3DEC thermal model 21
4.6 Large-scale model 22
4.7 Numerical considerations and code handling 24
4.7.1 General 24
4.7.2 Handling of temperature results using *FISH* 24
4.7.3 Step-wise fracture strength reductions 25
4.8 Calculation sequence 26
4.8.1 Near-field models 26
4.8.2 Large-scale model 26

5 Input data and links to site models 27
5.1 General 27
5.2 Rock mechanical, thermal and thermo-mechanical properties 27
5.2.1 General 27
5.2.2 Material parameter values 27
5.2.3 Initial stresses 29
5.2.4 Initial temperatures 31
5.3 Layout 31
5.3.1 Repository scale 31
5.3.2 Tunnel scale 32
5.4 Map of near-field models 33
5.4.1 General 33
5.4.2 Forsmark 33
5.4.3 Simpevarp 34
5.4.4 Laxemar 34

6 Results 35
6.1 Temperatures 35
6.2 Fracture shear displacement and fracture normal stress 37
6.2.1 General 37
6.2.2 Base case 37
6.2.3 Sensitivity to fracture strength, pore pressure and in situ stress state 57

6.3 Rock stresses 60
6.3.1 General 60
6.3.2 Elastic conditions 63
6.3.3 Sensitivity to fracture strength, pore pressure and thermal expansion 68
6.4 Intact rock failure 73
6.4.1 General 73
6.4.2 Forsmark 73
6.4.3 Simpevarp 76
6.4.4 Laxemar 79
6.5 Results from large-scale model 81
6.5.1 Time dependent boundary conditions used in near-field models 81
6.5.2 Thermal stresses between the repository and the ground surface 82

7 Conclusions and discussion 85
7.1 General 85
7.2 Relevance and validity 85
7.2.1 Data 85
7.2.2 Thermal model 85
7.2.3 Fracture system 85
7.2.4 Boundary conditions 86
7.3 Near-field model results 86
7.3.1 Fracture shear displacements and normal stresses 86
7.3.2 Rock stresses 86
7.3.3 Intact rock failure 87
7.4 Large-scale model results 88
7.5 FISH routine for handling of temperature results 88

References 89

1 Introduction

The KBS-3 repository concept for spent nuclear fuel is based on horizontal tunnels at 400–700 m depth in crystalline rock. The spent fuel is deposited in copper canisters which are placed in vertical deposition holes in the tunnel floor. The canisters are surrounded by a low-permeability, flexible barrier of highly compacted bentonite for isolation and mechanical protection. The spent fuel will be dangerous for hundreds of thousands of years and it is important for the repository safety that the barrier system's sealing properties are stable over long times.

During the life-time of the repository, the mechanical conditions of the bedrock will change due to future changes in load conditions. The heat from the decaying spent fuel will introduce a period of increased rock temperature that will last for thousands of years. The temperature increase will create thermal stresses in the rock. There is also the possibility of future glaciations, which will change the state of stress in the rock mass. These changes in the rock mechanical conditions will give both fracture shear displacements and fracture normal stress changes. The shear displacements and stress changes will cause changes in the fracture hydraulic properties, both on a near-field scale and on a larger scale. In the present work, the fracture normal stress changes and fracture shear displacements caused by the heat pulse and of ice loads have been studied.

If the in situ stresses are high at the repository site, high tangential stresses may develop around the openings. If these tangential stresses exceed a level corresponding to a certain ratio of the rock's uniaxial compressive strength, stress-induced failure (spalling) may occur at the opening walls /Martin et al. 2001/. Even if spalling does not occur during the operational phase, it may take place at a later stage due to thermally induced stresses. The scope of spalling in a deposition hole has been studied as a part of this work.

The heat generation within the repository gives thermal compressive stresses at repository depth and a reduction of the compressive horizontal in situ stresses at some distance above and below the repository horizon. At some depth between the repository and the ground surface, the stress reduction may become large enough that the normal stresses in steeply oriented fracture zones become low or even approach zero. This will have implications for the hydraulic properties of such zones. The scope of the thermal horizontal stress evolution between the repository horizon and the ground was one of the issues that were addressed here.

The work discussed above has been carried out by use of *3DEC*, which is a three-dimensional computer code based on the distinct element method. The code simulates the response of a discontinuous medium subjected to either dynamic or static loads /Itasca 2003/. Embedded within *3DEC*, there is a programming language called *FISH,* which enables the user to define new variables and functions that may be used to add user-defined features to the code. *FISH* was used here for the development of a technique for storage and repeated use of temperature calculation results. This was done in order to make the thermal calculations computationally efficient.

Data to the models was obtained from the on-going site investigations at the Forsmark, Simpevarp and Laxemar sites and on current repository design premises.

2 Objectives

The main objective of this work has been to analyze thermo-mechanical discrete fracture near-field models based on preliminary data from the Forsmark, Simpevarp and Laxemar site investigations /SKB 2005ab, 2006a/ and on the current repository design premises /SKB 2004/. The models were used as tools in the study of heating- and glaciation effects on fractures and the rock surrounding deposition tunnels and deposition holes in a KBS-3 repository. The specific items that have been addressed are:

- Fracture normal stresses and shear displacements. The influences of pore pressure and of different fracture strength parameter settings were considered.
- Rock stresses. The influences of fractures were considered.
- The extent of stress-induced failure (spalling) around deposition holes due to excavation and heating.

In addition to the near-field models, a large-scale model also was analyzed. The model was used for the following:

- Provide alternative boundary conditions to the near-field models.
- Study the influence of the thermal development inside the repository on the thermal stresses between the repository horizon and the ground surface.

The *3DEC* results of this report have provided input to the SR-CAN THM background report dealing with the general THM evolution of the sites /Hökmark et al. 2006/.

3 Loads and time perspectives

3.1 General

During the repository's life time, there are a number of possible changes of conditions that may have implications for the mechanical conditions in the repository. In the present work, three main episodes were considered for the near-field models:

1. *Transition from initial state to state at the time of closure:* When the repository is constructed, the in situ conditions (rock stresses, pore water pressure) will be disturbed. The excavation of openings in the rock will cause pore pressure reductions and redistribution of stresses around the openings.
2. *Thermal pulse:* The heat generated by the spent fuel will increase the temperature within and around the repository. This will induce thermal stresses both within the repository and in the rock mass around the repository.
3. *Glaciation:* When a period of glaciation takes place, the ice load will cause stress changes in the repository.

In the near-field models, all three points were considered whereas only point two was considered in the large-scale model.

3.2 Transition from initial state to state at the time of closure

The transition from the initial state to the state after closure comprises the following:

- Reduction of the pore pressure in connection with drilling of pilot holes and blast holes.
- Formation of an Excavation Damaged Zone (EDZ) in connection with blasting and removal of rock (not considered here).
- Stress redistribution around openings in connection with removal of rock.

Some time after deposition the bentonite surrounding the individual canisters will reach full water-saturation and start to exert a swelling pressure on the walls of the deposition holes. The time-scale for the development of the swelling pressure depends on the availability to water. If the rock mass permeability is high and the water pressure in the surrounding rock is high, the swelling pressure may be fully developed after four or five years /Börgesson and Hernelind 1999/. After yet some time, the deposition tunnels will be resaturated and the ground water pressure will start to increase and eventually approach the initial undisturbed conditions.

Both the development of swelling pressure and the development of a pore pressure in the near-field have uncertain time-scales that will overlap with the period of the thermal pulse. The scope and extent of that overlapping is uncertain and not very important to the mechanical evolution. Here, three scenarios regarding pore pressure and swelling pressure development were analyzed:

- Both swelling pressure and pore pressure are fully established before the heat generation starts.
- Swelling pressure is fully established before the heat generation starts. No pore pressure developed.
- No swelling pressure and no pore pressure developed.

The stress redistribution around openings in connection with removal of rock was considered in the models. The effects of tunnelling and the effects of deposition hole drilling were considered separately. For each of these stages, the rock was removed in one single step. The effects of a step-wise removal of rock were not considered.

3.3 Thermal pulse, 0 years to 20,000 years

3.3.1 General

As soon as the canisters have been deposited, the decaying fuel will start to heat the near-field. The heat propagation in the geosphere is sufficiently slow that it will not be important that the heat generation starts at different times in neighbouring tunnels, rather than simultaneously in all tunnels /Hökmark and Fälth 2003/. Thus, in the thermal model used here, the heat generation of some 5,000 canisters is assumed to start simultaneously in all tunnels. The thermal volume expansion of the intact rock blocks is the fundamental process that governs the mechanical evolution. The heat load and the rock mass heat transport properties determine the temperature evolution, whereas the stress development is controlled by the degree of confinement, the rock's compressibility and thermal expansion properties.

3.3.2 Fuel initial power and power decay

Canisters will have the heating power $P(0)$ = 1,700 W each at the time of deposition /SKB 2006c/. Here, the power decay is expressed as:

$$P(t) = P(0)\sum_{i=1}^{7} a_i \exp(-t / t_i) \qquad (3\text{-}1)$$

where t is time. The values of t_i and a_i are listed in Figure 3-1.

Equation 3-1 is valid for 20,000 years and more. Soon after deposition there may be some uncertainty in the decay function, because individual canisters will contain fuel elements of different age. The decay function coefficients above are obtained by interpolating between values for 30-year-old and 40-year-old fuel /Hökmark and Fälth 2003/.

i	t_i (years)	a_i
1	20	0.060
2	50	0.705
3	200	-0.055
4	500	0.250
5	2000	0.025
6	5000	-0.009
7	20000	0.024

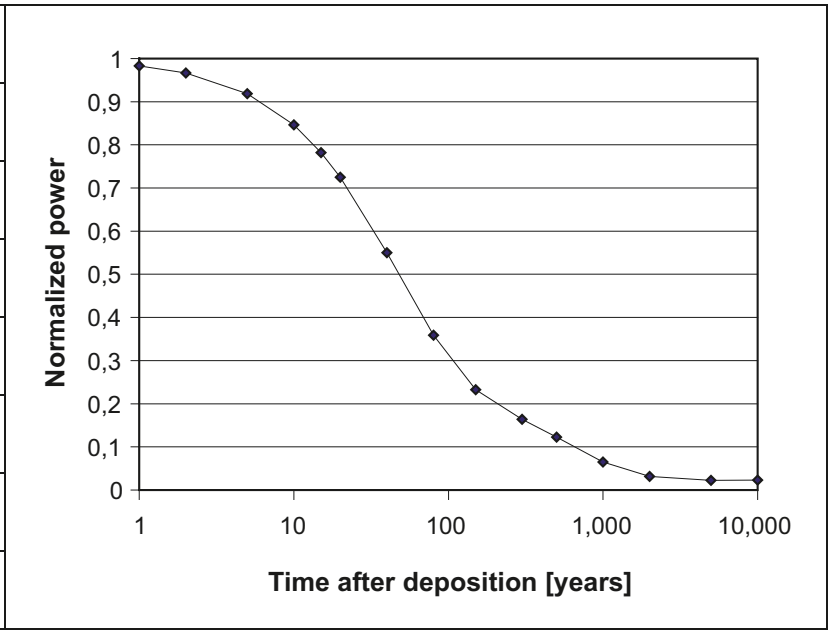

Figure 3-1. *Decay function for the fuel.*

3.4 Ice load

The repository host rock must be assumed to be subjected to the effect of a glaciation load in the future. No detailed predictions can be made of how a future ice-cover will form, grow, change in thickness and extension over time, or how it will finally melt away. The best estimate is to assume that the next glaciation will follow a pattern similar to that of the most recent one, the Weichselian Glacier. Figure 3-2 shows the load along a NW-SE scan-line across the northern part of the shield as found from an ice model proposed by Lambeck /Lund 2005/.

The mechanical load that will be transferred to the near-field is not a straightforward consequence of the increased overburden. The finite thickness of the elastic/brittle crust and the interaction of that crust with the viscous mantle will generate flexural stresses which will vary over time. These flexural stresses will depend on the proximity to the edge of the ice and will give variations in horizontal stresses at repository depth. Here, preliminary results from 2D finite element method (FEM) analyses of ice/crust/mantle models of the most recent glacial cycle /Lund 2005/ were used to find stress boundary conditions for the near-field models.

For the models analyzed here, the ice load is assumed to appear sufficiently long after deposition that the temperature will have dropped back to the initial, undisturbed present-day values. This is not likely to be exactly correct, since there will be a few degrees of excess temperature even some 10,000 years after deposition. We nevertheless consider this approximation as adequate, and within the margins of the overall uncertainty.

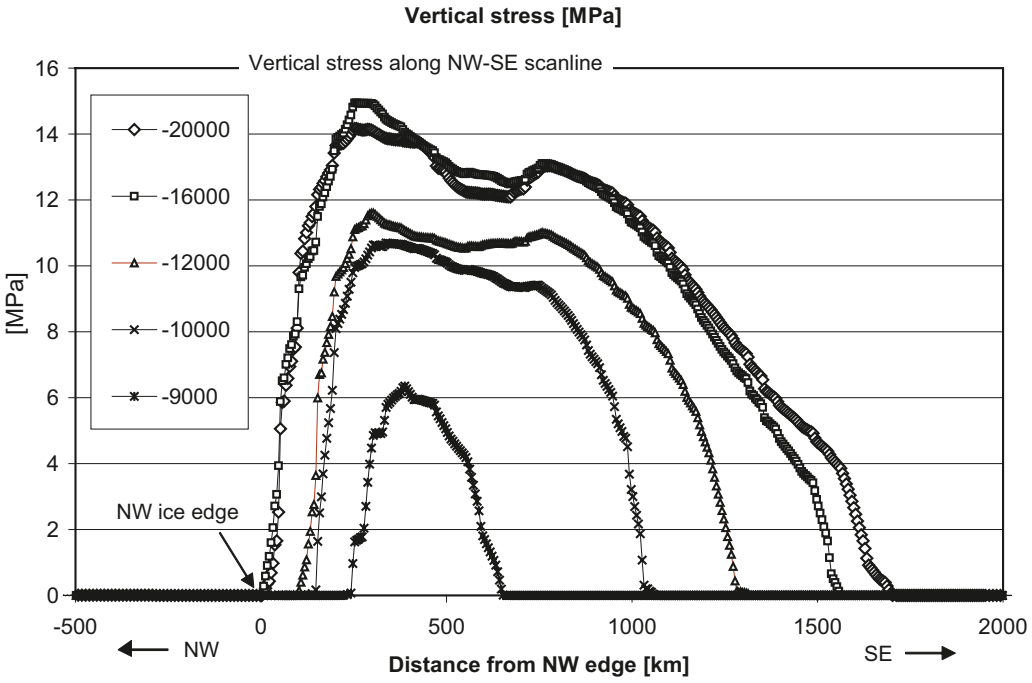

Figure 3-2. *Ice load on the crust along NW-SE scan-line according to Lambeck's ice model /Lund 2005/. Legends give time in years before present.*

4 Description of models

4.1 General

The work was carried out by use of *3DEC,* which is a numerical three-dimensional program based on the distinct element method /Itasca 2003/. Two types of models were analyzed:

- Near-field models
- Large-scale model

The near-field models were divided into three model groups: Forsmark models, Simpevarp models and Laxemar models. The models include 4,756 heat sources, a portion of a deposition tunnel, three deposition holes and a number of fractures. Some models were analyzed without fractures.

The large-scale model was used to study rock thermal stresses on a large-scale and also for evaluation of the relevance and validity of the near-field model mechanical boundary conditions. In the large-scale model, no fractures and no in situ stresses were included.

4.2 Geometric outlines of the thermo-mechanical near-field 3DEC model

Figure 4-1 (left) shows the outlines of the *3DEC* near-field model. Parts of the model are hidden in the figure. The model is 50 m in the tunnel direction, 40 m across tunnels and 50 m in the vertical direction. The right part of the figure shows the inner 30 m × 30 m × 30 m box which included the explicitly modeled fractures. The orthogonally aligned planes are construction planes which were used to define the model geometry and to facilitate discretization of the continuum, i.e. the intact rock.

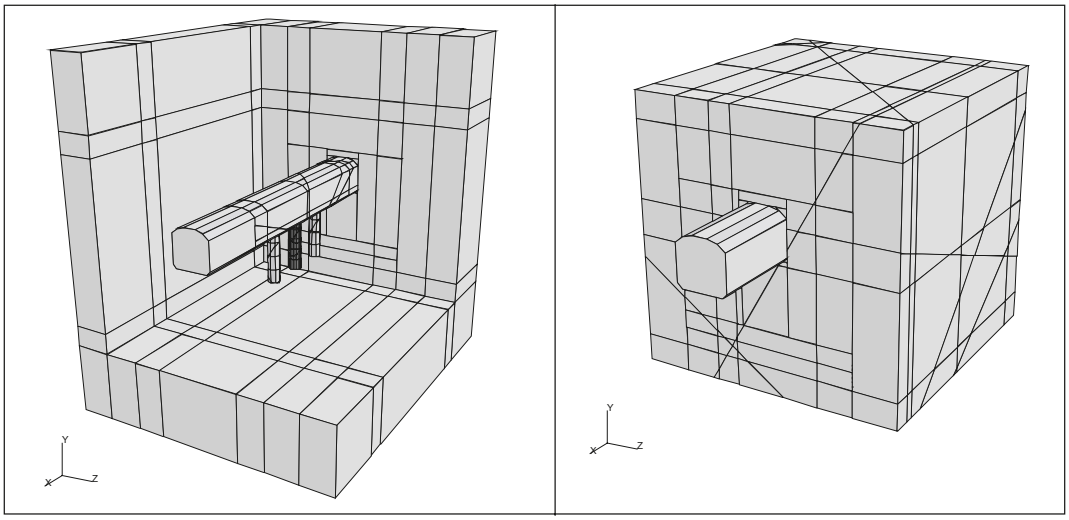

Figure 4-1. *Geometry of mechanical 3DEC model. Left: Outlines of entire model. Right: The inner 30 m × 30 m × 30 m box. This part of the model contains the fractures.*

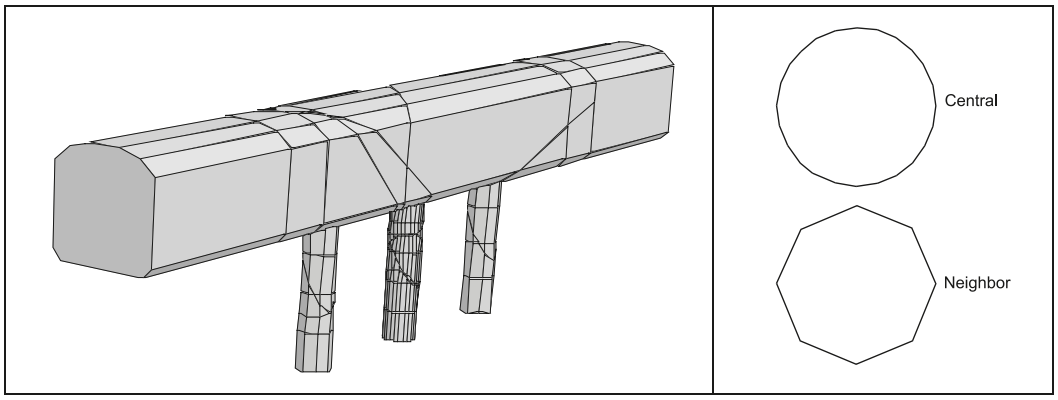

Figure 4-2. *Interior of 3DEC model with 24 tangential sections to represent the central hole and 8 to represent the two neighbouring holes.*

The analyses were focused on processes in the near-field of a deposition hole in the central parts of a deposition area. The two closest neighbour holes were included, but holes at larger distances will not have any mechanical influence on the region of interest and were not represented mechanically. The periphery of the central deposition hole was represented by 24 tangential sections. The other holes were represented by 8 sections (Figure 4-2).

4.3 Near-field model fracture geometry

The models contain a small set of fractures, identical for all models. The fracture geometry is not based on field data. Instead, a few, relatively large fractures with different orientations and locations relative to the near-field geometry were defined. The six fractures are listed in Table 4-1 and the fracture planes are shown in Figure 4-3.

All fractures extend to the boundaries of the inner 30 m × 30 m × 30 m box (cf Figure 4-1). This means maximum fracture sizes corresponding to radii between 20 and 25 m, depending on dip and strike angles. The fracture geometry is given relative to the geometry of the tunnel and the central deposition hole, irrespective of the canister spacing and the tunnel orientation. For the volume of interest here, i.e. the volume around the central deposition hole, the fracture density (P32) is about 1.5 units of fracture area per unit rock volume.

Table 4-1. List of fractures incorporated in the near-field model.

Fracture	Description
#1	Vertical and perpendicular to tunnel, at 0.4 m distance from the wall of the central deposition hole
#2	Vertical and parallel to tunnel at 0.75 m distance from the tunnel wall
#3	Vertical, intersecting tunnel at 45° at 0.54 m distance from the wall of the central deposition hole.
#4	Dipping 20° with strike normal to tunnel. Intersecting the central deposition hole axis 2 m below tunnel floor.
#5	Dipping 45° with strike normal to tunnel. Intersecting the central deposition hole axis 5 m below tunnel floor.
#6	Dipping 45° with strike 45° relative to tunnel. Intersecting the central deposition hole axis 3 m below tunnel floor.

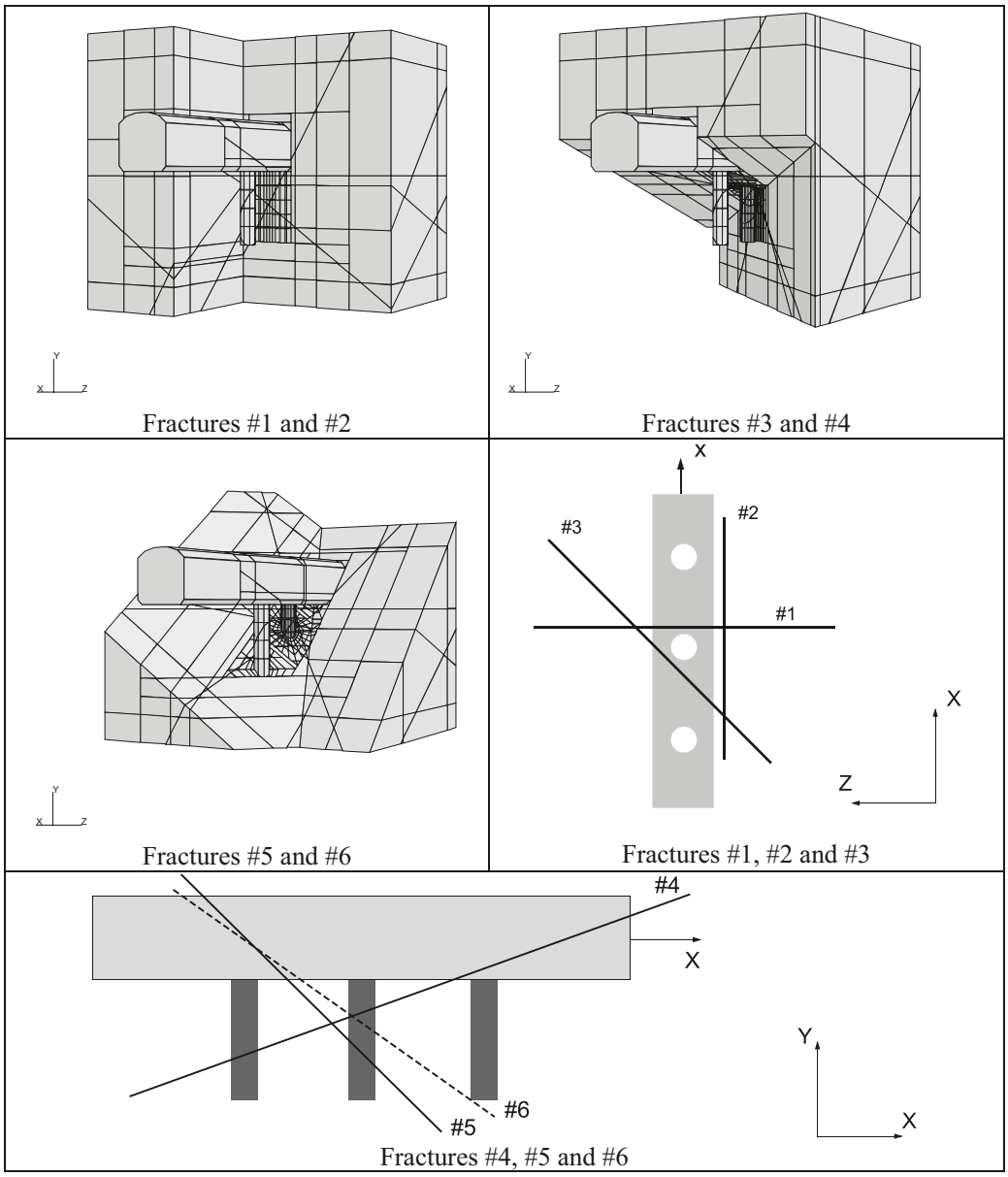

Figure 4-3. *Fractures in inner 30 m x 30 m x 30 m box. All fractures extend to the box boundaries.*

4.4 Near-field model boundary conditions

4.4.1 Thermal

The *3DEC* thermal logic is based on an analytical solution of the temperature field around individual point heat sources, and on the principle of superposition to find the total effect of numerous point sources. Linear heat conduction in a homogenous, isotropic medium is assumed. The point sources are arranged in lines and grids to represent the deposition geometry applied in the repository layout. The use of an analytical solution implies that there is no need for thermal boundary conditions, although it is possible to specify isothermal and adiabatic boundaries. Here, no such boundaries were specified, which means that the thermal influence of the ground surface was ignored. This gives a small overestimation of the temperatures at the repository level after 5,000 years and onwards /Hökmark 1996/.

4.4.2 Mechanical

Excavation/operation and temperate phase

For most of the cases analyzed here, the bottom boundary and the vertical boundaries were fixed in their normal directions and a constant stress was applied at the top of the model. The stress at the top was the same as the vertical in situ stress. For the excavation phase, these are relevant conditions. The boundaries were at sufficient distances (more than six tunnel radii) from the central tunnel section that the boundary effects could be ignored /Brady and Brown 1994/.

For the heated phase, two different sets of boundary condition were used.

1. *Base case:* The same as in the excavation phase, i.e. bottom and vertical boundaries locked in the normal direction and constant load on top of the model.
2. *Moving boundaries:* The vertical boundaries were allowed to displace in their normal directions and the stress on the top of the model was varied. The vertical boundary displacements and the stress at the top were varied with time according to results obtained from the large-scale model described in Section 4.6.

For the heated phase, the base case setting will introduce two errors:

- In reality there will be some horizontal expansion of the modelled volume. That expansion depends on the large-scale rock mass properties and on the repository layout. Figure 4-4 shows an example of horizontal deformations calculated in a previous study by /Hökmark 1996/. In that study, the assumptions regarding heat load and mechanical properties differed from what was used here and a uniformly heated square-shaped repository was assumed. In the present study, the heat sources are not uniformly distributed. Between the heated areas, there are unheated regions. This gives a more complicated time development of the boundary movements (Figure 4-5), but the time of maximum displacement (about 1,000 years) coincides with that of the study by /Hökmark 1996/.
- In reality there will be a small increase in vertical load due to the heating. According to a previous study this will not amount to more than 3 MPa /Probert and Claesson 1997/. In addition, that increase in vertical load will be different at different positions in the repository, for instance in the central region, in edge regions and in corner regions. The analysis made by Probert and Claesson regarded a repository with a square-shaped horizontal cross section with a uniformly distributed heat load. For the reference layout applied here (cf Chapter 5), with non-heated areas between the rectangular deposition areas, the picture is more complicated. However, even if the reference layout is used, the vertical stress will not exceed the 3 MPa level (Figure 4-5).

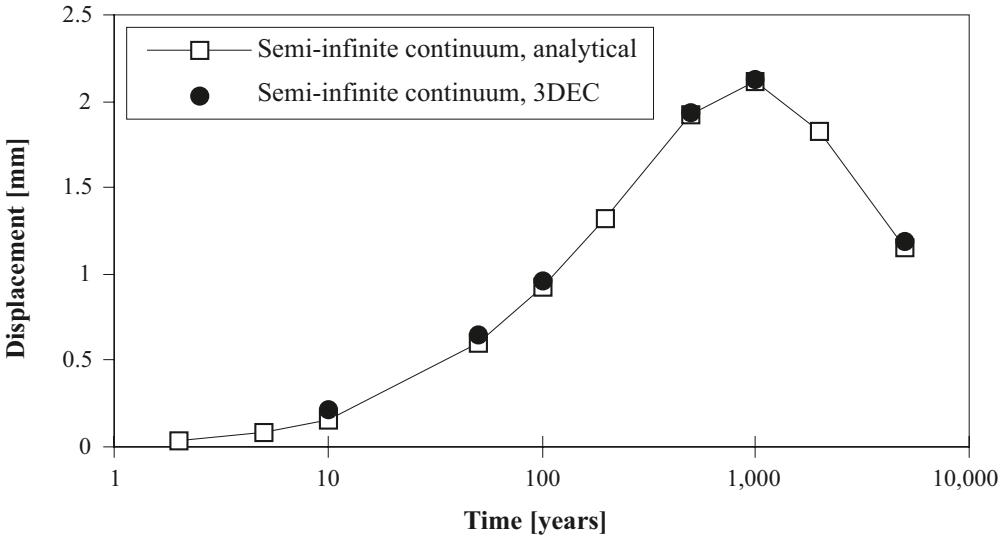

Figure 4-4. *Displacement of vertical boundary in previous study /Hökmark 1996/.*

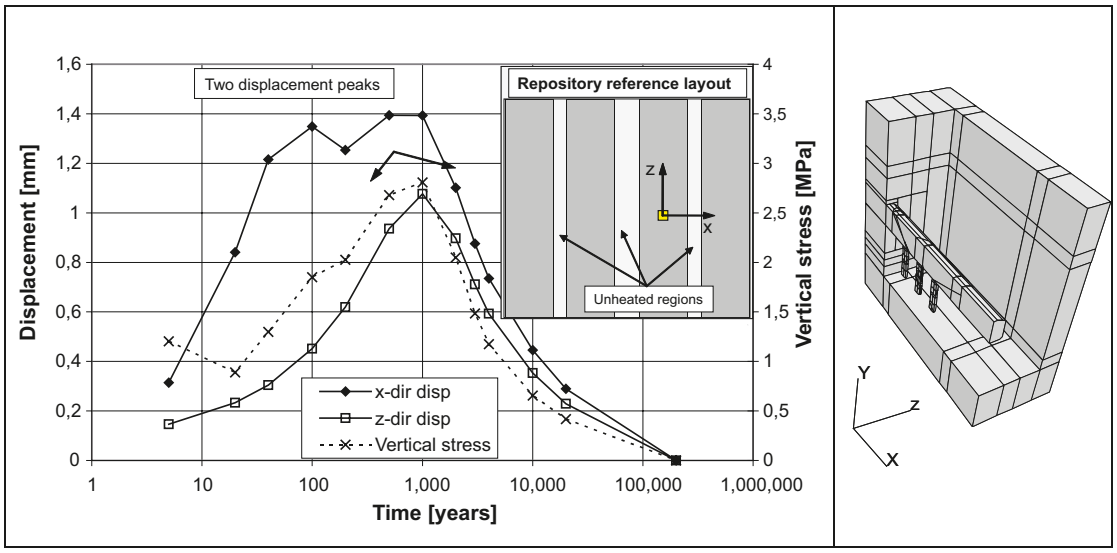

Figure 4-5. *Displacements of vertical boundaries and vertical stress at top of model. Boundary conditions derived from the large-scale thermo-mechanical 3DEC model described in Section 4.6. Note the double x-displacement peaks due to the repository layout with unheated regions between the local and the neighbouring deposition areas.*

In order to quantify the overestimation of the thermal stresses that is made when the base case assumption is applied, results from two models were compared. In one model (*Fors 8*), the basic assumption was applied. In the other model (*Fors 9*), the moving boundary assumption was used (cf Figure 4-5). Figure 4-6 shows thermal stress as a function of time at a point located close to the central deposition hole in the two models. After 100 years, when the thermal stresses reach their maxima, the stress in *Fors 8* is about 4 MPa higher than in *Fors 9*, i.e. an overestimation of the thermal stress of about 7% at the time of maximum stress. After 1,000 years, the difference in stress has increased to 11 MPa. However, after this time the stress level has decreased significantly and the stress overestimation at this time is less important. The stress overestimations made using the basic boundary condition settings are conservative and within reasonable bounds.

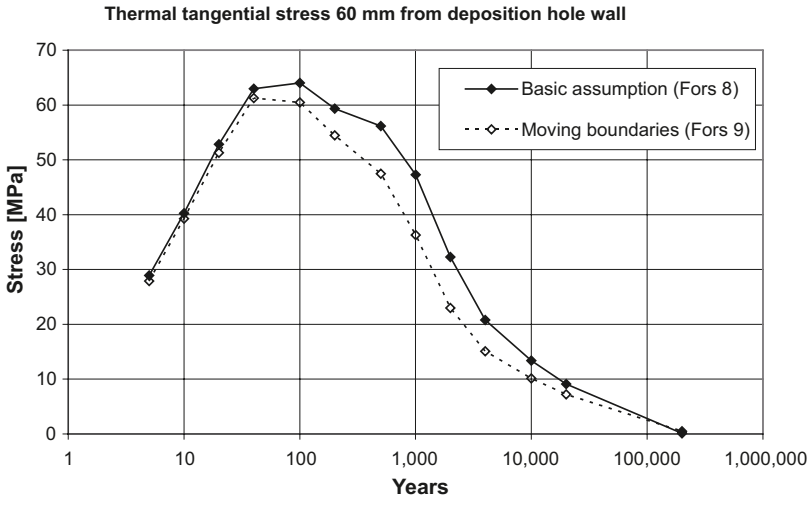

Figure 4-6. *The diagram shows the thermal tangential stress close to the central deposition hole wall at a point located 2 meters below the tunnel floor. Two cases are shown; Fors 8: Case with the vertical boundaries locked to normal displacements. Fors 9: Case with time dependent boundary movements in the x- and z-directions and time dependent vertical stress applied at model's upper boundary.*

Glaciation

For the modelling of the glaciation/deglaciation stage, results of preliminary 2D FEM ice/crust/mantle analysis (B Lund, Dep. of Earth Sciences, Uppsala University, personal communication, 2005) were used to specify stress boundaries (cf Figure 3-2). The 2D FEM analysis was based on the 1998 version of Lambeck's model of the most recent glaciation. The origin of the NW-SE scan-line was fixed at the point of the maximum North-Western ice sheet extension close to Lofoten, Norway.

The glaciation/deglaciation cycle was simulated only for the Forsmark model. The Forsmark site is not located directly on the NW-SE scan-line considered in the FEM analysis, but at an approximate distance of 800 km from the scan-line origin. Figure 4-7 shows stresses obtained from the ice-crust-mantle analysis for a point at 500 m depth 800 km southeast of the origin at the NW ice edge. Three sets of stress data corresponding to different stages of the cycle were selected for use as stress boundary conditions of the *3DEC* Forsmark near-field model: the stresses during maximum load (–15,000 years), the stresses at the time when the retreating ice margin passes the site (–9,000 years) and the stresses 9,000 years later (0 years).

In the Forsmark model, the major initial present-day stress is oriented in NW-SE and the tunnel is assumed to be sub-parallel to that stress. Therefore, the glaciation boundary principal stresses were assumed to coincide with the model axes (Figure 4-8).

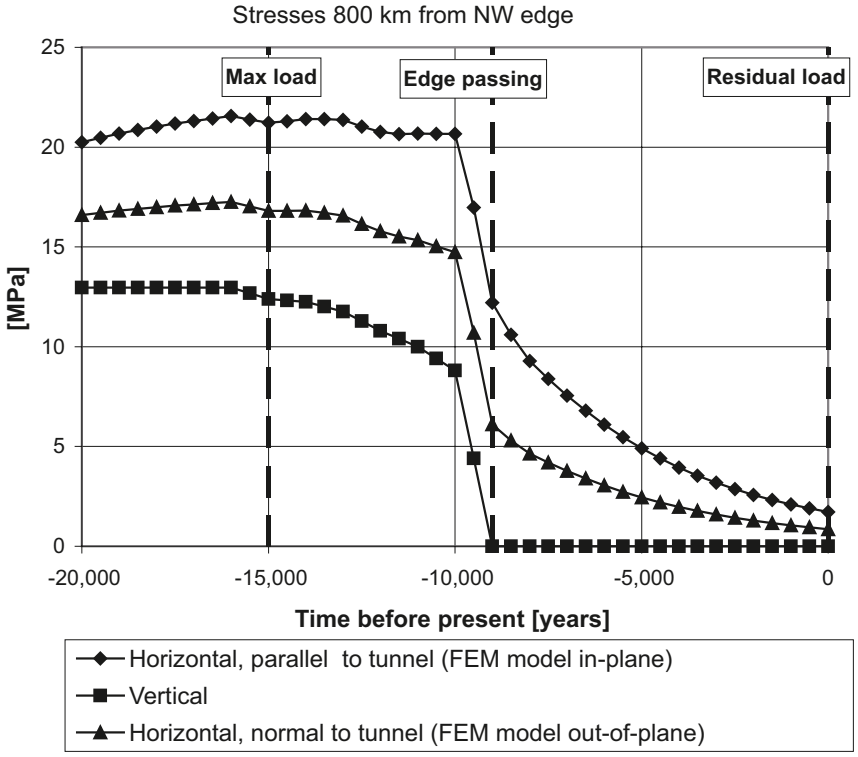

Figure 4-7. *Histories of stress increase at a point located 800 km from the northwest edge of the ice. The largest stress increase is in the plane of the 2D FEM study (i.e. oriented NW).*

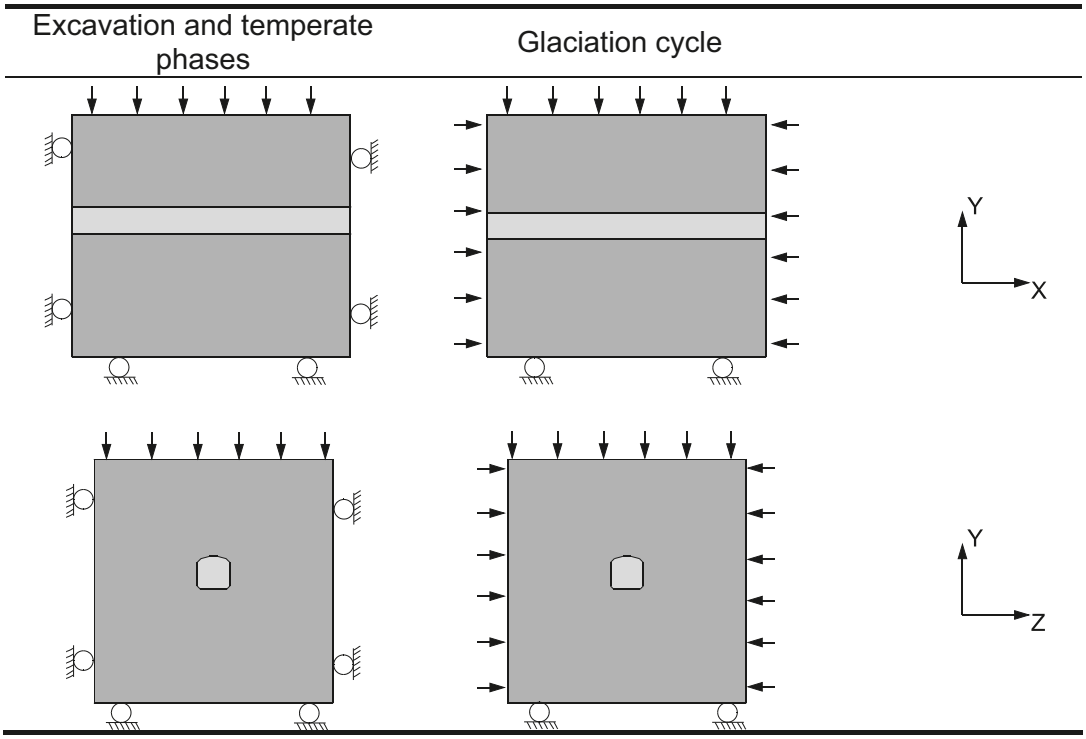

Figure 4-8. *Schematic of boundary condition used for excavation/operation and temperate phases (base case assumption) (left) and for glaciation cycle (right).*

The preliminary 2D ice-crust mantle analyses were based on a very schematic description of the earth with uniform, depth-independent, elastic crust properties and with an incompressible crust /Lund 2005/. In addition, the reference ice-load now considered in the safety assessment is about twice the one assumed in the preliminary 2D FEM analyses /SKB 2006b/. Some aspects of this are discussed in /Hökmark et al. 2006/. For the present study it is sufficient to note that that the horizontal stress additions have been overestimated and the vertical stress addition underestimated, which caused the in situ stress anisotropy found at all sites to increase very significantly in the *3DEC* near-field models as a result of the ice load. Recent crust stress results obtained using more realistic Earth models indicate that the ice load will reduce the stress anisotropy rather than increase it /Lund 2006/, meaning that the glacial cycle results were obtained using conservative load assumptions.

4.5 3DEC thermal model

Altogether 4,756 individual canisters are included in the thermal model. The geometrical arrangement of the canisters is described in the following chapter. The central canister is modelled as two vertical superimposed arrays of 20 positive and 20 negative point sources, as shown in Figure 4-9, upper left. The resulting compound line source reproduces the excess of heat output found around the bottom and top parts of real cylindrical canisters reasonably realistically /Hökmark and Fälth 2003/. The closest 20 neighbouring canisters are represented by simple vertical arrays consisting of 5 point sources each as shown in the lower left. The rest of the canisters were represented by point sources. The initial canister power and the decay function were set according to the fuel description in Chapter 3.

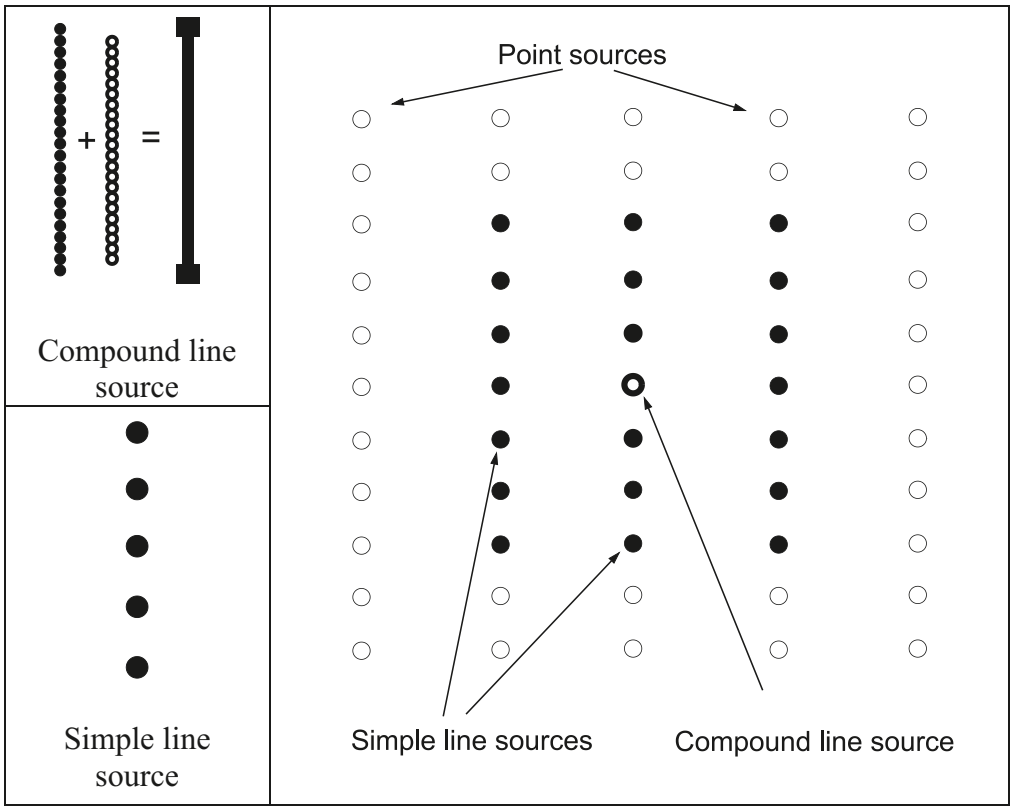

Figure 4-9. *Schematics of canister representation with a refined representation of the central canister (upper left). The compound line source parameters are calibrated to represent the axial distribution of heat output around a real cylindrical canister.*

4.6 Large-scale model

The main reasons for generating and analyzing the large-scale model were the following:

- Provide alternative boundary conditions to the near-field models. These boundary conditions were used to check the validity of the mechanical boundary conditions applied to the near-field model (base case assumption, cf Section 4.4.2). They were also applied in a particular version of the Forsmark model, which was analyzed specifically to estimate the volumes of rock in which the spalling strength may be exceeded.
- Explore the way the thermal stresses vary over time around the repository, in particular in the region between the deposition areas and the ground surface.

Figure 4-10 shows the outlines of the large-scale *3DEC* model. The model consists of a large block where the top represents the ground surface. Parts of the model are made invisible to show the interior of the model, i.e. the deposition areas at 500 m depth. The model was used to simulate the thermo-elastic response only, i.e. without account of the initial stresses. No fractures were considered (elastic model), meaning that only one quarter of the problem needed to be modelled. This is also illustrated in Figure 4-11. The bottom and the vertical boundaries were fixed in the normal direction (roller boundaries) whereas the upper horizontal boundary was free. A box representing half the near-field model was defined (Figure 4-11). The box dimensions were the same as half of the near-field model (X × Y × Z = 50 m × 50 m × 20 m). The z- and x-displacements of the near-field box vertical boundaries as well as the vertical stress on its top boundary were recorded for use as boundary conditions for the corresponding near-field model. The thermal model used was that of the Forsmark near-field model (i.e. the same repository geometry was assumed). The thermo-mechanical properties were those applied for the rock mass in the Forsmark near-field model (cf Table 5-1).

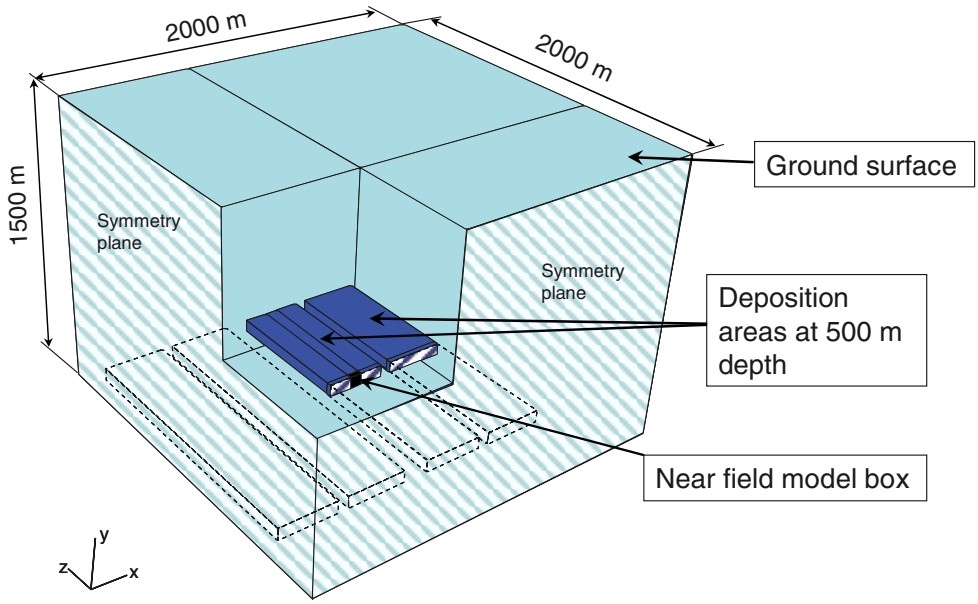

Figure 4-10. *The quarter-symmetry thermo-mechanical large-scale model. The outlines of the full repository are indicated by the dotted frames.*

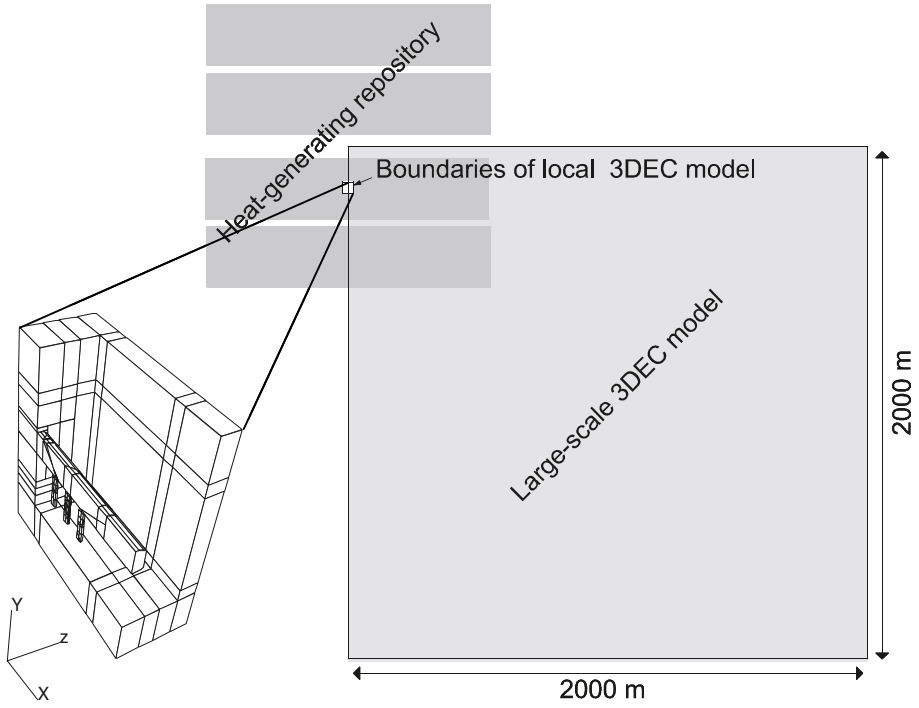

Figure 4-11. *Outline of the large-scale model. Only a quarter of the repository needed to be included in the model. The box in which the boundary displacements and stresses were recorded is indicated in the figure. These histories where used as boundary conditions in some of the Forsmark near-field cases. The box represents one half of the near-field model. No excavations or fractures were included in the large-scale model.*

4.7 Numerical considerations and code handling

4.7.1 General

3DEC is a numerical three-dimensional program, which is based on the distinct element method /Itasca 2003/. The code simulates the response of discontinuous media (e.g. jointed rock mass) subjected to either static or dynamic loads. The medium is represented by blocks that can be either rigid or deformable. Large displacements (i.e. translations and rotations) of the blocks are permitted. Deformable blocks are subdivided into a mesh of finite difference elements. The relative motions of the blocks are governed by linear or non-linear force-displacement relations along the discontinuities.

3DEC is based on a time domain solution scheme which solves the equations of motion using an explicit finite difference method. The law of motion and the constitutive relations are applied at each time step. The time step has to be shorter than the critical time step to ensure numerical stability. The critical time step is calculated by the code and it is based on the mass to stiffness ratio of the system /Itasca 2003/.

4.7.2 Handling of temperature results using *FISH*

Temperatures are calculated in *3DEC* without regular heat transport calculations. Instead, the temperature at each grid point at a given instance of time is calculated by use of an analytic solution. In general the analytic solution scheme is fast. However, the near-field models used here consist of many grid points (~80,000) and a large number of heat sources (~4,700). In addition, the heat power decay function consists of seven exponents. This means that when the temperature contributions from all heat sources are applied to all grid points, the basic time integral has to be evaluated $80{,}000 \times 4{,}700 \times 7 \approx 2.6 \cdot 10^9$ times. This operation has to be performed for every instance of time analyzed, which makes the temperature calculations time consuming.

The large number of near-field models analyzed here were divided into three main groups, Forsmark models, Simpevarp models and Laxemar models. The models within each group have the same geometry, the same grid and consequently the same thermal solution at each instance of time. This was used to speed up the calculations. For each group of models, the grid point temperatures at each instance of time were calculated only once and then saved on disk. The temperatures could then be read back into the model being analyzed, where the actual temperature increments (used in thermal stress calculation) were calculated. The scheme is shown in Figure 4-12. The export and import of temperature results as well as the temperature increment calculation was handled by use of the programming language *FISH* embedded within *3DEC*.

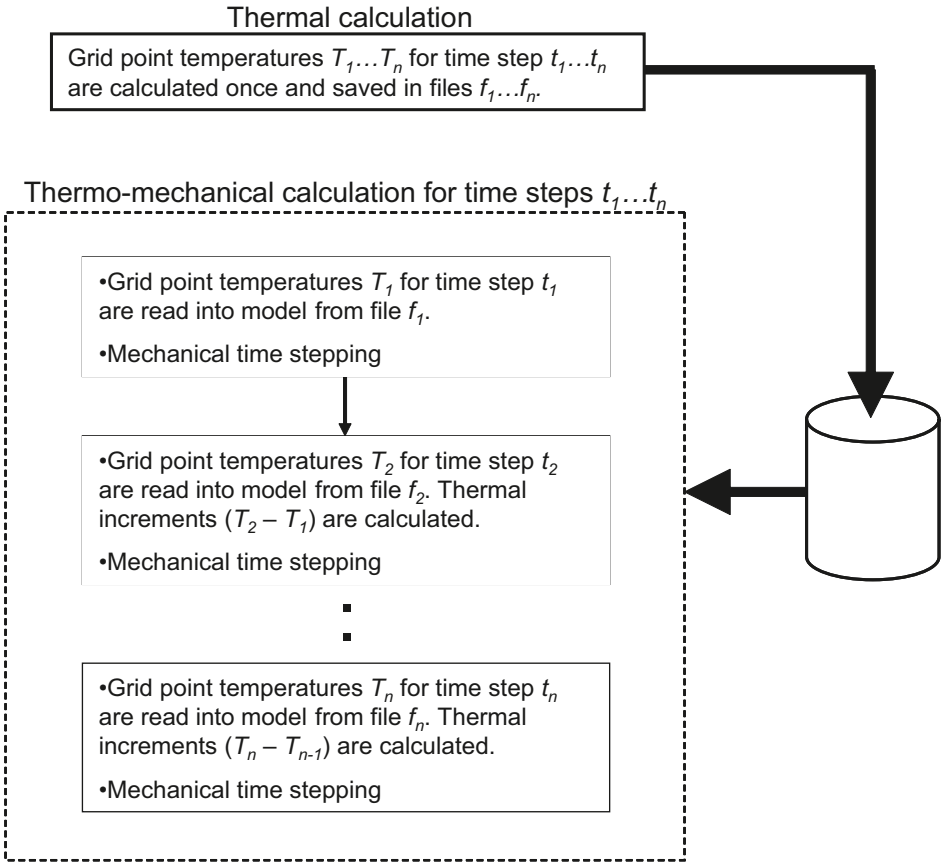

Figure 4-12. *Scheme for handling of temperature results. Here T denotes a complete set of grid point temperatures. The administration of the temperature results was done by use of FISH.*

4.7.3 Step-wise fracture strength reductions

During the calculations, *3DEC* performs a large number of small mechanical time steps. At each time step, the block forces, displacement and velocities are updated and at every 10th step, the contacts in the block interfaces are updated.

The thermal stress calculation for one instance of time comprises three steps:

1. The temperatures and the temperature increments in the model are calculated as described above.
2. Thermal stresses are calculated. The calculation is based on the calculated temperature increments.
3. A number of mechanical time steps are performed until mechanical equilibrium is achieved.

This means that large, thermally induced unbalanced forces will occur when the time stepping is started (step no. 3). In order to ensure that no irrelevant, non-physical fracture movements took place as a result of a sudden thermal stress release, the strength of the fractures was set to a high value initially and then reduced in steps until the intended fracture strength parameter value was reached. The initial fracture strength was high enough that the model behaved elastically. This fracture strength reduction scheme was applied each time a new temperature state was read into the model.

4.8 Calculation sequence

4.8.1 Near-field models

The near-field model simulations comprised the following steps:

1. Calculation of primary equilibrium under the given in situ stress state.
2. Excavation of deposition tunnel.
3. Excavation of deposition holes.
4. Establishment of 10 MPa swelling pressure in the deposition holes.
5. Establishment of 5 MPa pore pressure at tunnel walls, in all fractures and in deposition holes (10 MPa swelling pressure + 5 MPa pore pressure = 15 MPa total pressure in deposition holes).
6. Thermal load from 4,756 canisters, each generating 1,700 W of thermal power at the time of deposition and with decay function as specified for SKB reference fuel (cf. Figure 3-1). Temperatures/thermal stresses were calculated at the following times: 5, 10, 20, 40, 100, 200, 500, 1,000, 2,000, 4,000, 10,000, 20,000 and 200,000 years after deposition.
7. Mechanical effects of glacial load with boundary stresses obtained from preliminary results from on-going simulations of mechanical ice/crust/mantle interactions.

The above disturbances were applied in sequence although in reality there will be some overlapping, in particular between items 4, 5 and 6. Item 7, glaciation was analyzed only in the Forsmark model.

4.8.2 Large-scale model

The large-scale model calculation included only calculation of thermal stresses.

5 Input data and links to site models

5.1 General

The modelling work reported here was performed during a period of ongoing site investigations and establishment of site descriptive models. The data used here correspond to the knowledge and the views expressed in preliminary versions of the Forsmark, Simpevarp and Laxemar version 1.2 site descriptive models /SKB 2005ab, 2006a/. The site model data has been supplemented by information from the projecting teams (M Brantberger, Ramböll Sverige AB, personal communication 2004, R Glamheden, FB Engineering AB, personal communication 2004). Geometry data has also been obtained from the current repository design premises /SKB 2004/.

Some of the material property data and some of the layout input may change during the continued investigation and projecting work. Effects of spatial variations, anisotropy etc have not been considered. Instead mean values have been used throughout. All this means that the models analyzed here are not site models in a strict sense. The objectives of the modelling work are partly generic in nature.

5.2 Rock mechanical, thermal and thermo-mechanical properties

5.2.1 General

The following idealizations apply for all models presented here:

- The 30×30×30 m inner box (cf. Section 4.2) consists of intact rock intersected by a number of planar discontinuities (fractures). The volume outside the box consists of rock mass.
- Both the intact rock and the rock mass are approximated to be linear elastic.
- The fractures respond to loads according to an idealized elasto-plastic material model with linear joint stiffness, zero tensile strength and shear failure according to a Coulomb criterion.
- Heat transport takes place by linear conduction.

At some distance from the near-field (i.e. outside the inner box, cf. Figure 4-1), fractures are not explicitly modelled. The rock mass representation is identical to that of intact rock, but with parameter values conditioned to account for the presence of fractures according to the equivalent continuum representation given in the site descriptive models. The rock mass has the same heat conductivity, heat diffusivity and volumetric heat expansion coefficient as the intact rock.

5.2.2 Material parameter values

The base case material parameter values are presented in Table 5-1. The fracture strength parameter values derived from the reported site data should be compared with findings from laboratory work performed previously on hard rock joints in Ävrö granite. For shear displacements of 4 mm and less, /Olsson 1998/ reported total friction angles of 40°–50° and dilation angles of about 10° (cf. Figure 5-1). In the present models, the friction and dilation angles were 34° and 10°, respectively. This gives a total friction angle of 44°, which is in line with the results in the study by Olsson.

Table 5-1. Base case material parameter values.

Component	3DEC parameter	Unit	Forsmark	Simpevarp	Laxemar	Note
Intact rock	Density	kg/m^3	2,600			1
	Young's modulus	GPa	76	80	70	2
	Poisson's ratio	–	0.24	0.27	0.20	2
	Heat diffusivity	m^2/s	$1.75 \cdot 10^{-6}$	$1.25 \cdot 10^{-6}$	$1.36 \cdot 10^{-6}$	3
	Heat conductivity	W/(m·K)	3.65	2.61	2.82	3
	Heat expansion coefficient	K^{-1}	$7.7 \cdot 10^{-6}$	$6.2 \cdot 10^{-6}$	$7.2 \cdot 10^{-6}$	4
Fractures	Joint normal stiffness	GPa/m	128	100	220	5
	Joint shear stiffness	GPa/m	39	29	40	5
	Friction angle	deg	34			6
	Cohesion	MPa	0.6			6
	Dilation angle	deg	10			7
Rock mass	Young's modulus	GPa	68	62	55	8
	Poisson's ratio	–	0.22	0.28	0.28	8

1) Approximate and generic value used in all models.

2) Ver. 1.2 site model data. Values given for rock type *"granite to granodiorite"* (Forsmark), "*quartz monzonite to monzodiorite and Ävrö granite"* (Simpevarp) and "*granite to quartz monzodiorite (Ävrö granite)"* (Laxemar).

3) Values of heat conductivity (Forsmark and Simpevarp models) were obtained from early deliveries of site data to preliminary design projects (M Brantberger, Ramböll Sverige AB, personal communication 2004; R Glamheden, FB Engineering AB, personal communication 2004). These data were used to set the canister spacing in pilot layout work and have been kept in the *3DEC* models, although the thermal site models have been updated such that the RFM012 domain mean value is 3.46 W/(m·K) rather than 3.65 W/(m·K) /Sundberg et al. 2005b/ and the RSMA01 value is 2.80 W/(m·K) rather than 2.61 W/(m·K) /Sundberg et al. 2005a/. The thermal diffusivities are calculated from generic values of density (2,600 kg/m^3) and specific heat (800 J/(kg·K)). These values correspond to a volumetric heat capacity of 2.08 MJ/m^3, while the RFM012 and RSMA01 mean values are 2.15 MJ/m^3 and 2.23 MJ/m^3, respectively /Sundberg et al. 2005ab/. The Laxemar value, which regards rock domain RMSA, was picked from the Laxemar layout D1 report /Janson et al. 2006/

4) Values of heat expansion coefficients (Forsmark and Simpevarp) were obtained from draft site model versions. For the Forsmark model this value agrees with the one given for *granite to granodiorite* and, on the domain level, for domains RFM012 and RFM029 in /SKB 2005b/. For the Simpevarp model, the value now given for *Ävrö granite* is $6.0 \cdot 10^{-6}$ K^{-1}. /SKB 2005a/. For Laxemar the value regards *granite to quartz monzodiorite* /SKB 2006a/.

5) Ver. 1.2 site model data. In the site models, there are no differences between fractures belonging to different fracture sets or different domains within the sites. In the *3DEC* models mean values are used throughout. For the normal stiffness, the site reports give min-max ranges of 60–230 GPa/m (Forsmark), 49–179 GPa/m (Simpevarp) and 150–310 GPa/m (Laxemar). For the shear stiffness, corresponding ranges are 10–55 GPa/m, 10–49 GPa/m and 18–66 GPa/m, respectively.

6) Values of Coulomb parameters given here are approximated from data given in the site reports /SKB 2005ab, 2006a/. Similar to the stiffness values, the given strength data is not differentiated with respect to borehole or joint set. The data given for the three sites are sufficiently similar that (here) the same (averaged) parameter values are used for all sites.

7) Draft versions of the Forsmark and Simpevarp site reports (and the borehole primary data reports) did not include any values of the dilation angle. For the Simpevarp subarea there are no values in the final version /SKB 2005a/. Previous investigations of rock joints in *Ävrö Granite* have indicated that the dilation angle should be about 10° or more /Olsson 1998/, which is the value used in the *3DEC* models for both sites (cf. Figure 5-1). The values now given for the Forsmark and Laxemar areas range between 4° (for fractures in high compression) and 19.5° and 16°, respectively (for fractures in low compression) /SKB 2005b, 2006a/.

8) Ver. 1.2 site model data. Values given for rock domain RFM012 (Forsmark), rock domain A (Simpevarp) and rock domain A (Laxemar).

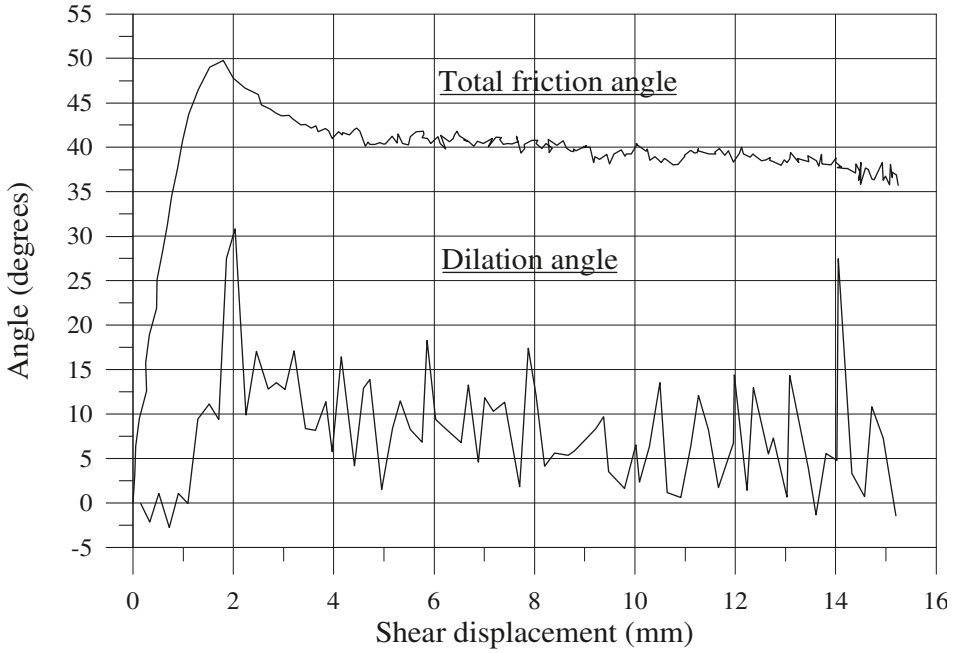

Figure 5-1. *Total friction angle and dilation angle for Ävrö granite joint obtained from constant normal load test /Olsson 1998/.*

5.2.3 Initial stresses

The initial stresses are presented in Table 5-2. All stresses apply at 500 m below ground surface with exception for the Forsmark alternative stress state, which applies at 400 m depth. For Simpevarp there are two stress regimes. The following applies:

- For the Forsmark model, and for the Simpevarp stress domain 1 model, there is a 15° angle between the deposition tunnel axis and the major horizontal stress (Figure 5-2, left) (M Brantberger, Ramböll Sverige AB, personal communication 2004; R Glamheden, FB Engineering AB, personal communication 2004). The Forsmark alternative stress state applies at 400 m depth and stress magnitudes were obtained from /SKB 2005b/.
- For the Simpevarp stress domain 2 model, which was assumed to be located in a low stress regime area, the major stress was perpendicular to the tunnel axis (Figure 5-2, middle) (R Glamheden, FB Engineering AB, personal communication 2004).
- In the Laxemar layout, the tunnel orientation differs between deposition areas /Janson et al. 2006/. In the Laxemar model, the angle between the major horizontal stress and the tunnel axis is 63° (Figure 5-2, right).

Table 5-2. Initial stresses.

	Stress [MPa]	Dip	Trend (related to tunnel axis)
Forsmark (base case):			
σ_1	45	0	15°
σ_2	18	0	105°
σ_3	13	90°	–
Forsmark, alt. stress state (apply at 400 m depth):			
σ_1	43	0	15°
σ_2	29	0	105°
σ_3	11	90°	–
Simpevarp, stress domain 1 (base case):			
σ_1	32	0	15°
σ_2	14	90°	–
σ_3	9.5	0	105°
Simpevarp, stress domain 2:			
σ_1	16	0	90°
σ_2	9.0	90°	–
σ_3	5.5	0	0°
Laxemar:			
σ_1	34	0	63°
σ_2	13.5	90°	–
σ_3	10	0	153°

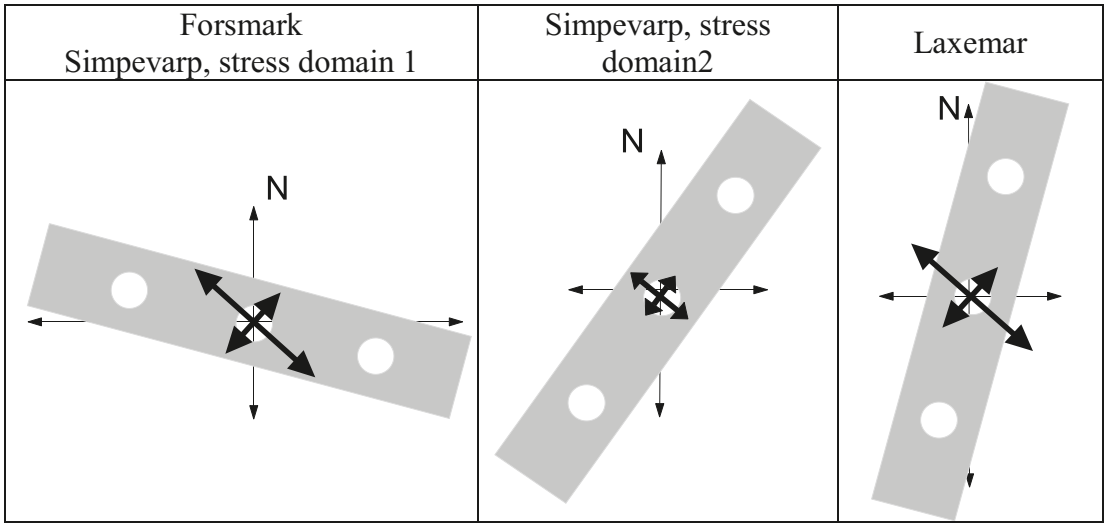

Figure 5-2. *Orientation of horizontal in situ stresses: Forsmark and Simpevarp stress domain 1 (left), Simpevarp stress domain 2 (middle) and Laxemar (right).*

5.2.4 Initial temperatures

The initial temperatures are not important to any of the calculations. Thermal stresses are obtained from changes in temperature, independently of the actual temperature level.

5.3 Layout

5.3.1 Repository scale

The repository layout is prescribed according to Figure 5-3 /SKB 2002/. The tunnel spacing is 40 m. The canister spacing in each model was set according to data obtained from the projecting teams (M Brantberger, Ramböll Sverige AB, personal communication 2004; R Glamheden, FB Engineering AB, personal communication 2004) /Janson et al. 2006/. It was set with regard to the thermal properties, i.e. the rock thermal conductivity, as shown in Figure 5-4. If the undisturbed geothermal temperature is higher or lower than the reference value 15°C, the curves must be offset accordingly. The following canister spacing values were applied:

- Forsmark model: 6 m
- Simpevarp model: 8 m
- Laxemar model: 7.2 m

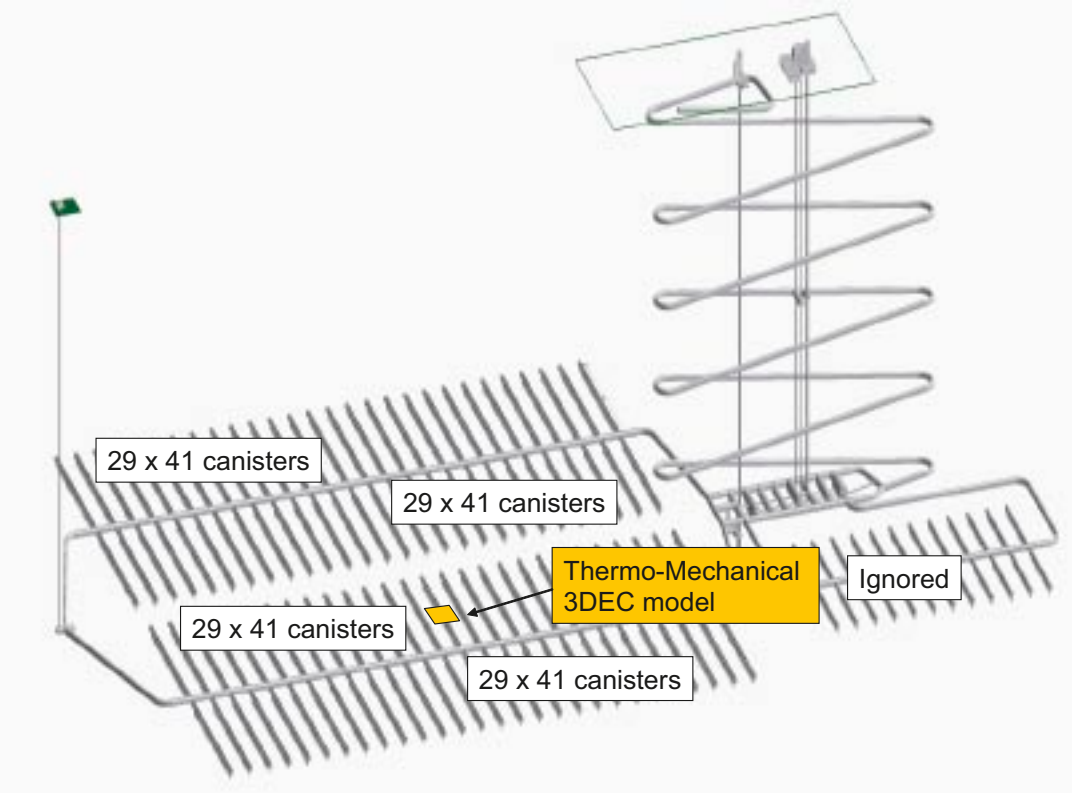

Figure 5-3. *Schematic figure of the general repository layout. The rock portion modelled in the near-field models corresponds to a rectangular area with a width across the tunnel of 40 m and length along the tunnel of 50 m. The total number of canisters in the repository was calculated based on dimensions according to Layout E /SKB 2002/.*

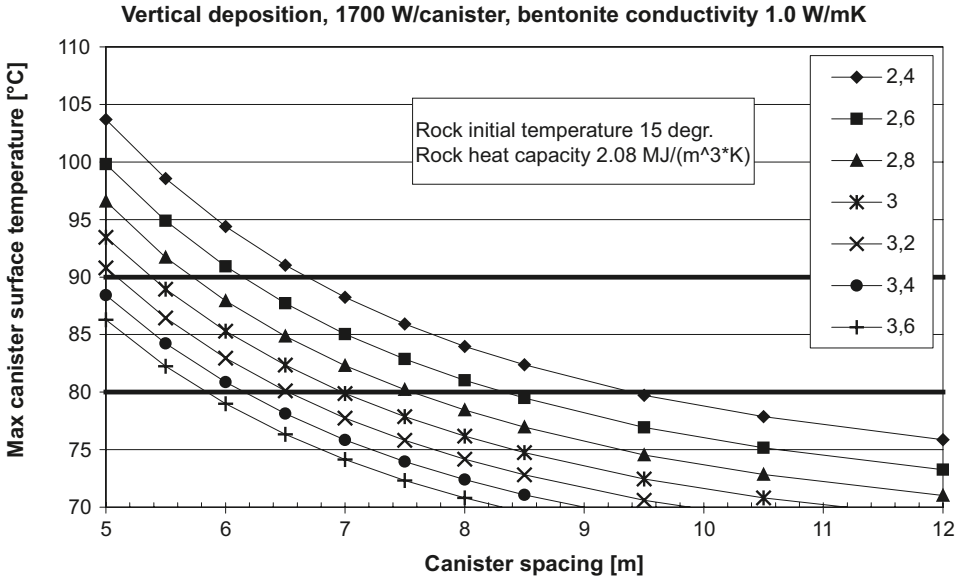

Figure 5-4. *Rule for determination of the canister spacing. The calculated canister surface temperature must not exceed 80°C. From /SKB 2004/.*

5.3.2 Tunnel scale

The geometry of the excavated openings is in accordance with Layout E /SKB 2002/, (Figure 5-5). Deposition tunnels are horse-shoe shaped, 5.5 m in height and 5.5 m wide. Deposition holes are 8 m deep and 1.75 m in diameter. Tunnel floor corners are assumed to be cut at 45° 0.5 m above the floor as shown in the right part.

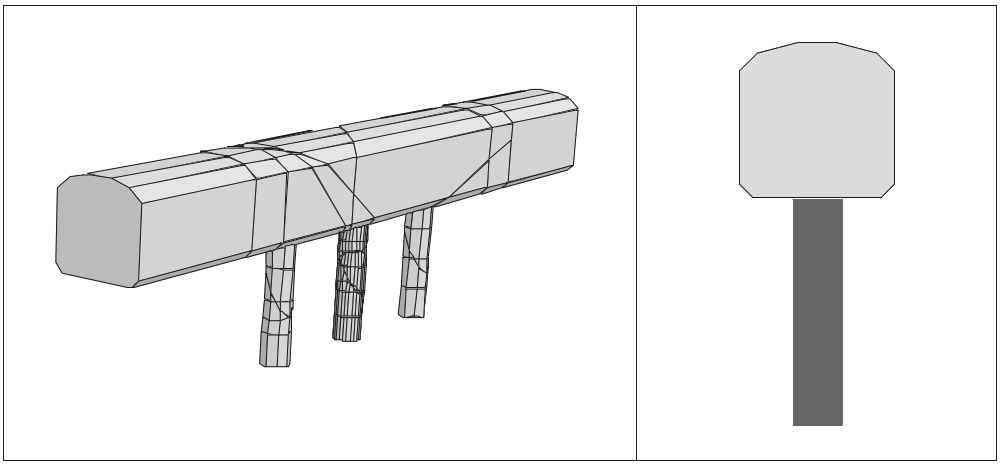

Figure 5-5. *Geometry of tunnels and deposition holes. The region analyzed here is the near-field of one deposition hole. Only the two closest neighbour holes are explicitly included in the mechanical model.*

5.4 Map of near-field models

5.4.1 General

A number of cases based on Forsmark, Simpevarp and Laxemar site data have been analyzed. The base case assumption made for all sites was to apply the material parameter values presented in Table 5-1, apply 10 MPa swelling pressure in the deposition holes and a 5 MPa pore pressure in all fractures and inside the tunnel. For Forsmark, the base case implies that the base case in situ stresses were applied and for Simpevarp, stress domain 1 in situ stresses were used (cf. Table 5-2). An alternative in situ stress state for Forsmark was also studied. This stress state applies at 400 m depth. There was also an alternative case for Simpevarp using the in situ stress state in stress domain 2.

Parameter variations regarding the fracture shear strength and thermal expansion properties have been made. To limit the number of cases, all parameters have not been varied in all models. In the Forsmark model, the fracture strength has been varied and in the Simpevarp model, a variation of the thermal expansion coefficient was made.

The pore pressure was assumed to be fully developed at the time of waste deposition. This is a simplification, which was made since it gives a possibility to distinguish between the effects of pore pressure and the thermal effects. In reality, the time scale for the re-establishment of the pore pressure in the rock mass is tens of years (see e.g. /Jaquet and Siegel 2004/). The time scale is dependent on the rock's hydraulic properties. The effect of having a slow pore pressure re-establishment was studied by analyzing cases without pore pressure. Both the pore pressure assumptions and the non-pore pressure assumption are idealizations. The non-pore pressure assumption is most relevant in the beginning of the heating phase, but after some time, the pore pressure case is the most relevant.

5.4.2 Forsmark

Table 5-3 shows a list of all the Forsmark cases. The base case was a case where all six fractures were active and pore pressure was included (*Fors 1*). An equivalent model but without pore pressure was also studied (*Fors 2*). In model *Fors 3,* only fracture #4 was active.

One uncertainty in the site data regards the fracture strength properties. To examine the effect of variations in fracture strength, two alternative values of the friction angle were tried, 27° (*Fors 6*) and 45° (*Fors 4* and *Fors 5*). In the case with 27°, the cohesion was set to 0.1 MPa.

In most models, the outer vertical boundaries were locked against normal displacements. This gives some overprediction of the induced thermal stresses (cf. Section 4.4.2). In order to examine the extent of the overprediction, the results of the two cases *Fors 8* and *Fors 9* were compared. In these two cases, only the thermal stresses were calculated. In *Fors 8,* base case mechanical boundary conditions were applied whereas in *Fors 9* the moving boundary conditions were applied.

During excavation of deposition holes, the tangential stresses at the deposition hole walls may become close to or even exceed the rock's spalling strength. These stresses will become even higher during the heated phase. In order to make a more detailed study of the stress distribution around the central deposition hole during excavation and heating, the *Fors 10* case was analyzed. To increase the accuracy of the stress-deformation analysis, this particular version of the model was specifically densely meshed in the immediate vicinity of the central deposition hole. To avoid overprediction of the thermal stresses, the same boundary condition scheme as in *Fors 9* was applied. In the *Fors 10* case there were no fractures, no swelling pressure and no pore pressure.

The alternative in situ stress state, which applies at 400 m depth (cf. Table 5-2), was analyzed in case *Fors 11*. In all other aspects, this case was identical to *Fors 1*. An elastic variant of *Fors 11* was also analyzed. This case was called *Fors 12*.

Table 5-3. List of near-field models based on Forsmark site data.

Case	Fractures	Pore pressure	Swelling pressure	Comment
Fors 1	x	x	x	Base case
Fors 2	x		x	
Fors 3	Only #4 active	x	x	
Fors 4	x	x	x	Fric angle 45°
Fors 5	x		x	Fric angle 45°
Fors 6	x	x	x	Fric angle 27°, Cohesion 0.1 MPa
Fors 7			x	Equal to Fors 2 but fully elastic
Fors 8				Elastic, no in situ stress
Fors 9				Elastic, no in situ stress, moving boundaries
Fors 10				Elastic, finer mesh around central hole, moving boundaries
Fors 11	x	x	x	Fric angle 34°, alternative stress data, 400 m depth
Fors 12			x	Equal to Fors 11 but fully elastic

5.4.3 Simpevarp

In Table 5-4, the cases based on Simpevarp data are presented. The base case for the Simpevarp model included all six fractures, swelling pressure and pore pressure (*Simp 1*). The *Simp 2* case was equal to *Simp 1* but without pore pressure. The effects of a higher thermal expansion coefficient were studied by running two cases (*Simp 3* and *Simp 4*) with alternative values of the thermal expansion coefficient (The expansion coefficient in *Simp 4* is equal to that of the Forsmark model). The *Simp 5* case is equal to *Simp 2* but without any fractures (fully elastic) and *Simp 6* is a case including fractures, swelling pressure and pore pressure but with in situ stresses according to stress domain 2 (cf. Section 5.2.3). The *Simp 7* case is equal to *Simp 6* but fully elastic.

5.4.4 Laxemar

For Laxemar, two cases were analyzed (Table 5-5). *Lax 1* is the base case for the Laxemar model. In that case all fractures were active, and pore pressure and swelling pressure were applied. The *Lax 2* case is an elastic model with no fractures active.

Table 5-4. List of near-field models based on Simpevarp site data.

Case	Fractures	Pore pressure	Swelling pressure	Comment
Simp 1	x	x	x	Base case
Simp 2	x		x	
Simp 3	x	x	x	Thermal expansion $7.0 \cdot 10^{-6}$ K^{-1}
Simp 4	x	x	x	Thermal expansion $7.7 \cdot 10^{-6}$ K^{-1}
Simp 5			x	Elastic
Simp 6	x	x	x	Stress domain 2
Simp 7			x	Elastic, Stress domain 2

Table 5-5. List of near-field models based on Laxemar site data.

Case	Fractures	Pore pressure	Swelling pressure	Comment
Lax 1	x	x	x	Base case
Lax 2			x	Elastic

6 Results

6.1 Temperatures

Figure 6-1 shows the general repository layout assumed for all sites. The near-field model (indicated with a yellow square) is located in the central part of deposition Area 1.

Figure 6-2, Figure 6-3, and Figure 6-4 show the temperature increase at the mid-height of the central deposition hole wall in the Forsmark, Simpevarp and Laxemar models, respectively. In addition to the *3DEC* results, the figures also show results obtained from independent analytical solutions. Here, the analytical solution is a superposition of solutions of the temperature field generated by time-dependent line sources /Hökmark and Fälth 2003/ and temperature fields generated by time-dependent rectangular heat sources /Claesson and Probert 1996/.

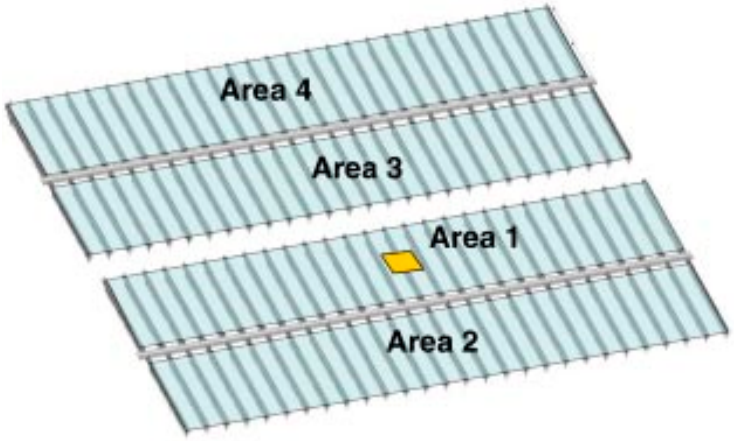

Figure 6-1. *Overview of the repository layout used in the 3DEC thermal model showing the four deposition areas. The yellow square in Area 1 indicates the location of the near-field model.*

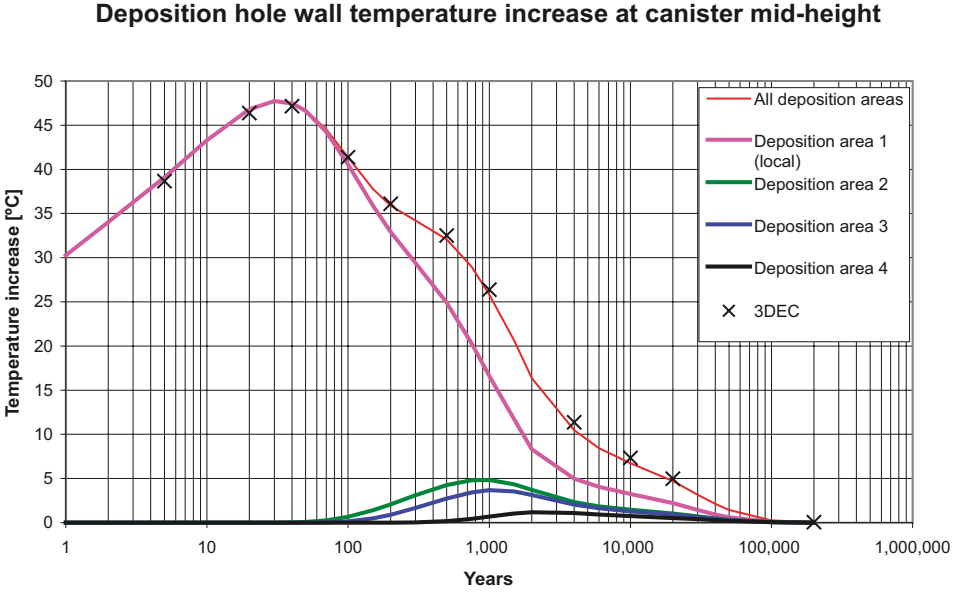

Figure 6-2. *The temperature increase at mid-height of the central deposition hole in the Forsmark model. The deposition area numbering is according to Figure 6-1. The contributions from areas other than Area 1 are relatively unimportant and do not influence the local conditions until some 100–200 years after deposition.*

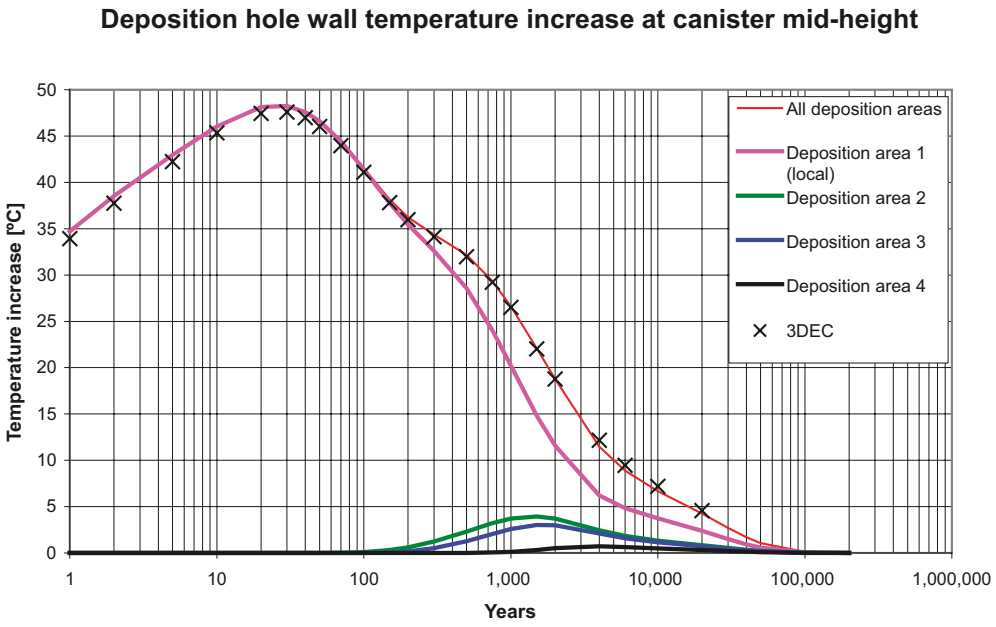

Figure 6-3. *Temperature increase at mid-height of the central deposition hole in the Simpevarp model. The deposition area numbering is according to Figure 6-1. The contributions from areas other than Area 1 are relatively unimportant and do not influence the local conditions until some 100–200 years after deposition.*

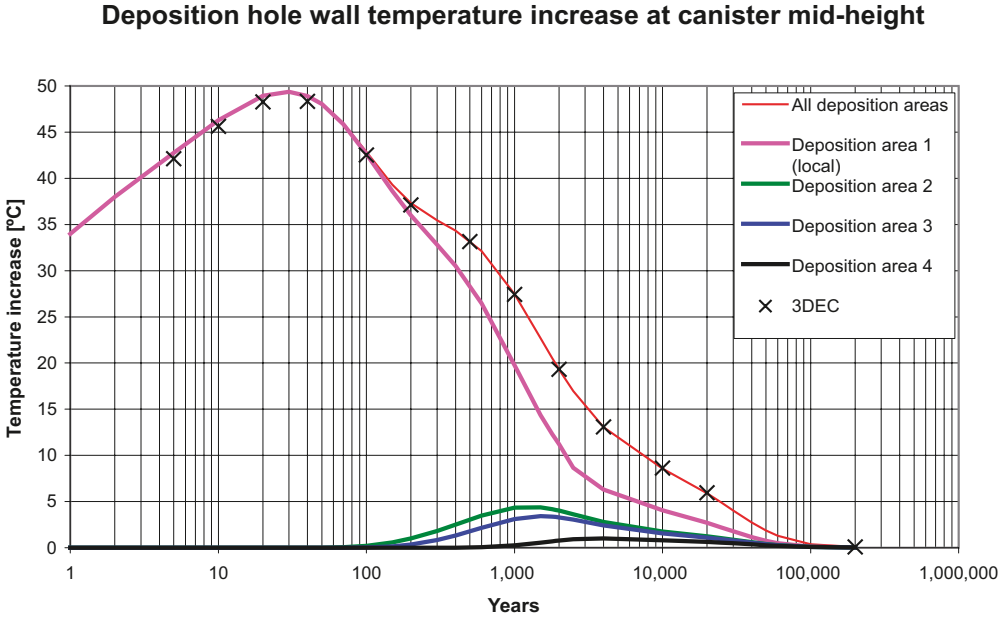

Figure 6-4. *Temperature increase at mid-height of the central deposition hole in the Laxemar model. The deposition area numbering is according to Figure 6-1. The contributions from areas other than Area 1 are relatively unimportant and do not influence the local conditions until some 100–200 years after deposition.*

The agreement between the *3DEC* results and the independent analytical solutions is good. For all three sites, the max temperature increase is 47–49°C, although the heat dissipation is much more efficient in Forsmark. This is an expected result of the different canister spacing in the models. According to the nomographic chart (Figure 5-4) and considering the low initial temperature in Forsmark, it would be possible to set the canisters even closer at that site and allow for a few degrees more of increased temperature.

For all three sites it is also clear that the contribution from deposition areas other than the local one are relatively unimportant and do not influence the local conditions until some 100–200 years after deposition.

6.2 Fracture shear displacement and fracture normal stress

6.2.1 General

The amount of fracture shear displacement and normal stress changes are important results and can be used when estimations of changes in fracture hydraulic transmissivity are made. Fracture normal stress changes and shear displacements may cause changes of fracture apertures with consequent changes in fracture transmissivity.

In Section 6.2.2 below, results from the base case models are presented. In Section 6.2.3, the sensitivity to fracture strength properties, pore pressure conditions and thermal expansion is studied.

6.2.2 Base case

In this section, fracture normal stress- and fracture shear displacement results for the *Fors 1-, Simp 1-* and *Lax 1-*cases are presented. These three cases are base cases for the Forsmark, Simpevarp and Laxemar models, respectively. In *Fors 1, Simp 1* and *Lax 1,* all fractures are active, swelling pressure is applied in the deposition holes and a 5 MPa pore pressure is applied in all fractures and in the tunnel.

The results are presented mainly as history plots of fracture shear displacements and fracture normal stress. Besides, vector plots of fracture shear displacements after 200,000 years and contour plots of normal stresses after 100 years are shown. The results are organized according to Table 6-1. Each figure shows results for one fracture.

Table 6-1. Figure reference to results.

Figure nr.	Case	Fracture number	Figure nr.	Case	Fracture number	Figure nr.	Case	Fracture number
6-5	Fors 1	1	6-11	Simp 1	1	6-17	Lax 1	1
6-6	Fors 1	2	6-12	Simp 1	2	6-18	Lax 1	2
6-7	Fors 1	3	6-13	Simp 1	3	6-19	Lax 1	3
6-8	Fors 1	4	6-14	Simp 1	4	6-20	Lax 1	4
6-9	Fors 1	5	6-15	Simp 1	5	6-21	Lax 1	5
6-10	Fors 1	6	6-16	Simp 1	6	6-22	Lax 1	6

Fracture shear displacement

The fracture shear displacements are in general larger in the Forsmark model compared to the other models. This may be explained by the higher stresses and the higher stress anisotropy assumed in the Forsmark models and by the difference in thermal volume expansion coefficient ($7.7 \cdot 10^{-6}$ K^{-1} for Forsmark; $6.2 \cdot 10^{-6}$ K^{-1} and $7.2 \cdot 10^{-6}$ K^{-1} for Simpevarp and Laxemar, respectively). Table 6-2 summarizes the maximum values found among the monitored points. For Forsmark, values obtained during the glacial cycle are given in parenthesis.

The values shown in Table 6-2 are not necessarily the absolute maximum values, which are usually found in small regions at intersections with the tunnel periphery (cf. the vector plots in following figures). The table shows that the displacements along the vertical fractures are insignificant in comparison to the displacements on the gently dipping fractures that intersect the tunnel floor and the central deposition hole.

It is clear from the vector plots of fractures #4, #5 and #6 that residual shear displacements (after 200,000 years) are significant only locally. The regions where the shear displacements exceed 3 mm do not extend more than about 1 m from the openings. One exception is the gently dipping fracture #4 in the Forsmark model. In that particular fracture, the regions where the residual shear displacements exceed 3 mm extend about 5 m from the openings (Figure 6-8, right).

The maximum residual shear displacements in fracture #4, #5 and #6 at the intersection with the openings are presented in Table 6-3. Results for the Forsmark, Simpevarp and Laxemar models are shown. The largest residual shear displacement of 6 mm is found in fracture #4 at the intersection with the tunnel in the Forsmark model.

Table 6-2. Maximum fracture shear displacement at monitored points (mm). Values obtained during glacial cycle are given in parenthesis.

Fracture number	Forsmark	Simpevarp	Laxemar
#1	0.16 (0.16)	0.095	0.28
#2	0.78 (0.95)	0.51	0.30
#3	0.92 (1.55)	0.33	0.45
#4	4.20 (4.25)	1.54	1.97
#5	1.30 (1.55)	0.72	0.27
#6	1.25 (1.75)	0.70	1.91

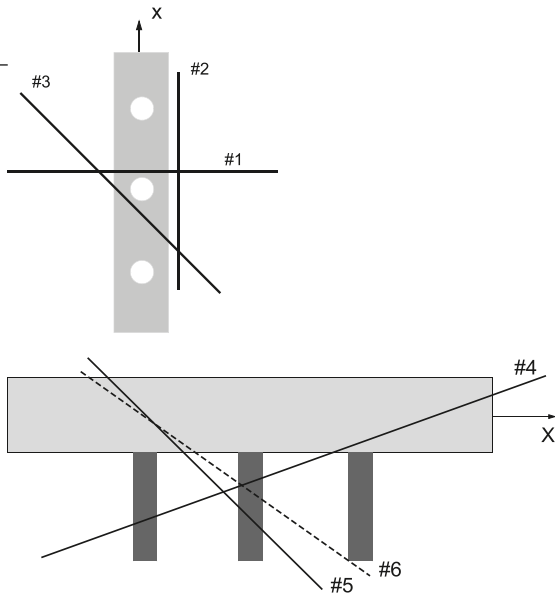

Table 6-3. Maximum residual shear displacements in fracture #4, #5 and #6 at intersection with deposition tunnel and with central deposition hole (mm).

Intersection with	Fracture #4			Fracture #5			Fracture #6		
	Forsmark	Simpevarp	Laxemar	Forsmark	Simpevarp	Laxemar	Forsmark	Simpevarp	Laxemar
Tunnel	6	3.5	3.5	2	1.5	1.5	4	1.5	4.5
Dep. hole	5	0.5	1	0.5	0.5	0.5	2	0.5	1.5

Normal stresses

Regarding the fracture normal stresses, the following can be observed:

- According to the recorded normal stress histories, the fracture normal stresses are in general of the same magnitude after heating and glaciation as they are before. This indicates that the inelastic fracture shear displacements that take place during the period of the heat load and during the glacial cycle have little importance for the end state of fracture normal stresses.
- In Fracture #2, there is a region where the normal stresses become low due to excavation and heating. This is due to the fracture's proximity to the tunnel. (Figure 6-6, Figure 6-12 and Figure 6-18). This is particular true in the Forsmark and Simpevarp models where the major principal in situ stress is sub-parallel to the strike of fracture #2.

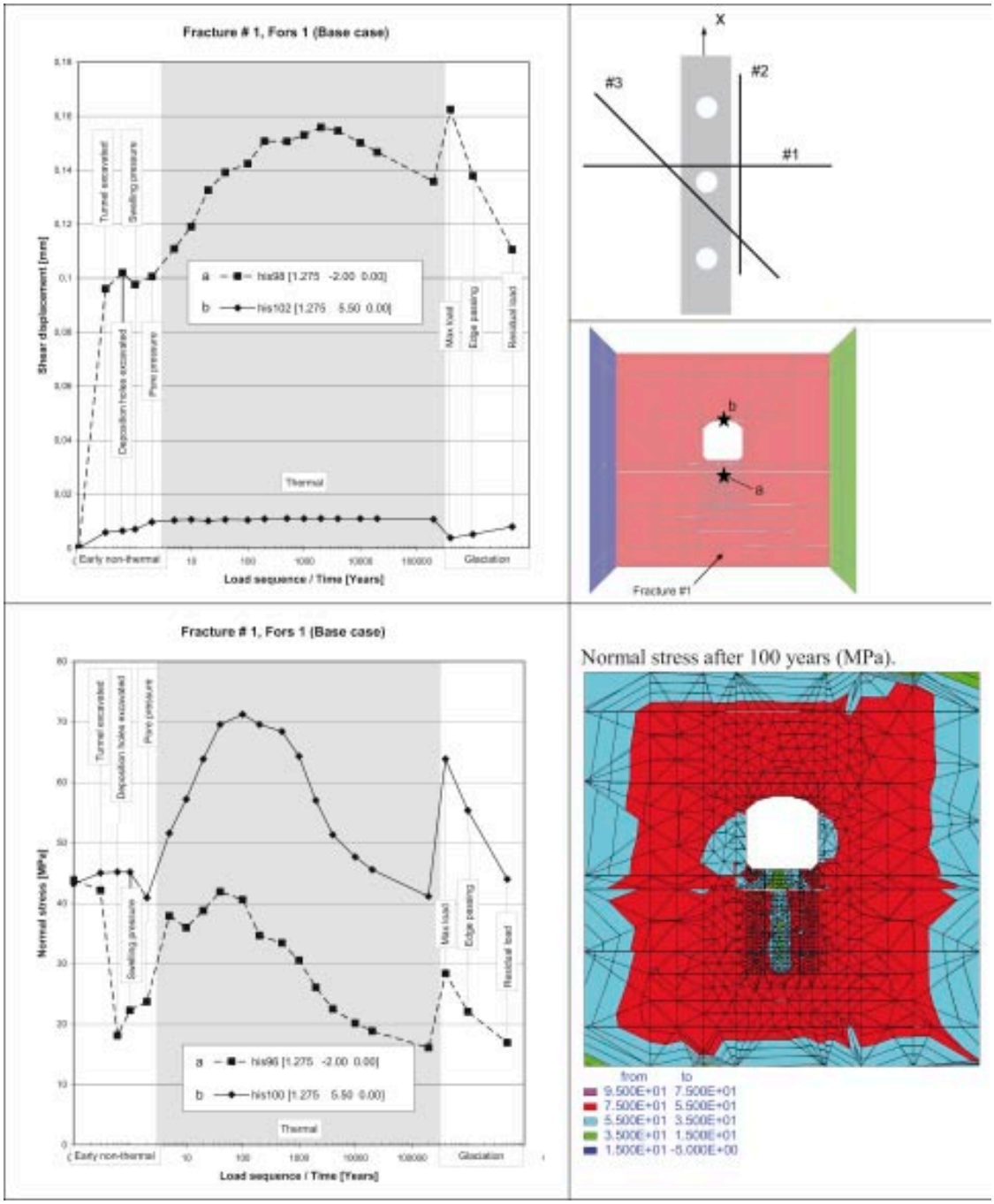

Figure 6-5. *The figure shows results from the Forsmark base case (Fors 1). The results are presented as fracture shear displacement and normal stress history plots for two points in Fracture #1. The contour plot at bottom right shows the fracture normal stress after 100 years heating.*

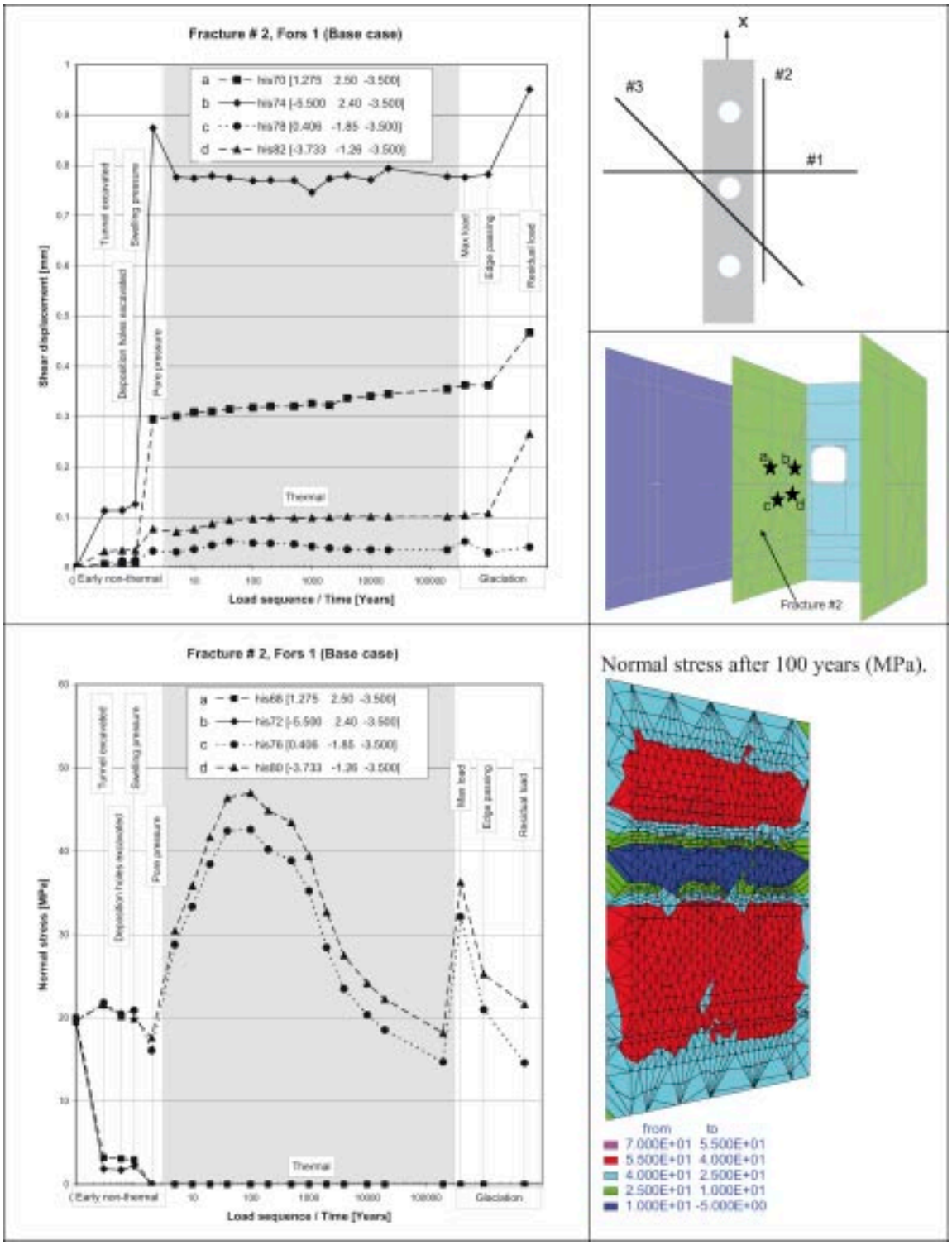

Figure 6-6. *The figure shows results from the Forsmark base case (Fors 1). The results are presented as shear displacement and normal stress history plots for some points in Fracture #2. The contour plot at bottom right shows the fracture normal stress after 100 years heating.*

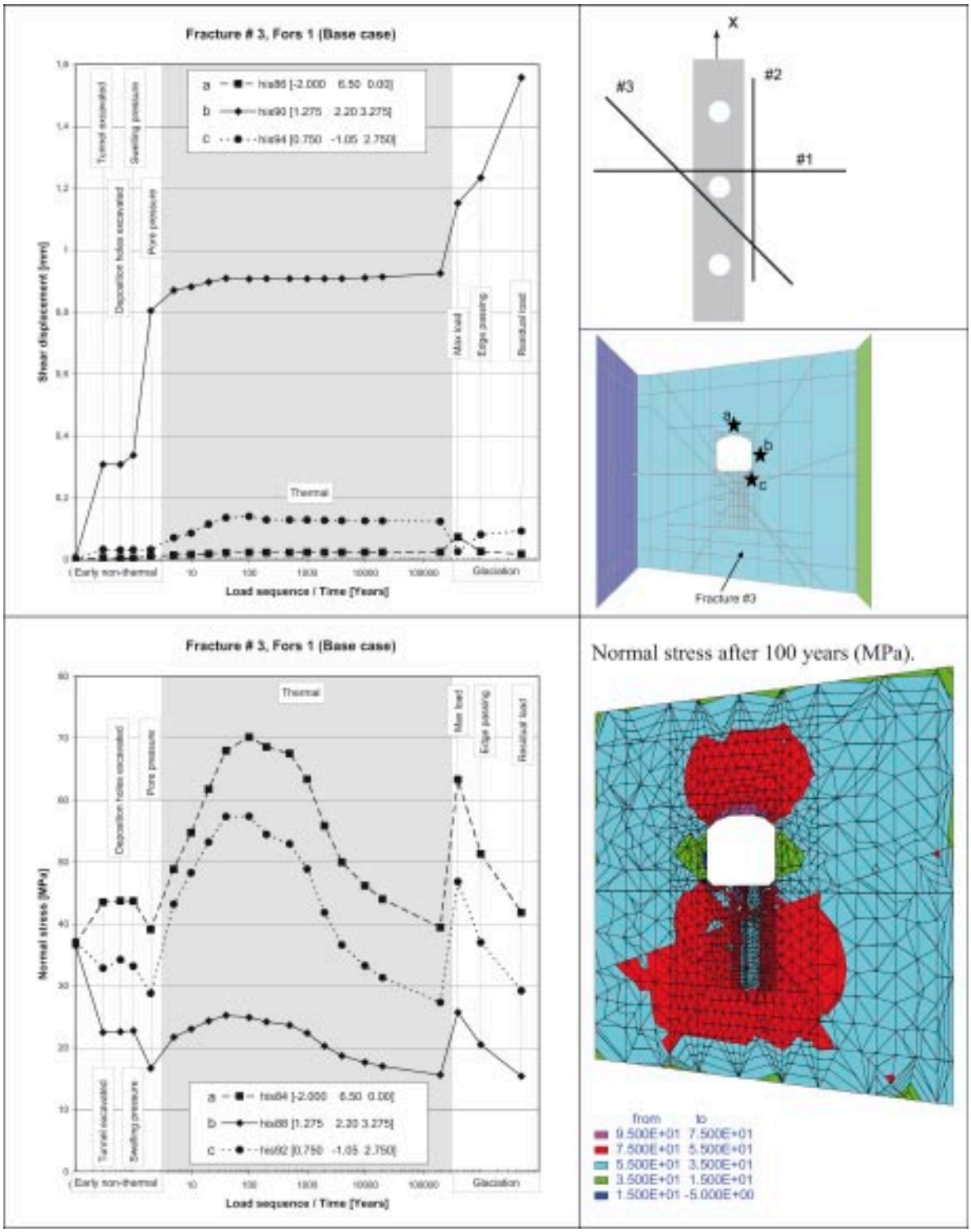

Figure 6-7. *The figure shows results from the Forsmark base case (Fors 1). The results are presented as shear displacement and normal stress history plots for some points in Fracture #3. The contour plot at bottom right shows the fracture normal stress after 100 years heating.*

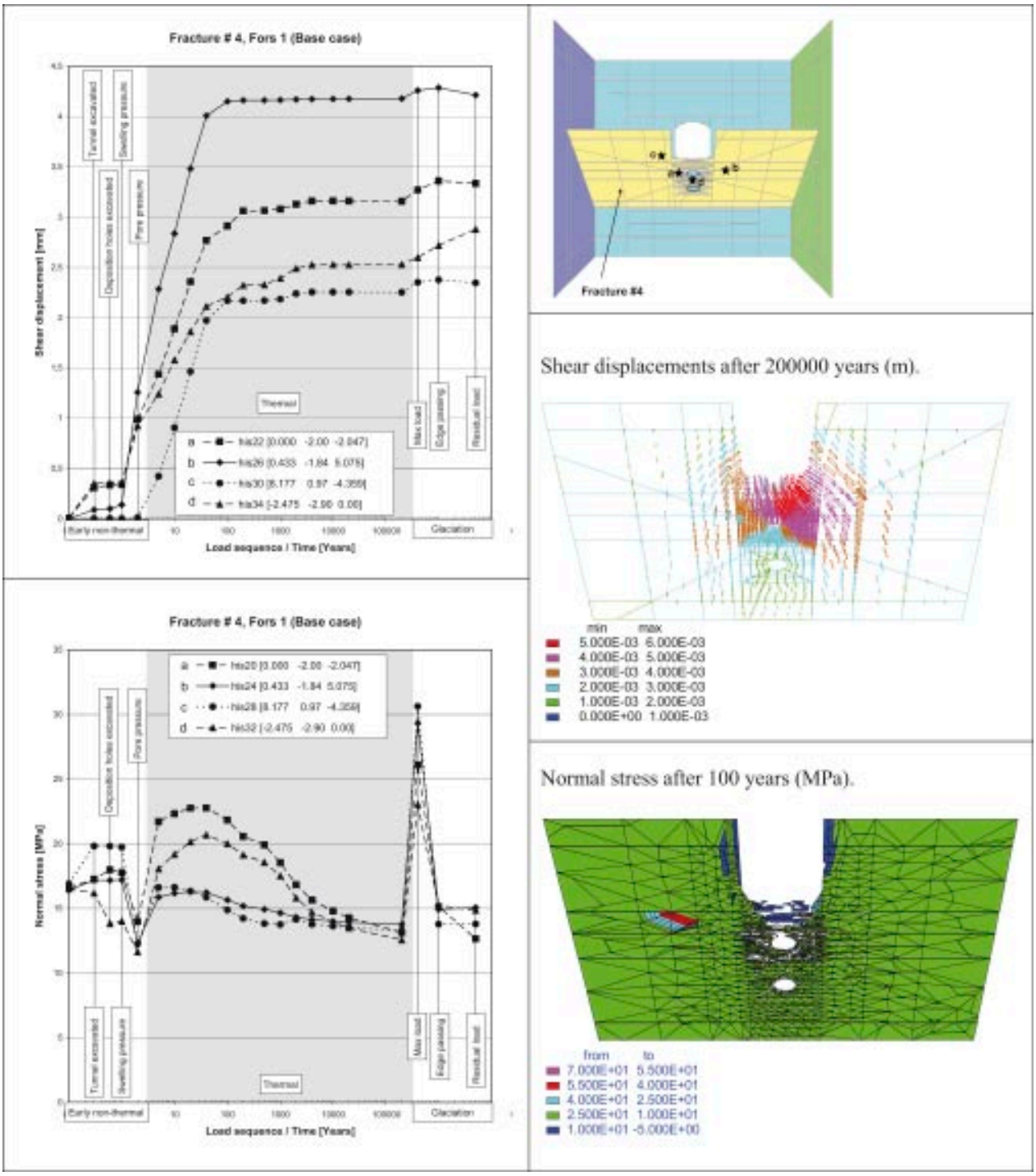

Figure 6-8. *The figure shows results from the Forsmark base case (Fors 1). The results are presented as shear displacement and normal stress history plots for some points in Fracture #4. The vector plot at middle right shows the fracture shear displacements after 200,000 years of heating. The contour plot at bottom right shows the fracture normal stress after 100 years of heating. Note: The invisible areas are due to an anomaly in 3DEC's plotting logic.*

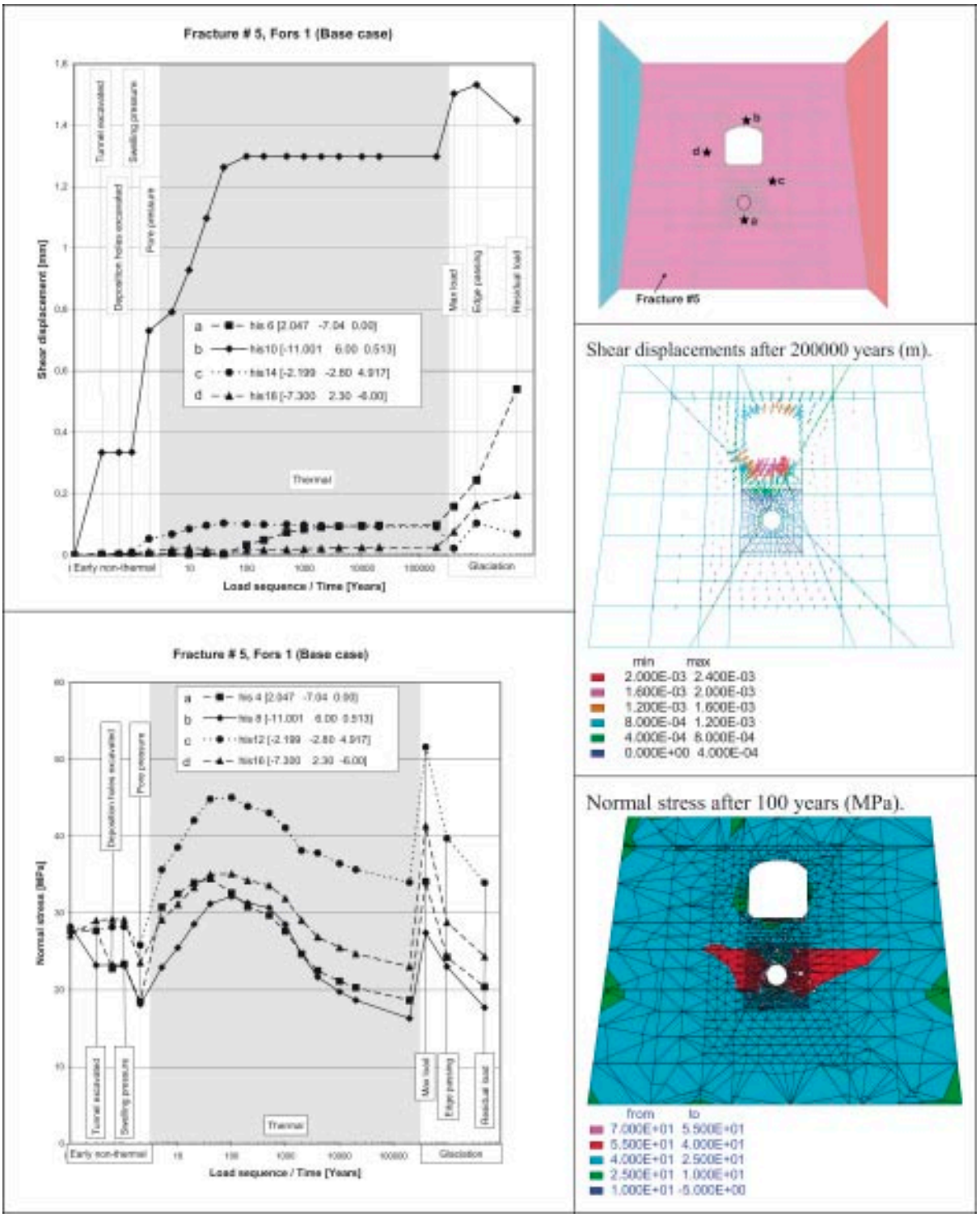

Figure 6-9. *The figure shows results from the Forsmark base case (Fors 1). The results are presented as shear displacement and normal stress history plots for some points in Fracture #5. The vector plot at middle right shows the fracture shear displacements after 200,000 years of heating. The contour plot at bottom right shows the fracture normal stress after 100 years heating.*

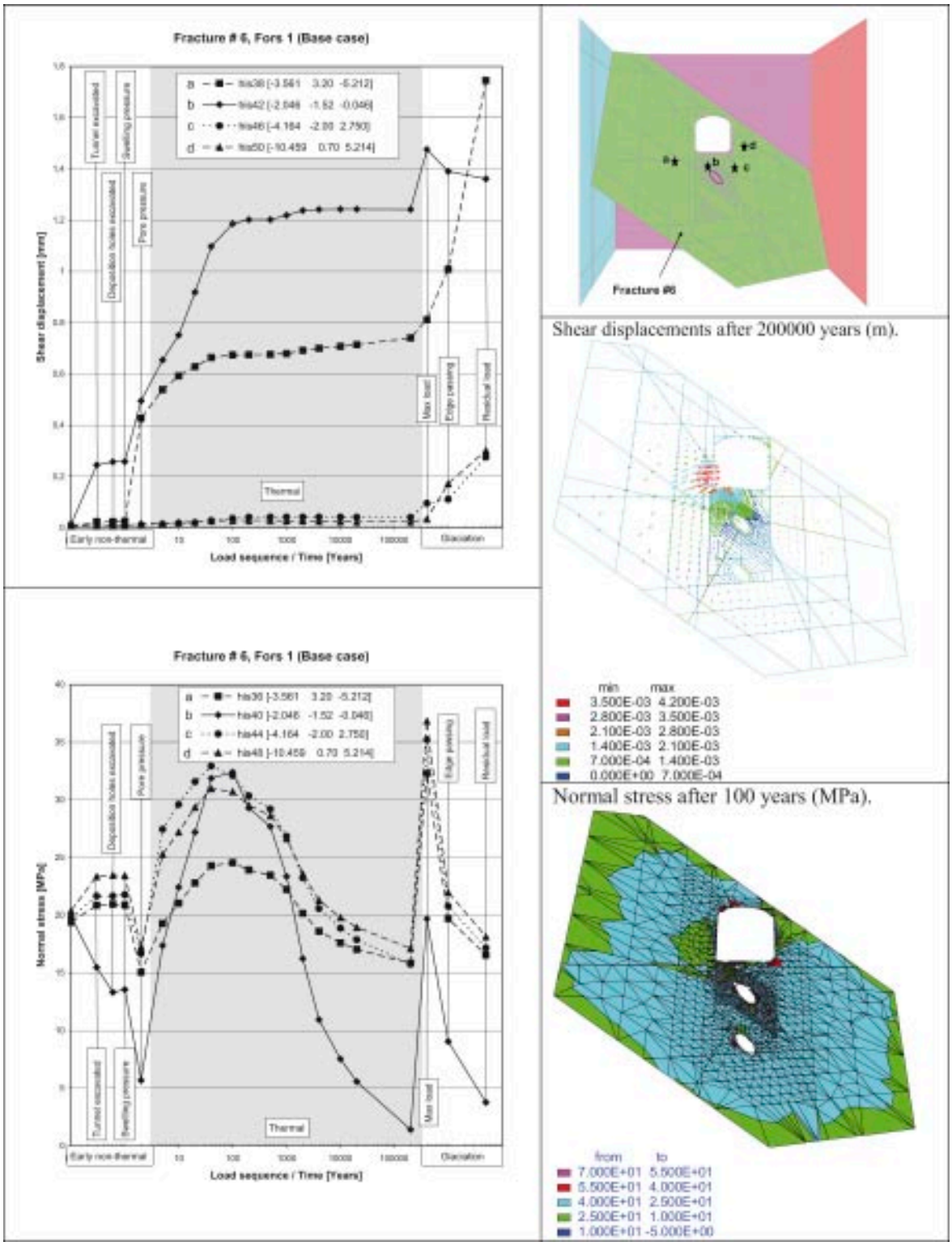

Figure 6-10. *The figure shows results from the Forsmark base case (Fors 1). The results are presented as shear displacement and normal stress history plots for some points in Fracture #6. The vector plot at middle right shows the fracture shear displacements after 200,000 years of heating. The contour plot at bottom right shows the fracture normal stress after 100 years heating.*

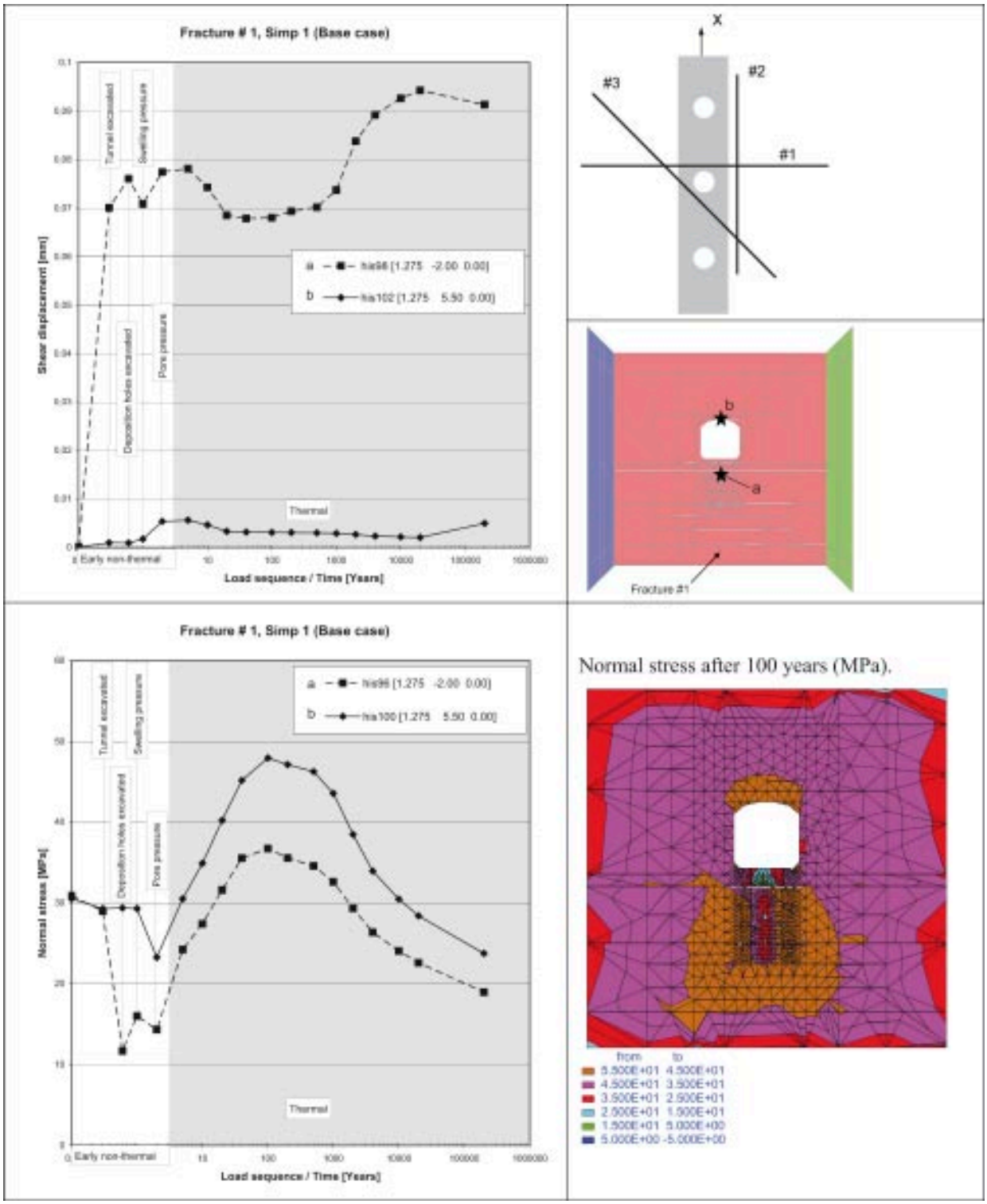

Figure 6-11. *The figure shows results from the Simpevarp base case (Simp 1). The results are presented as shear displacement and normal stress history plots for two points in Fracture #1. The contour plot at bottom right shows the fracture normal stress after 100 years heating.*

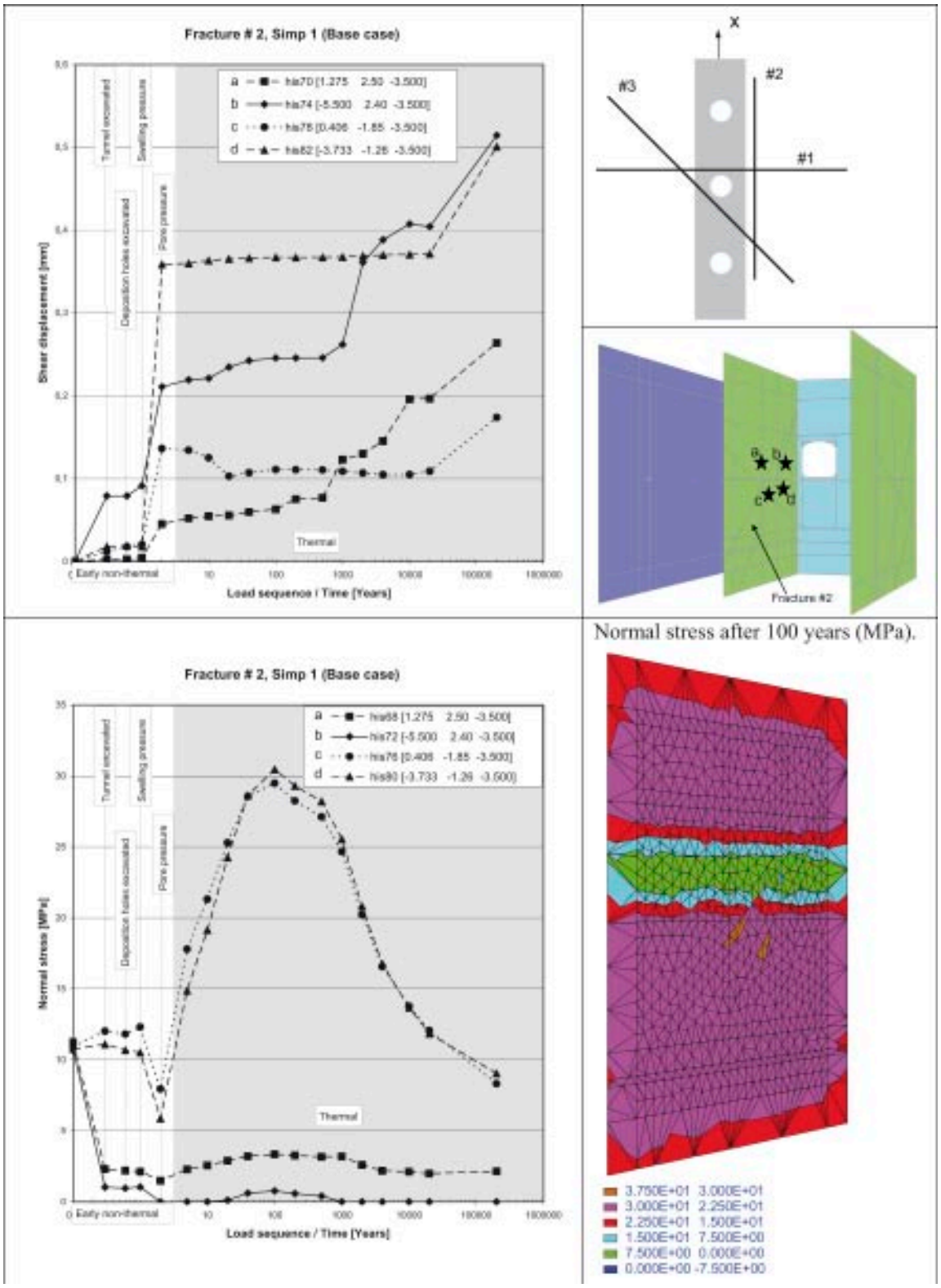

Figure 6-12. *The figure shows results from the Simpevarp base case (Simp 1). The results are presented as shear displacement and normal stress history plots for some points in Fracture #2. The contour plot at bottom right shows the fracture normal stress after 100 years heating.*

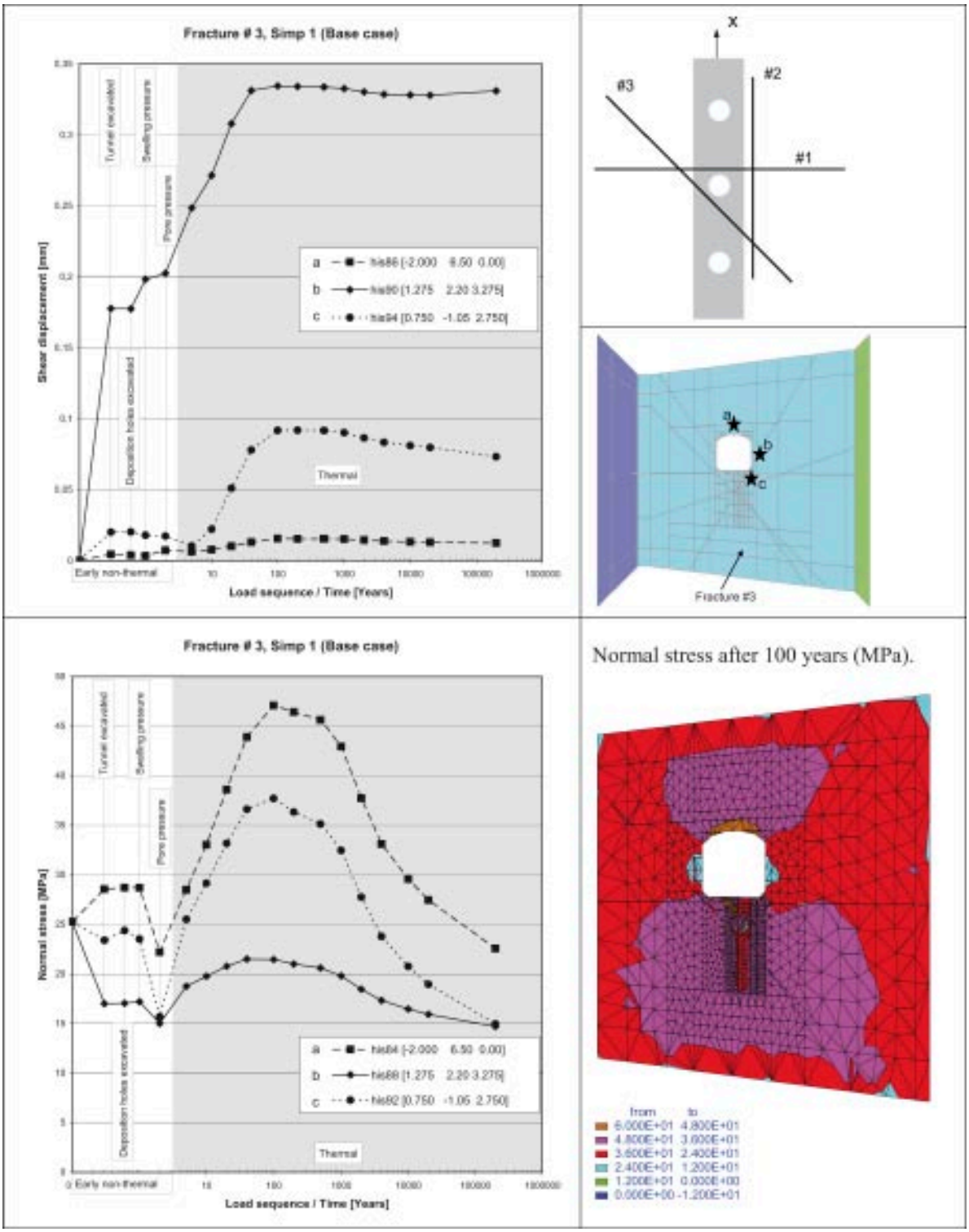

Figure 6-13. *The figure shows results from the Simpevarp base case (Simp 1). The results are presented as shear displacement and normal stress history plots for some points in Fracture #3. The contour plot at bottom right shows the fracture normal stress after 100 years heating.*

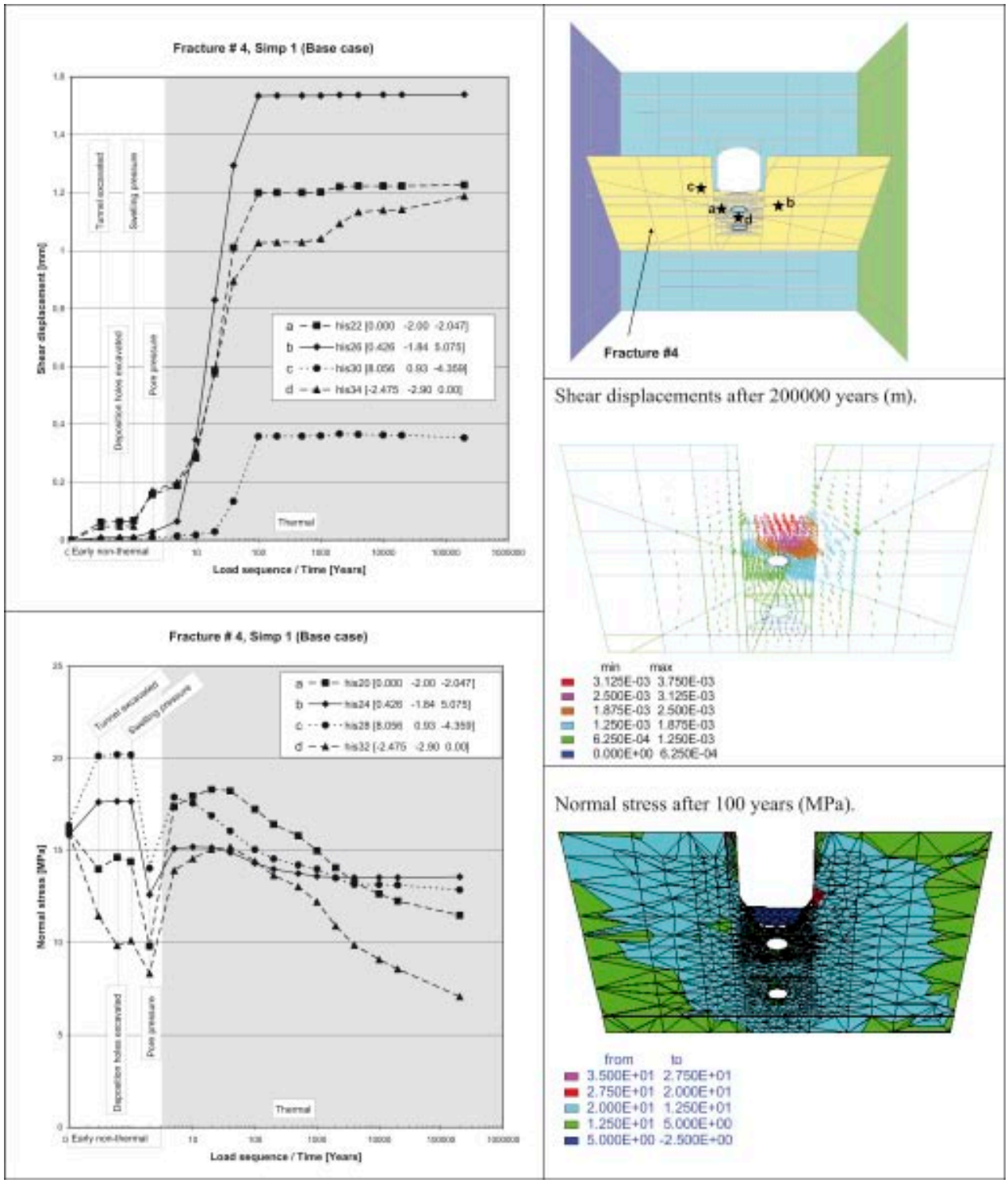

Figure 6-14. *The figure shows results from the Simpevarp base case (Simp 1). The results are presented as shear displacement and normal stress history plots for some points in Fracture #4. The vector plot at middle right shows the fracture shear displacements after 200,000 years of heating. The contour plot at bottom right shows the fracture normal stress after 100 years heating.*

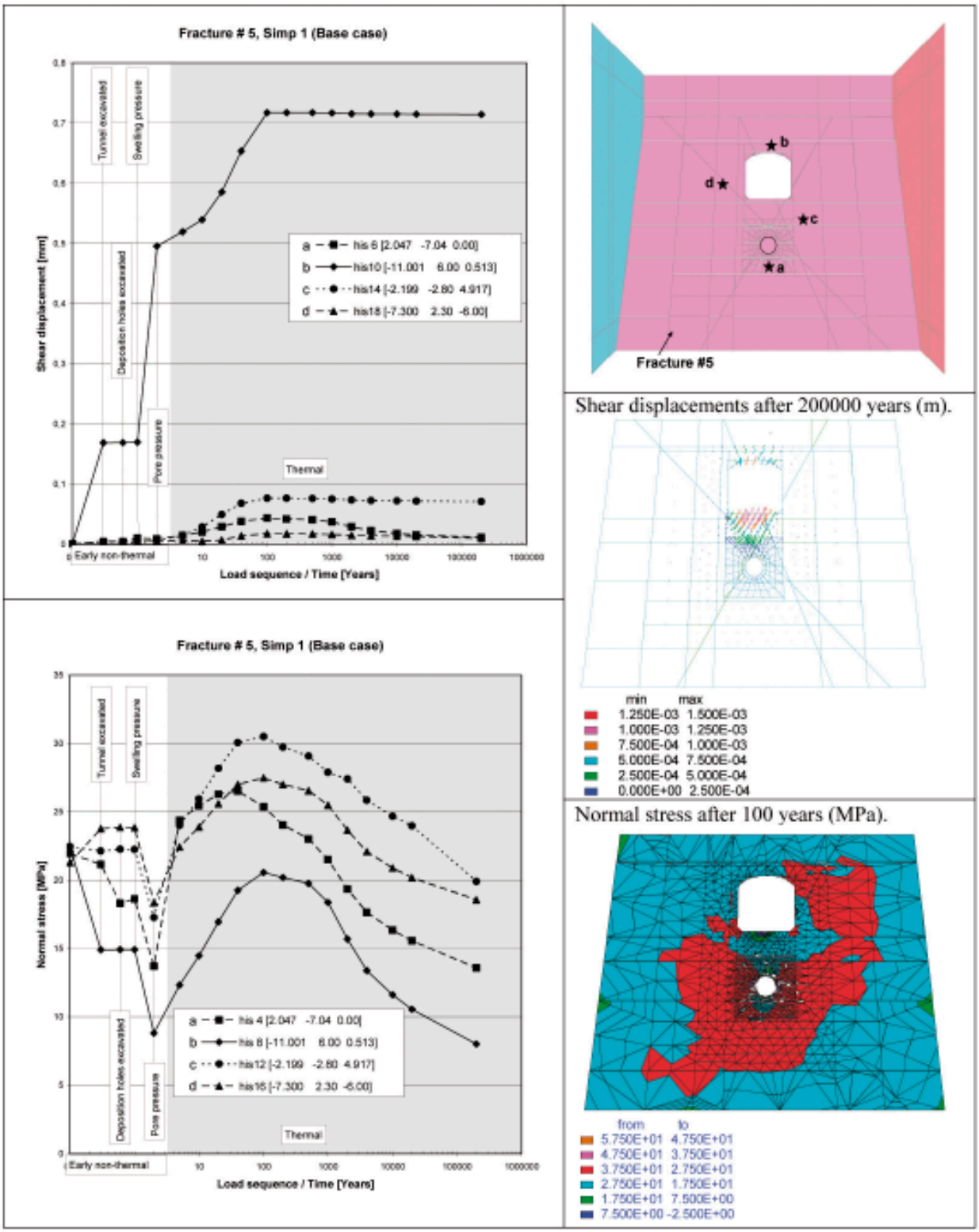

Figure 6-15. *The figure shows results from the Simpevarp base case (Simp 1). The results are presented as shear displacement and normal stress history plots for some points in Fracture #5. The vector plot at middle right shows the fracture shear displacements after 200,000 years of heating. The contour plot at bottom right shows the fracture normal stress after 100 years heating.*

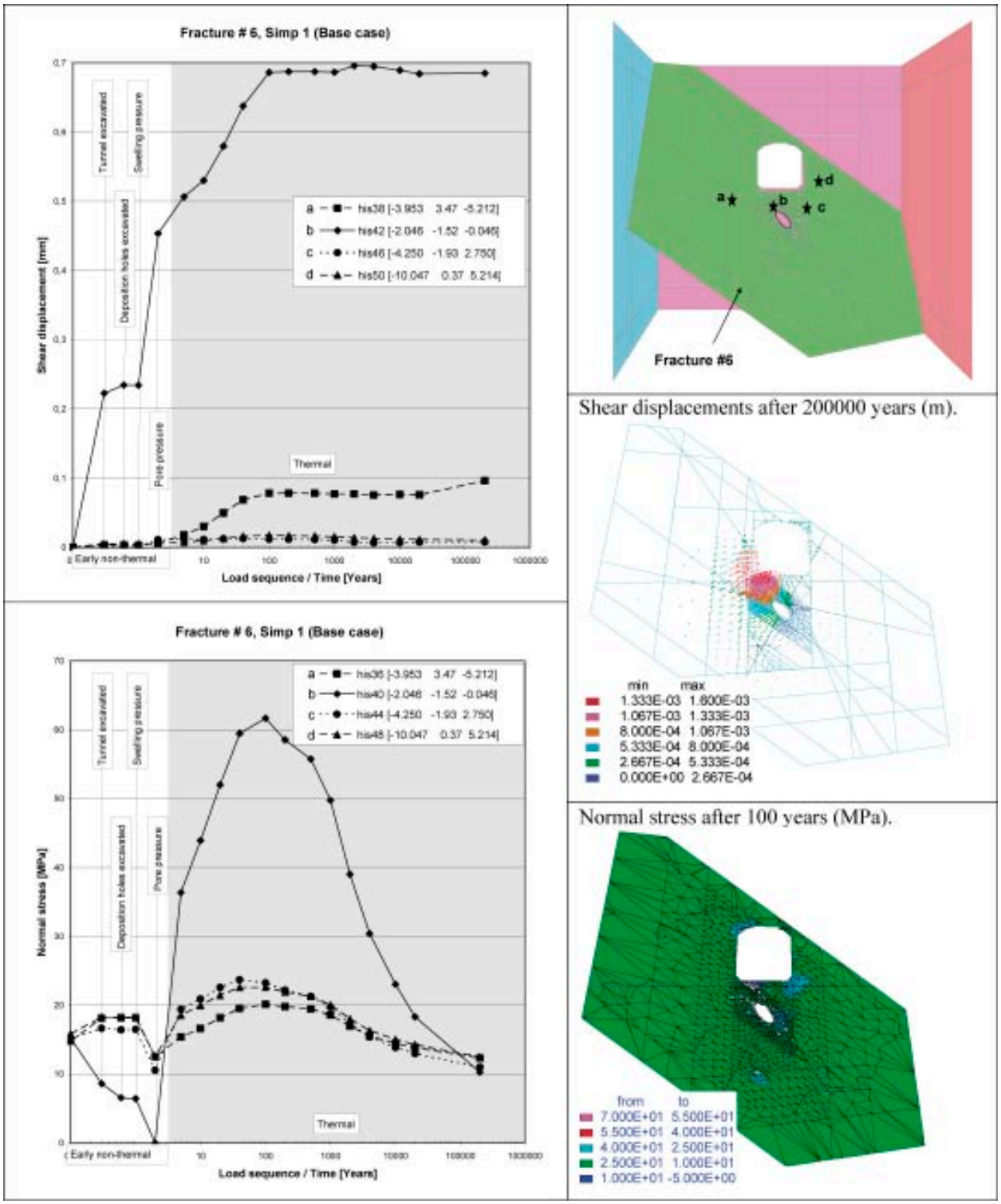

Figure 6-16. *The figure shows results from the Simpevarp base case (Simp 1). The results are presented as shear displacement and normal stress history plots for some points in Fracture #6. The vector plot at middle right shows the fracture shear displacements after 200,000 years of heating. The contour plot at bottom right shows the fracture normal stress after 100 years heating.*

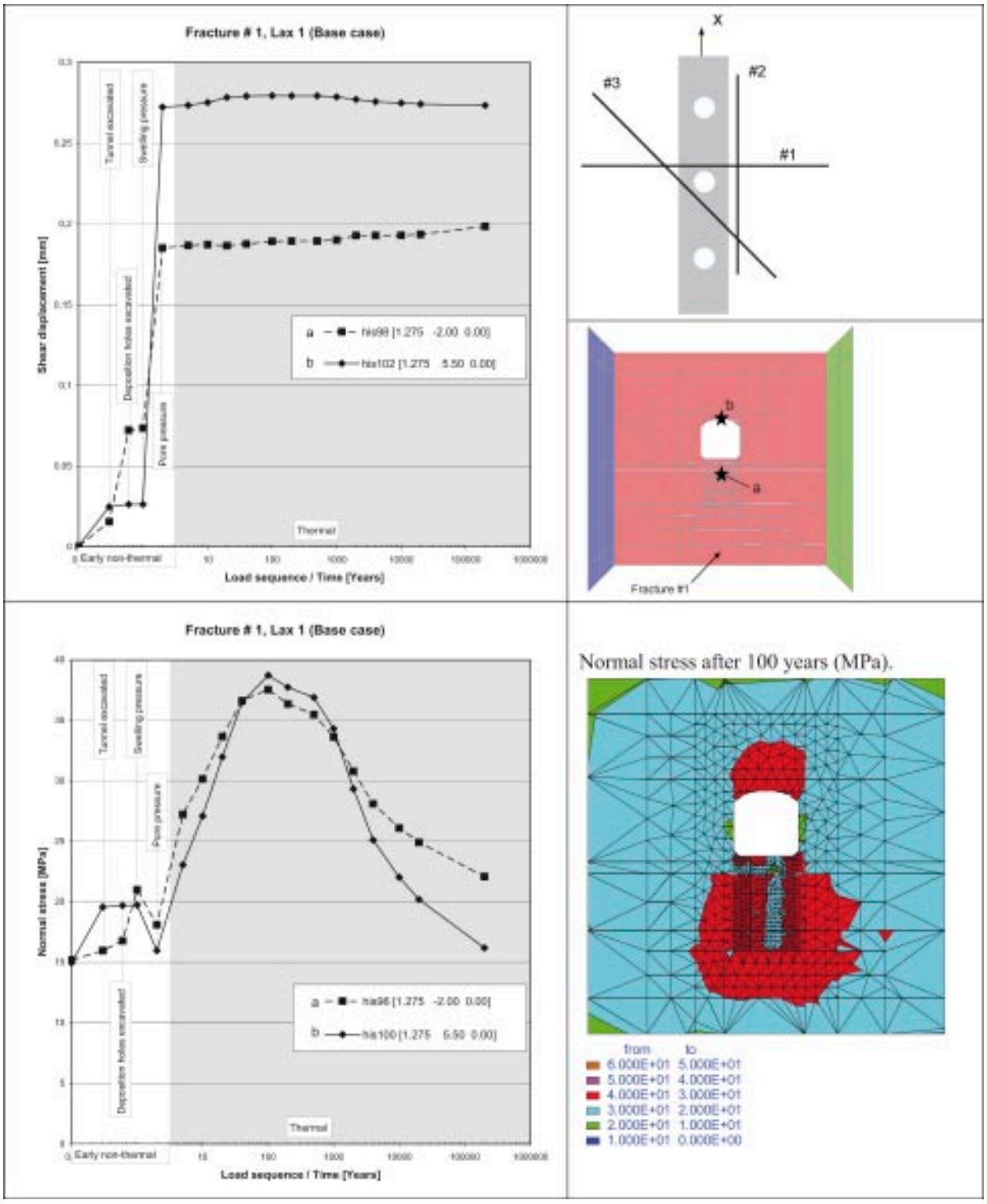

Figure 6-17. *The figure shows results from the Laxemar base case (Lax 1). The results are presented as shear displacement and normal stress history plots for two points in Fracture #1. The contour plot at bottom right shows the fracture normal stress after 100 years heating.*

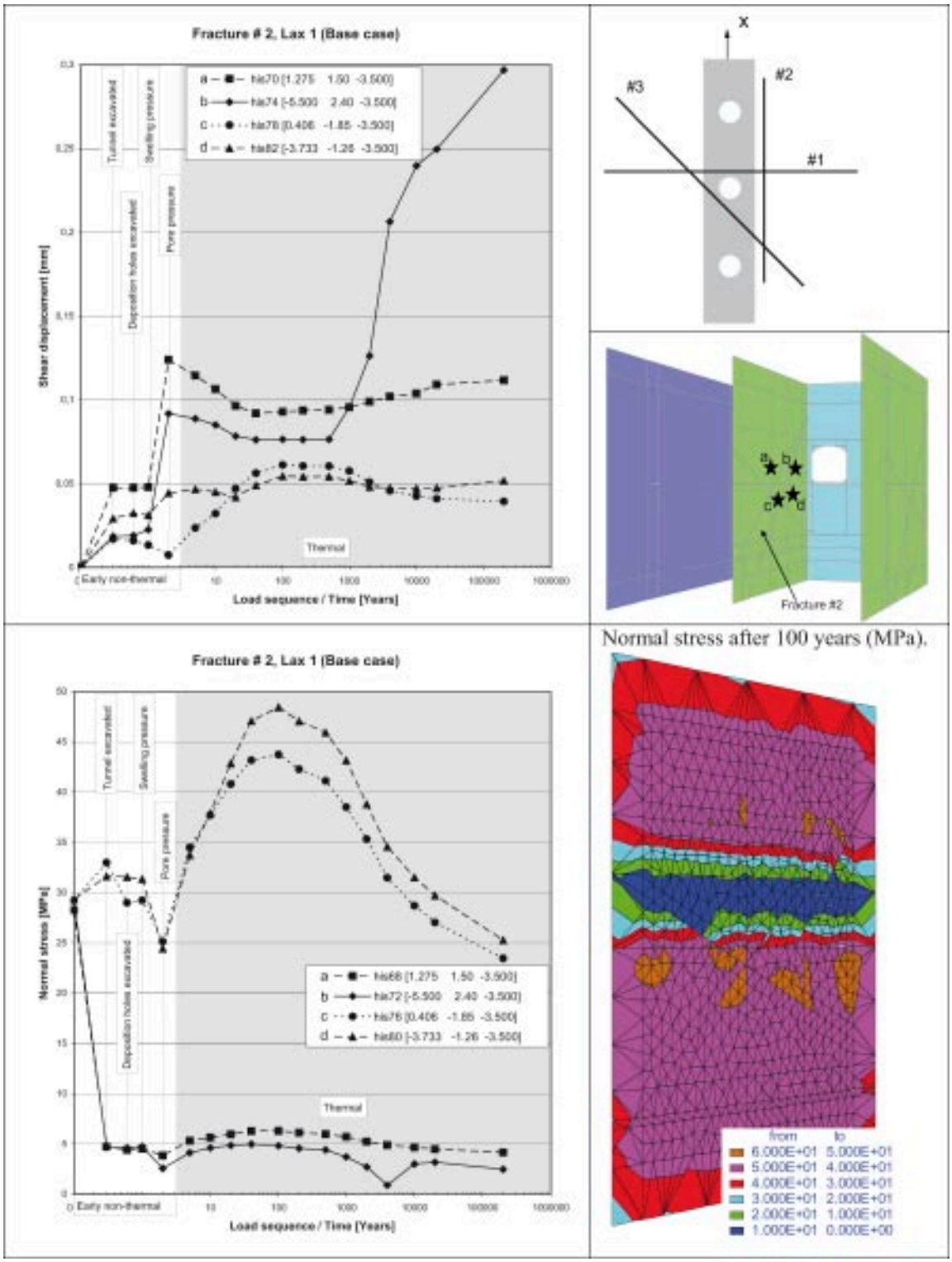

Figure 6-18. *The figure shows results from the Laxemar base case (Lax 1). The results are presented as shear displacement and normal stress history plots for some points in Fracture #2. The contour plot at bottom right shows the fracture normal stress after 100 years heating.*

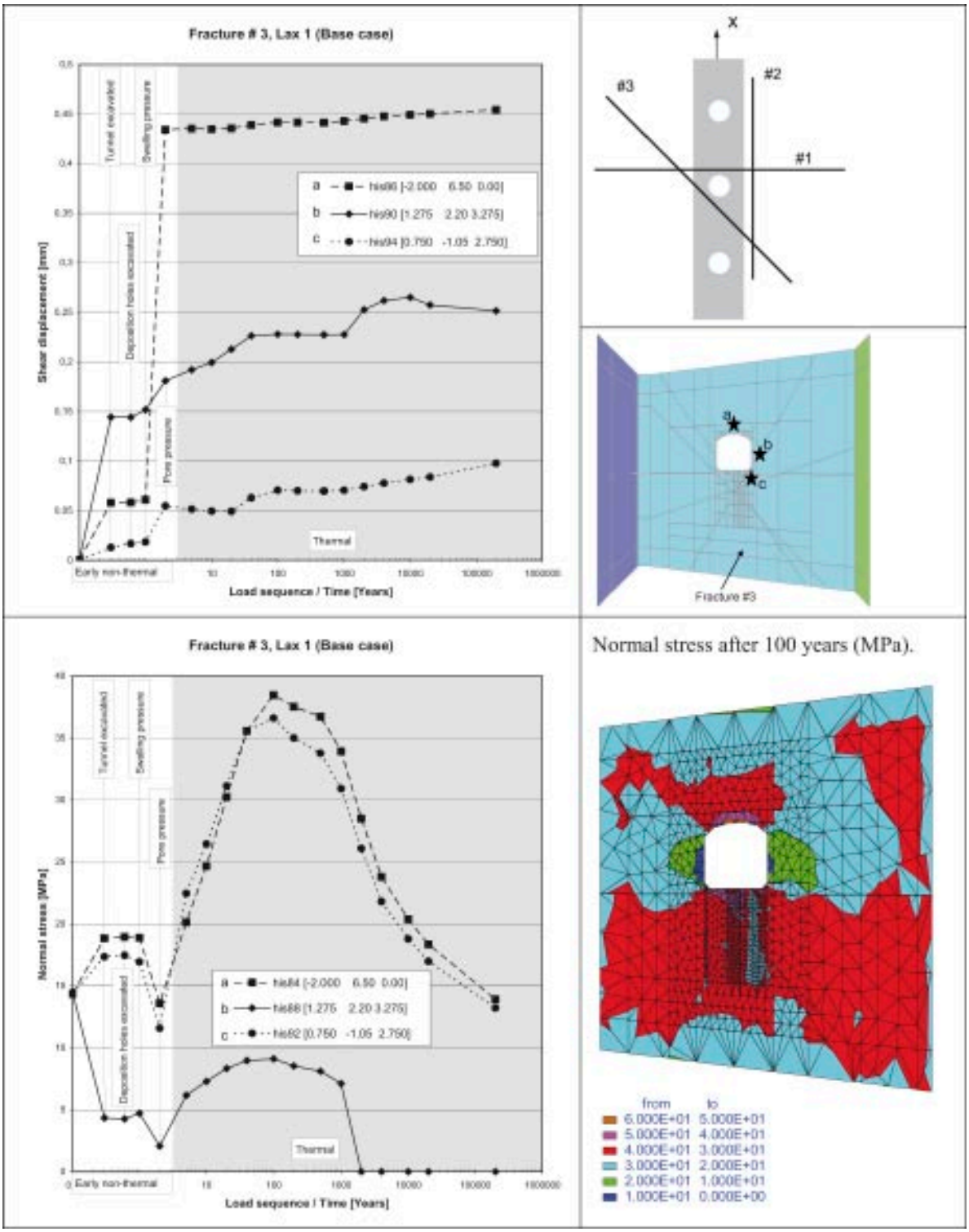

Figure 6-19. *The figure shows results from the Laxemar base case (Lax 1). The results are presented as shear displacement and normal stress history plots for some points in Fracture #3. The contour plot at bottom right shows the fracture normal stress after 100 years heating.*

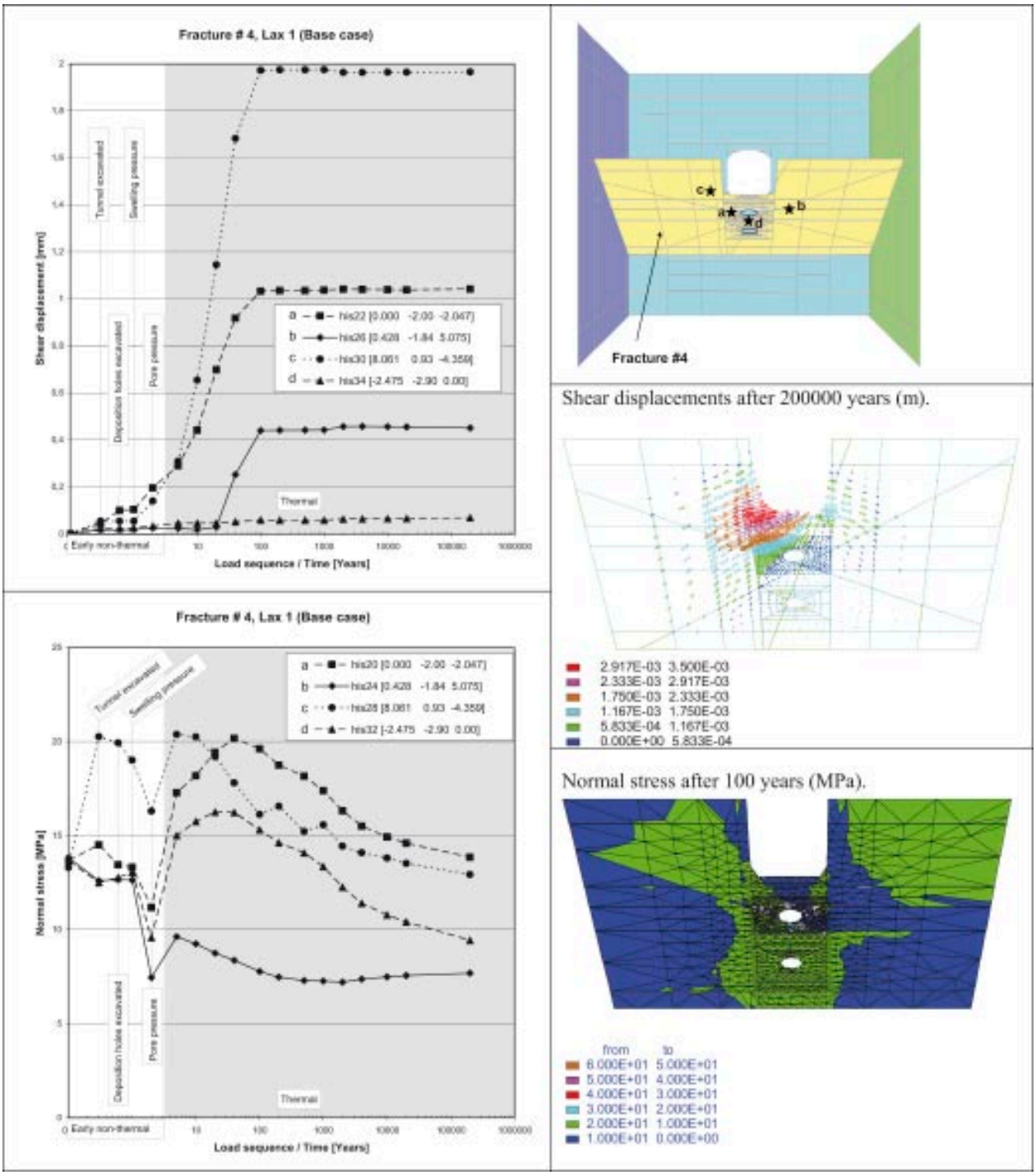

Figure 6-20. *The figure shows results from the Laxemar base case (Lax 1). The results are presented as shear displacement and normal stress history plots for some points in Fracture #4. The vector plot at middle right shows the fracture shear displacements after 200,000 years of heating. The contour plot at bottom right shows the fracture normal stress after 100 years heating.*

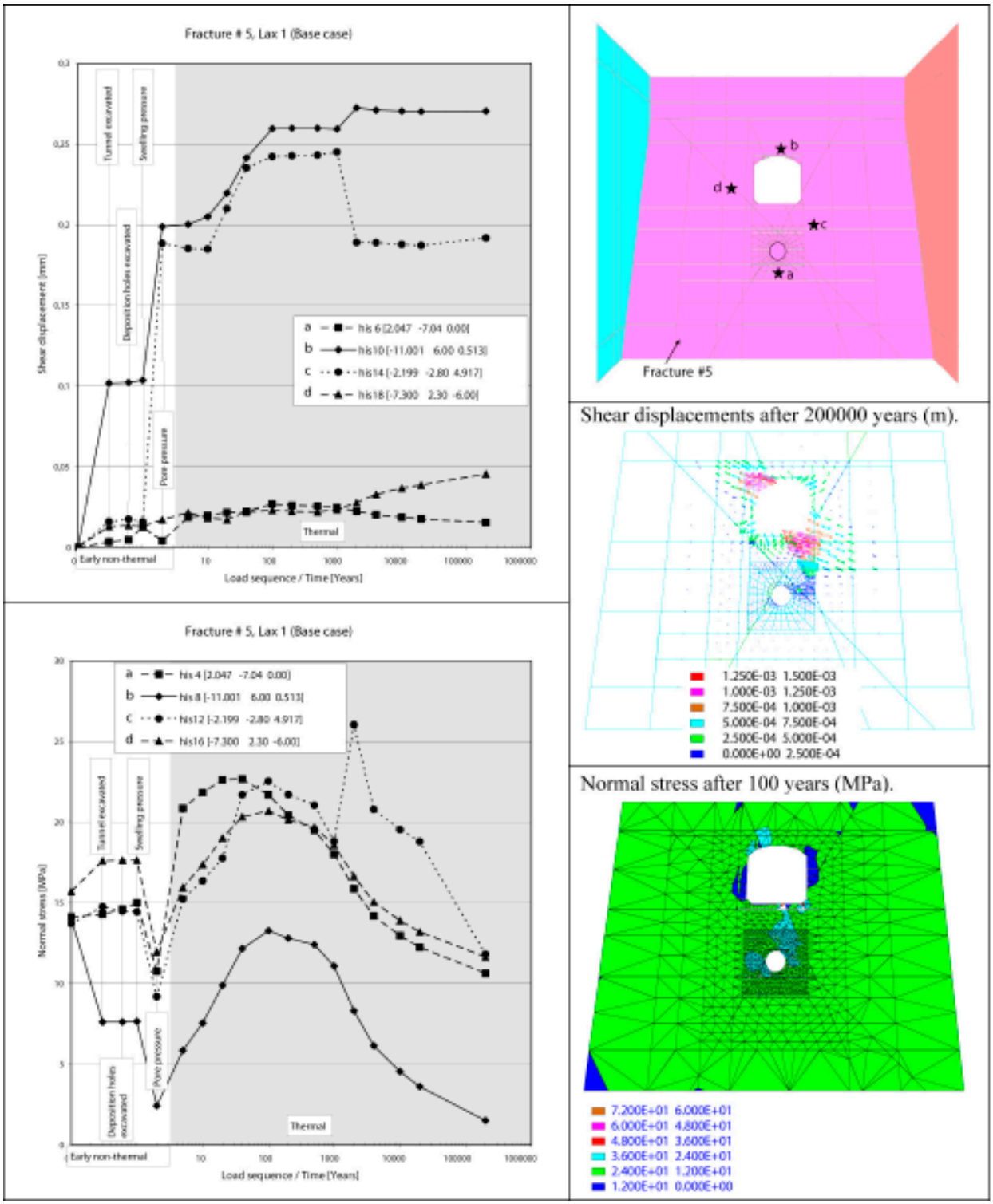

Figure 6-21. *The figure shows results from the Laxemar base case (Lax 1). The results are presented as shear displacement and normal stress history plots for some points in Fracture #5. The vector plot at middle right shows the fracture shear displacements after 200,000 years of heating. The contour plot at bottom right shows the fracture normal stress after 100 years heating.*

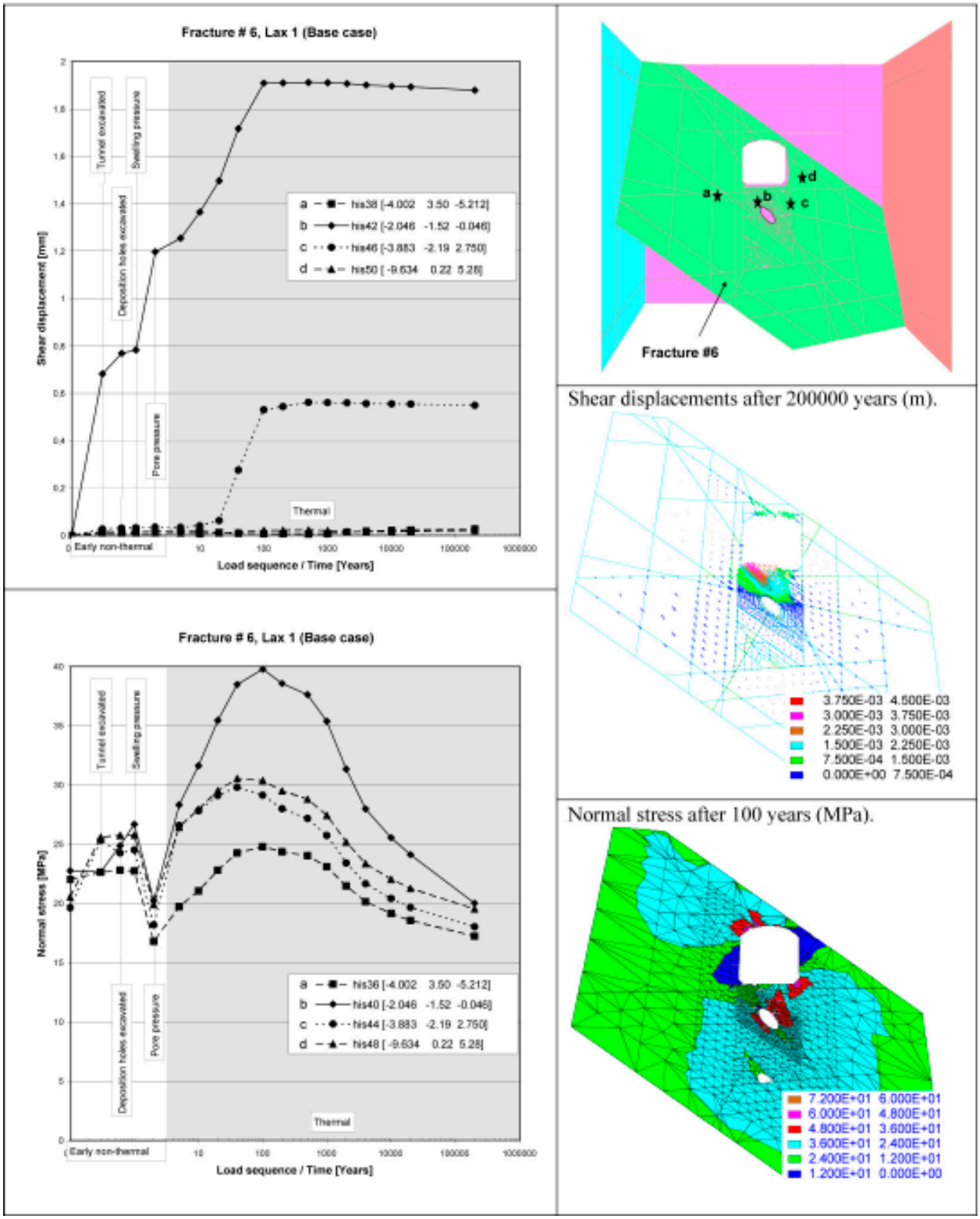

Figure 6-22. *The figure shows results from the Laxemar base case (Lax 1). The results are presented as shear displacement and normal stress history plots for some points in Fracture #6. The vector plot at middle right shows the fracture shear displacements after 200,000 years of heating. The contour plot at bottom right shows the fracture normal stress after 100 years heating.*

6.2.3 Sensitivity to fracture strength, pore pressure and in situ stress state

A number of alternative cases were analyzed in addition to the base case models discussed in the previous section. These cases were analyzed in order to study the influence of pore pressure, fracture strength and the in situ stress state on the fracture shear displacements and normal stresses. Fracture shear displacement and normal stress results from the alternative cases are presented and compared with results from the corresponding base case models (*Fors 1* and *Simp 1*). Results regarding four history points in fracture #4, #5 and #6 are used for the comparison.

In order to limit the number of calculation cases, the same parameters have not been varied both in the Forsmark model and in the Simpevarp model. In the Forsmark model, different fracture friction angles were tried whereas in the Simpevarp model, the thermal expansion coefficient was varied.

In the Forsmark model, two alternative values of the friction angle have been applied (27° and 45°). There is one case where only fracture #4 was active and in two cases no pore pressure was applied. In addition, there is one case where the base case assumptions were used (34° friction angle and with account of pore pressure) together with the alternative in situ stress state.

In the Simpevarp model, there is one case without pore pressure and two cases where alternative values of the rock thermal expansion coefficient were used. The highest expansion coefficient value ($7.7 \cdot 10^{-6}$ K^{-1}) is the same as in the Forsmark model. There is also a case where the in situ stresses were set according to stress domain 2.

Fracture shear displacement

Fracture shear displacement results from the Forsmark and Simpevarp cases are presented in Figure 6-23 and Figure 6-24, respectively. The following observations can be made:

- The presence of pore pressure has a significant effect on the fracture shear displacement. The cases with no pore pressure show significantly smaller amounts of displacement compared to the pore pressure cases (about 40–90% reduction). However, the zero pore pressure assumption is most relevant for early times and for situations where the time scale for the reestablishment of the in situ pore pressure conditions is long. For later times, when the in situ pore pressure situation in the repository rock mass has been re-established, the pore pressure case will be the most relevant. The time scale for pore pressure reestablishment is dependent on the rock's hydraulic properties.
- The variations of the fracture strength (friction angle) give significant variations of the shear displacement (Figure 6-23). The history point in fracture #5 shows an increase in the shear displacement of about 20 times (from 0.1 mm to 2 mm) when the friction angle is reduced from 34° to 27° (case *Fors 1* and *Fors 6*), and at point b in fracture #6, the same friction angle reduction gives a doubled displacement. Correspondingly, there are significant reductions of the displacements in fracture #4, point b when the friction angle is increased from 34° to 45°. (from 4 mm (*Fors 1*) to 2 mm (*Fors 4*); from 2.5 mm (*Fors 2*) to 0.1 mm (*Fors 5*)).
- The shear displacements in the *Fors 3* case (only fracture #4 active) are of the same magnitude as in the *Fors 1* case (Figure 6-23, upper left). Since the model includes only few fractures which thus influence each other to a limited extent, this is a reasonable result.
- The variation of the thermal expansion coefficient has some influence on the results (Figure 6-24). The fracture #4 point displaces about 2.1 mm in the *Simp 4* case, whereas the displacement is about 1.5 mm in *Simp 1*. However, *Simp 4* could also be compared with *Fors 1* (base case in the Forsmark model), which has the same thermal expansion coefficient value. In *Fors 1*, the shear displacement at the same point is yet larger, about 4.2 mm (Figure 6-23, upper left). This can probably be explained by the larger stress anisotropy found in the Forsmark model. These results indicate that, during the present conditions, the difference in in situ stress state has larger importance for the fracture shear displacement than the difference in thermal expansion.
- Just like in the *Simp 1* case (stress domain 1), the fracture shear displacements in the *Simp 6* case (stress domain 2) are small, i.e. below about 1.5 mm (Figure 6-24).

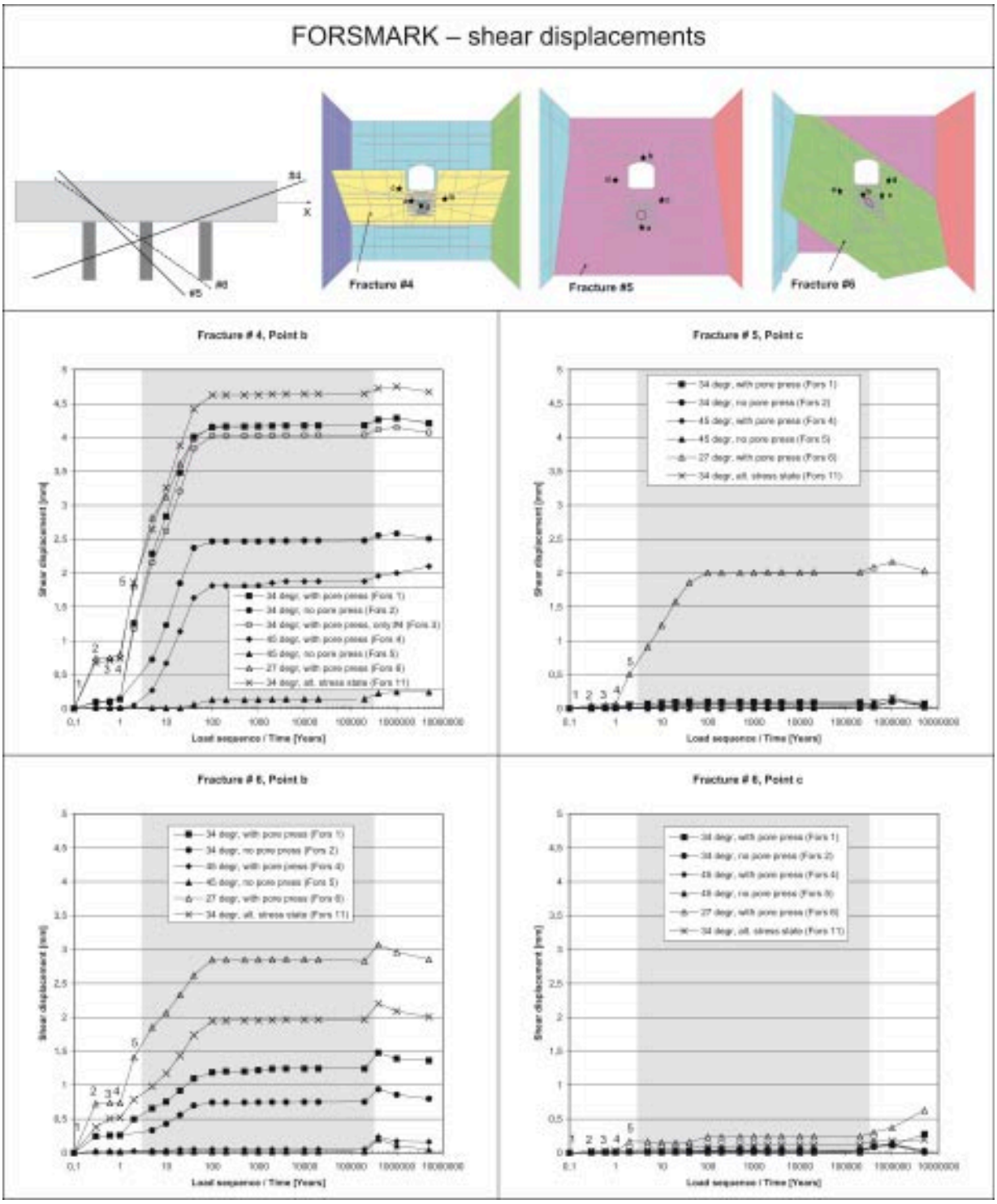

Figure 6-23. *Shear displacements in fracture #4 (upper left), #5(upper right) and #6 (bottom) in the Forsmark model. The labels in the diagrams denote the following equilibrium states: 1: Primary equilibrium, 2: Tunnel excavated, 3: Deposition holes excavated, 4: Swelling pressure in deposition hole, 5: Pore pressure*

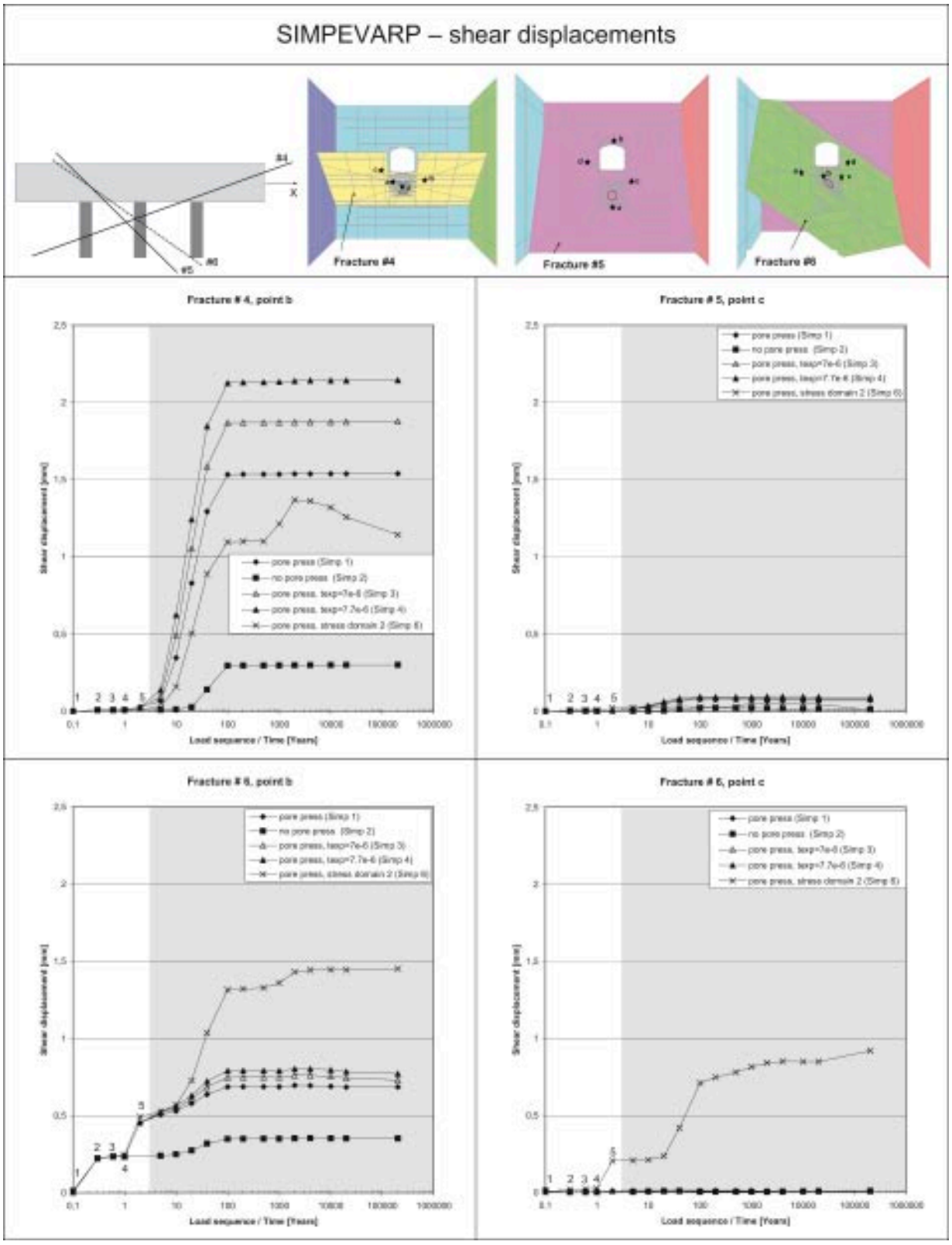

Figure 6-24. *Shear displacements in fracture #4 (upper left), #5(upper right) and #6 (bottom) in the Simpevarp model. The labels in the diagrams denote the following equilibrium states: 1: Primary equilibrium, 2: Tunnel excavated, 3: Deposition holes excavated, 4: Swelling pressure in deposition hole, 5: Pore pressure*

Fracture normal stress

In Figure 6-25, the effective normal stress results regarding the Forsmark model are presented. The following can be observed:

- At two of the points (fracture #5, point c and fracture #6, point b), significant stress differences due to friction angle variations can be observed. The influence is strongest at the end of the heated phase. The largest influence is found in fracture #5, point c. The maximum stress after 200,000 years is about 12 MPa higher in *Fors 1* (34°) than in *Fors 4* (45°) (i.e. 50% higher). The variations in normal stress are due to the different amounts of shear displacement which give different stress distributions.
- The influence on the effective normal stress of applying 5 MPa pore pressure is not equal at all points and in all cases. The reduction in effective normal stress ranges between about 3 MPa (fracture #5, point c, *Fors 6*) and 7.5 MPa (fracture #6, point b, *Fors 1*). The differences in changes of the effective normal stress relates to the difference in fracture shear strength.

The effective normal stress results regarding the Simpevarp model are presented in Figure 6-26. The following can be observed:

- The inclusion of pore pressure gives approximately the same stress reduction as the magnitude of the pore pressure (5 MPa) at the fracture #4 and #5 points. In fracture #6, point c, the stress reduction is little bit larger (about 6 MPa at maximum).
- The 24% increase of the thermal expansion coefficient gives a difference between *Simp1* and *Simp 4* in maximum stress of about 4 MPa (fracture #6, point c), i.e. 17% stress increase. The largest difference in fracture normal stress after ended heating period is about 5 MPa (fracture #5, point c).
- The normal stress levels are in general lower in *Simp 6* (stress domain 2) than in the other cases. This is due to the lower in situ stress levels in this case.

6.3 Rock stresses

6.3.1 General

The presentation of the rock stress results is divided into two parts. In Section 6.3.2, stresses calculated when assuming elastic conditions are presented. Elastic calculations give a good picture of the stresses which result from excavations of openings and heating since it turns out that the fractures in general have a limited influence on the stresses. The fractures may result in stress concentrations, but these are local effects. This is what is indicated by the results in Section 6.3.3, where the influence of the fractures is discussed.

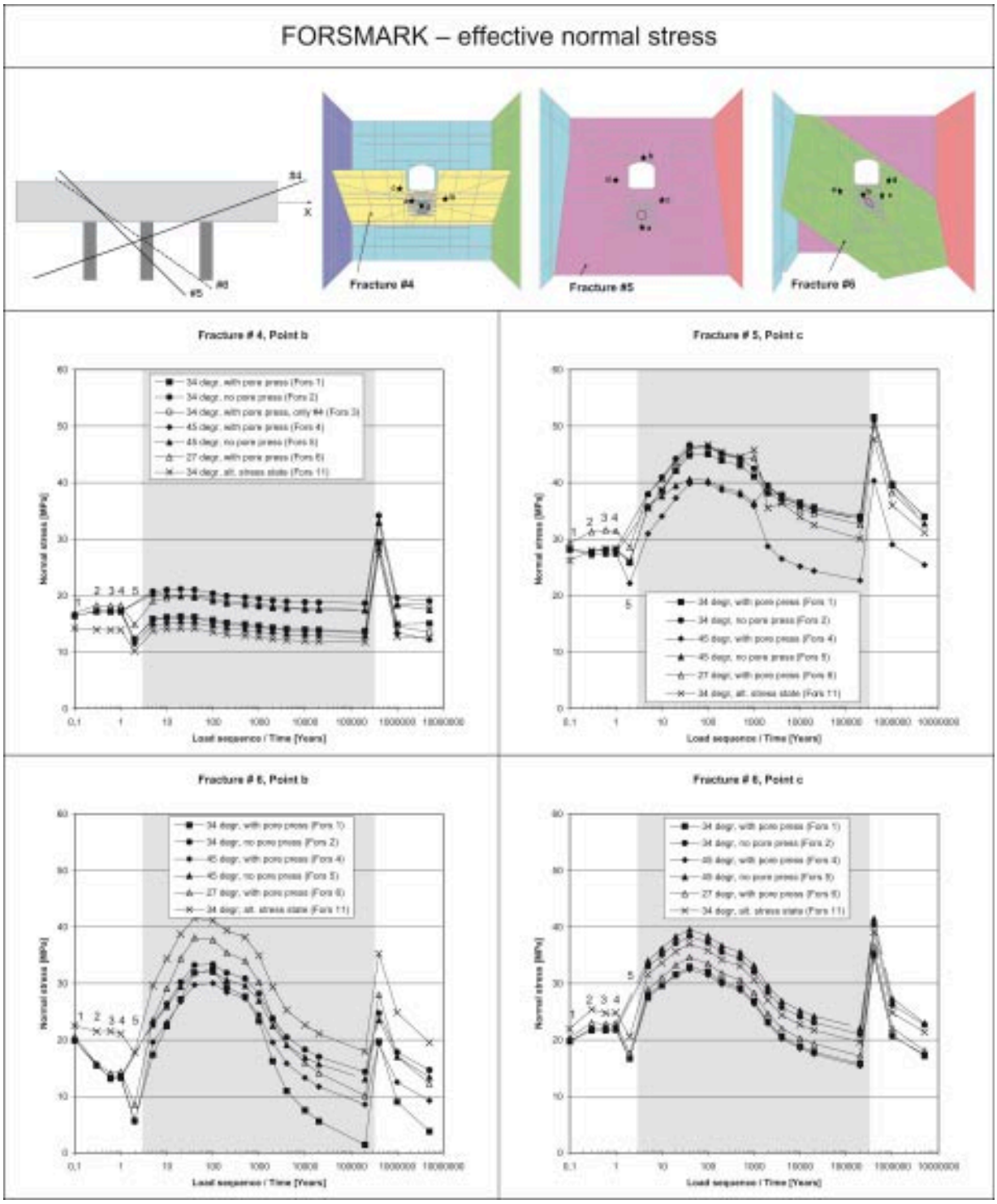

Figure 6-25. *Effective normal stresses in fracture #4 (upper left), #5 (upper right) and #6 (bottom) in the Forsmark model. The labels in the diagrams denote the following equilibrium states: 1: Primary equilibrium, 2: Tunnel excavated, 3: Deposition holes excavated, 4: Swelling pressure in deposition hole, 5: Pore pressure*

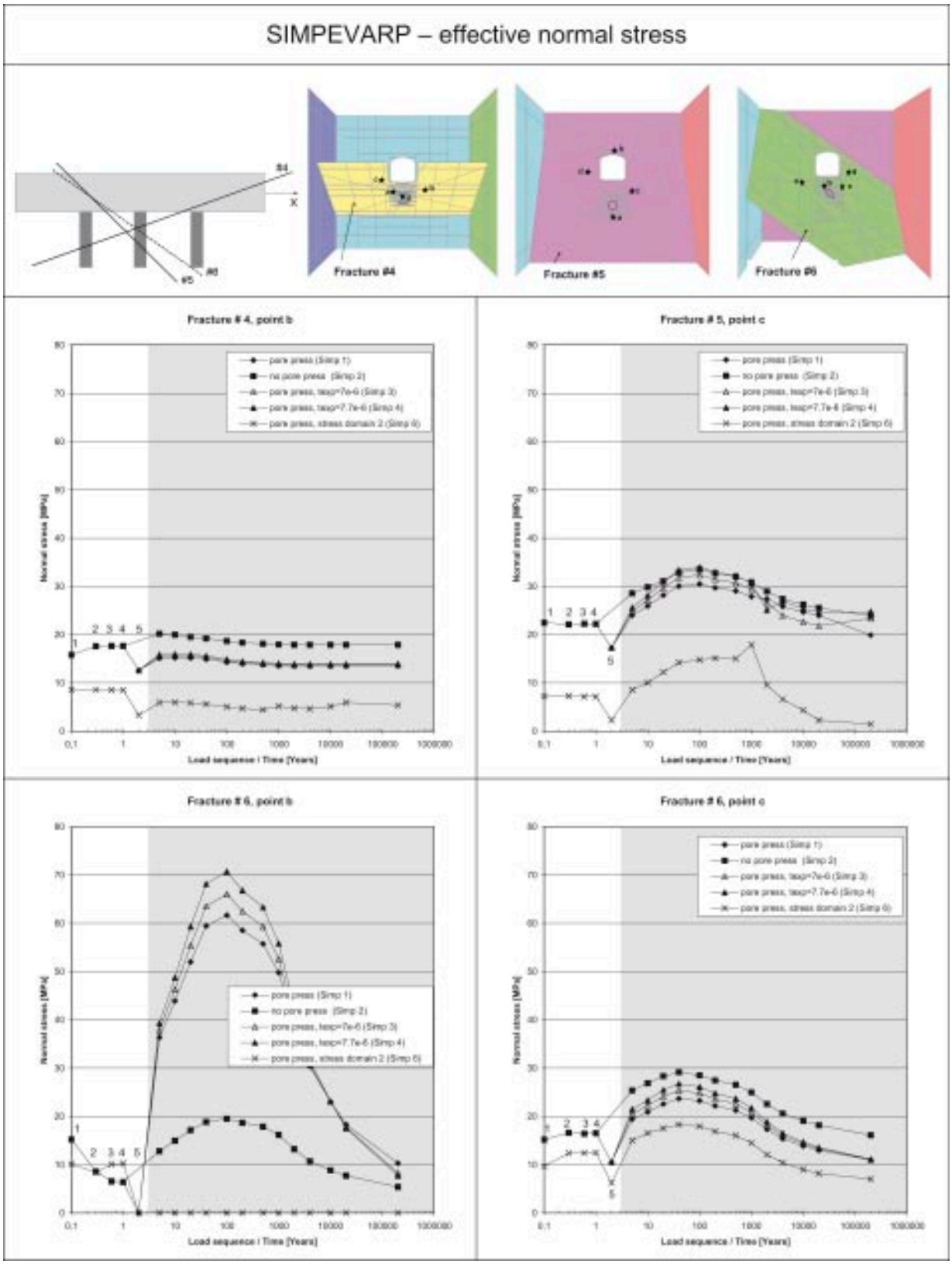

Figure 6-26. *Effective normal stresses in fracture #4 (upper left), #5(upper right) and #6 (bottom) in the Simpevarp model. The labels in the diagrams denote the following equilibrium states: 1: Primary equilibrium, 2: Tunnel excavated, 3: Deposition holes excavated, 4: Swelling pressure in deposition hole, 5: Pore pressure*

6.3.2 Elastic conditions

The major principal stress was recorded at different points close to the central deposition hole wall (Figure 6-27). The points were located at three azimuths (corresponding to locations *a, b* and *c*) and at two depths below the tunnel floor (1 m and 4 m). The two depths are here denoted *Level 1* and *Level 2,* respectively, and the history points are denoted according to Table 6-4. In the table, the distances between the points and the deposition hole wall are given in parenthesis.

The history points were located at the azimuths where the highest tangential stresses were expected to be found. In the Forsmark model and in the Simpevarp case where stress domain 1 was applied, there was a 15° angle between the major horizontal principal stress and the tunnel axis (Figure 6-27, bottom left). This stress orientation results in high stresses at location *a*. When the Simpevarp stress domain 2 was applied, the major horizontal in situ stress was directed perpendicularly to the tunnel axis, which results in high stresses at location *b* (bottom middle). These effects can be seen in Figure 6-28, which shows principal vector plots in a horizontal section 1 m below tunnel floor in case *Simp5* and *Simp 7.* Results from two stages are shown: 1) After deposition hole excavation, and 2) after 100 years of heating. In the Laxemar model, there was a 63° angle between the major principal stress and the tunnel axis (Figure 6-27, bottom right). For this case, the stresses were recorded at the locations *a* and *c*.

Table 6-4. History points. Distance from deposition hole wall in parenthesis (mm).

Level	Location a	b	c	Depth below floor
1	1a (36)	1b (62)	1c (36)	1 m
2	2a (35)	2b (28)	2c (36)	4 m

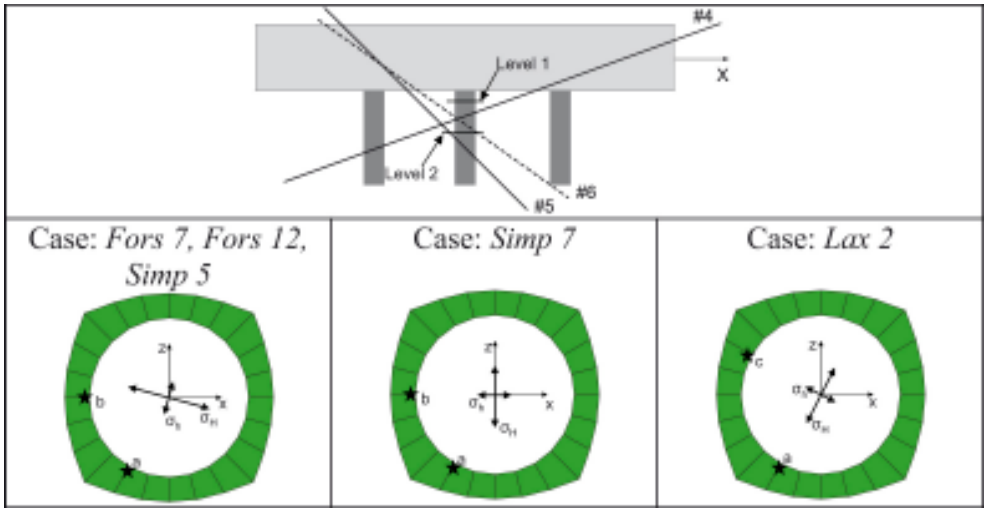

Figure 6-27. *History points were located at three azimuths (corresponding to locations a, b and c) and at two levels (1 m and 4 m below the tunnel floor). The figure also shows the directions of the major and minor horizontal in situ stresses in the different cases considered (x-axis along the tunnel and z-axis perpendicular to tunnel).*

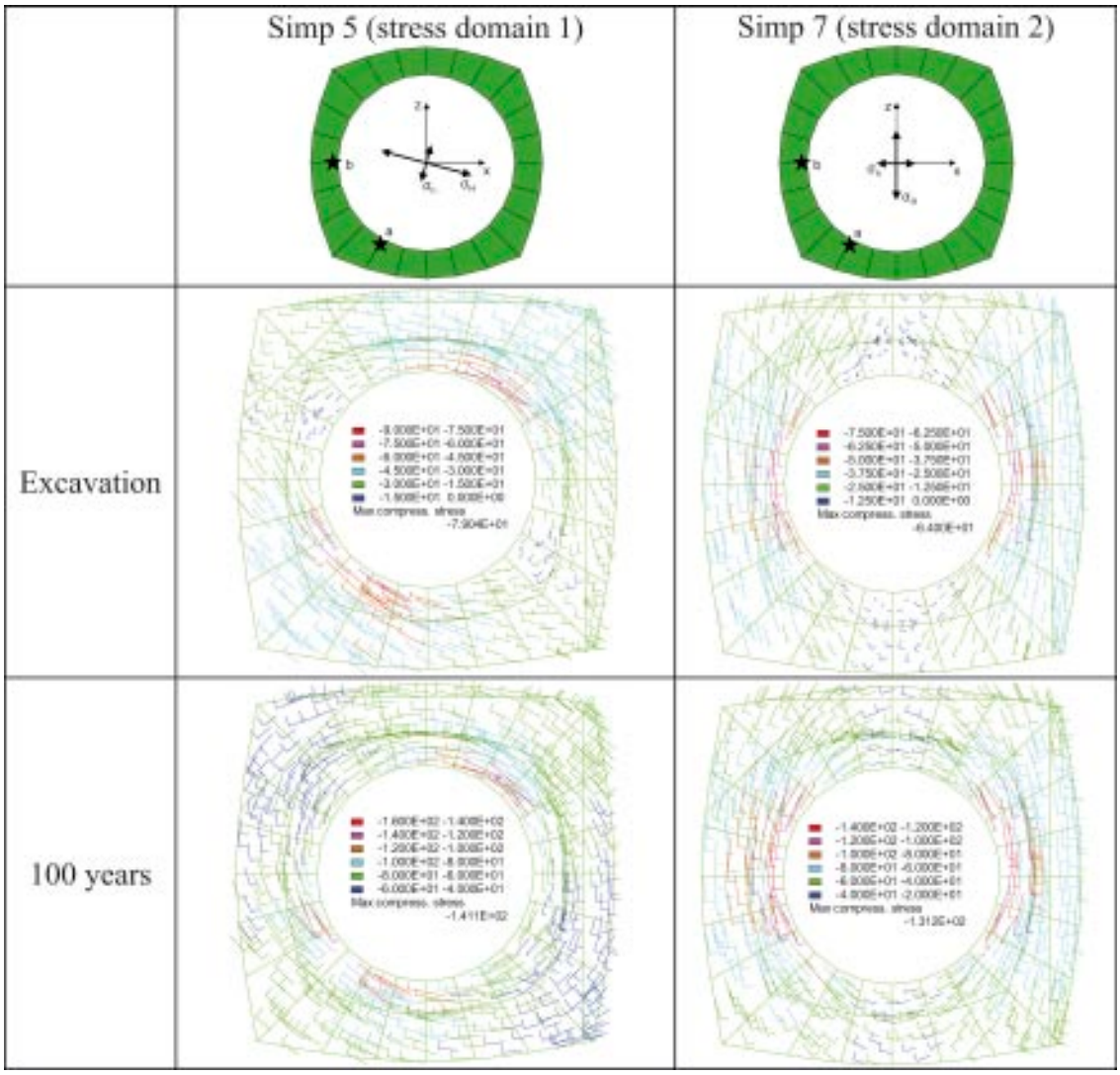

Figure 6-28. *Principal stress vector plots for two cases: Simp 5 (stress domain 1) and Simp 7 (stress domain 2). The vectors are colored according to the magnitude of the major principal stress. The results are taken from a horizontal section 1 m below the tunnel floor. At the top of the figure, the directions of the major and minor horizontal in situ stresses are shown (x-axis along the tunnel and z-axis perpendicular to tunnel).*

Stress histories from the following four elastic cases are presented in Figure 6-29:

- *Fors 7*: Forsmark base case in situ stress conditions.
- *Fors 12*: Alternative Forsmark in situ stress model and assuming repository to be located at 400 m depth (instead of 500 m, cf. Table 5-2).
- *Simp 5*: Simpevarp stress domain 1.
- *Simp 7*: Simpevarp stress domain 2.

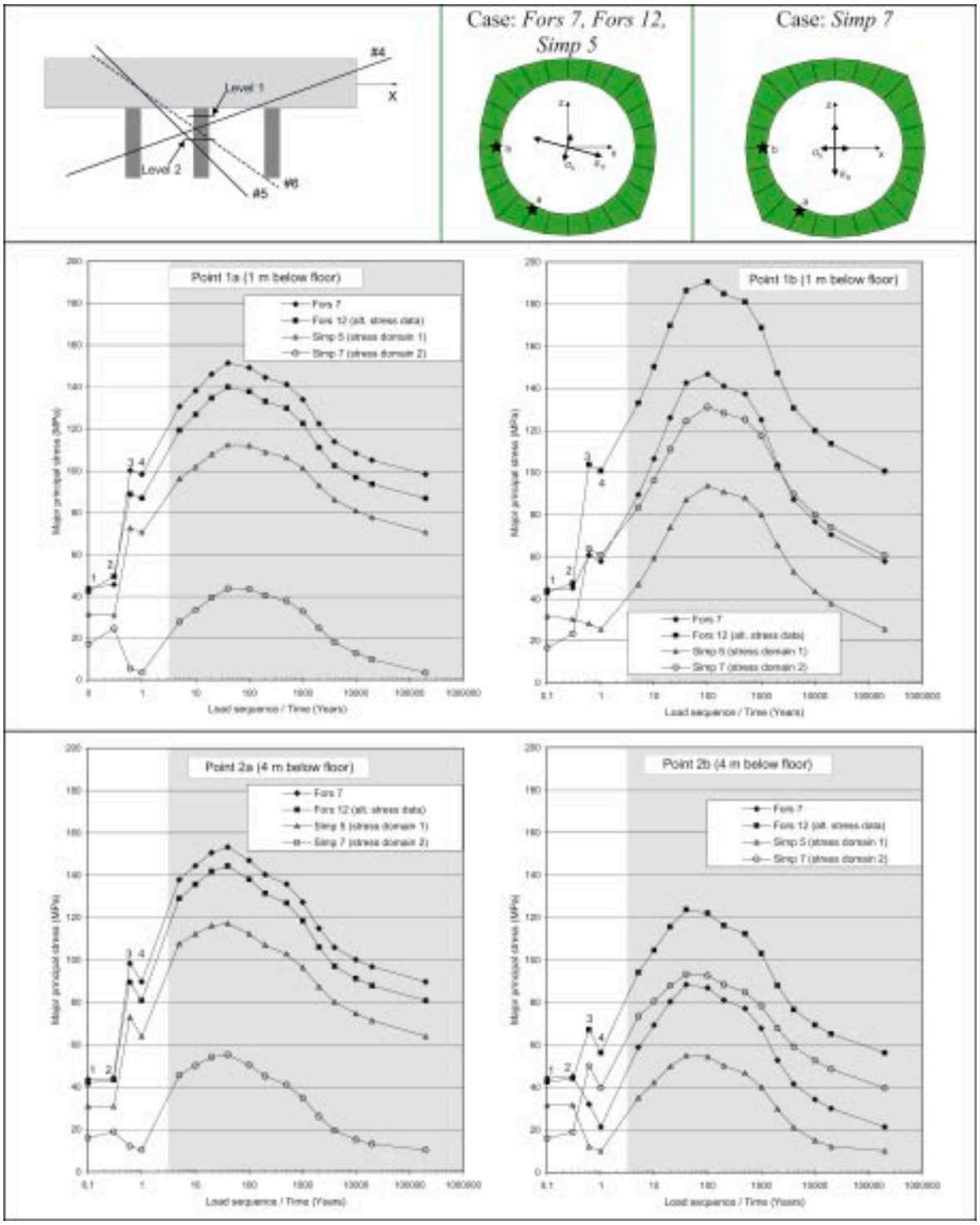

Figure 6-29. *Time histories of major principal stress at four points close to the central deposition hole wall. The points are located at two levels (upper left): Level 1: 1 m below floor, Level 2: 4 m below floor. Upper right picture shows the two different azimuths at which the points are located and the directions of the horizontal in situ principal stresses. Results from case Fors 7, Fors 12, Simp 5 and Simp 7 are presented. The labels in the diagrams denote the following equilibrium states: 1: Primary equilibrium; 2: Tunnel excavated; 3: Deposition holes excavated; 4: Swelling pressure in deposition hole.*

The following observations can be made:

- The stress levels are in general higher in the Forsmark cases due to higher in situ stresses.
- In the Forsmark cases, the deposition hole excavation results in a maximum stress increase of about 50 MPa and in the Simpevarp cases about 40 MPa. After completed excavation, the stresses reach about 100 MPa in *Fors 7* and *Fors 12* (point 1a, 1b, and 2a) and about 75 MPa in *Simp 5* (Point 1a, 2a). At point 2b, the effect of the hole excavation is less (maximum increase 32 MPa in *Simp 7*). In the other cases, the stresses are decreased at this point.
- The highest stress (190 MPa) was recorded after 100 years at point 1b for case *Fors 12*. The stress level during the heated phase was about 45 MPa higher in *Fors 12* compared to *Fors 7*. This is due to the higher value of the minor horizontal stress, σ_h, in *Fors 12*.
- In position *b,* the stress increase due to excavation is higher at level 1 than at level 2 due to the stress concentrations in the vicinity of the tunnel. This is also true for the stress increase due to the heat load. The higher stress magnitudes close to the tunnel floor are illustrated by the principal vector plot in Figure 6-30.

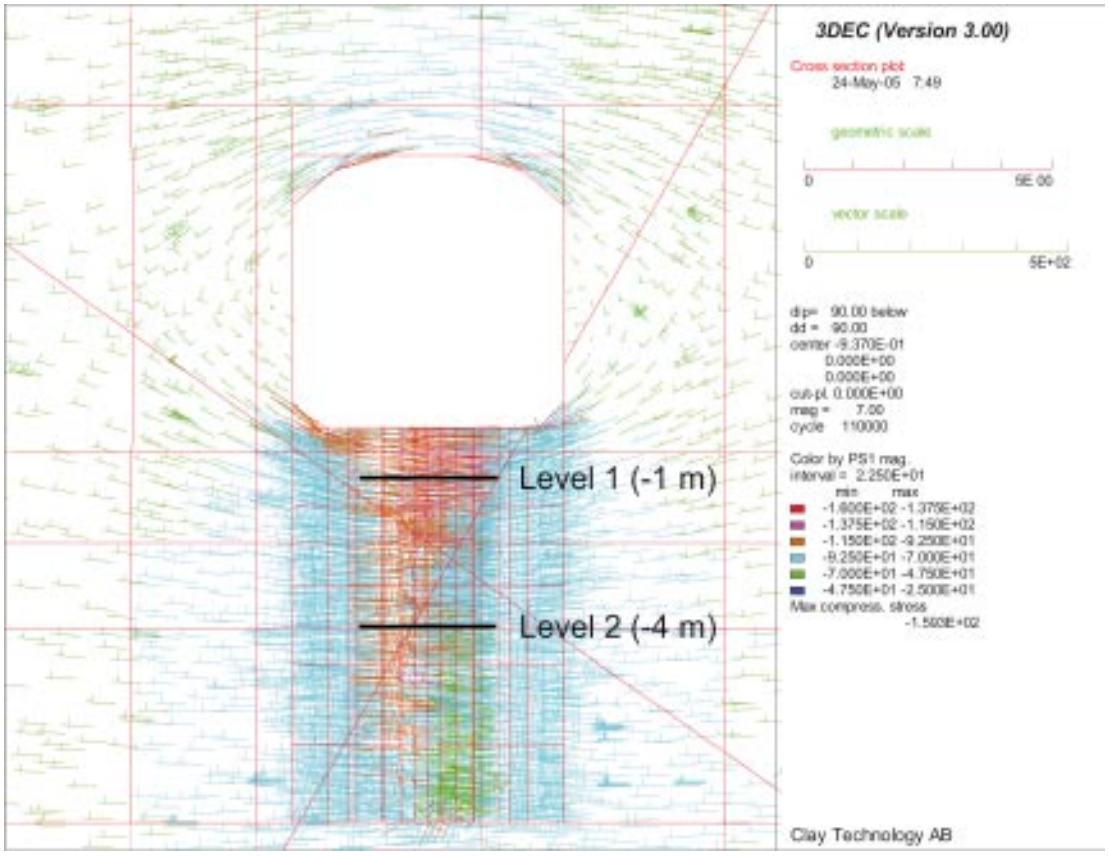

Figure 6-30. *The figure shows a principal stress vector plot from case Fors 7 after 100 years of heating in a vertical section transversal to the tunnel and located 62 mm from the deposition hole wall. The vectors are colored according to the magnitude of the major principal stress. The labels indicate the two levels at which the history points are located. The thermal stresses are more emphasized in the region close to the tunnel floor. The high plot symbol density close to the deposition hole is caused by the fine zoning in this region.*

In Figure 6-31, the results from the *Lax 2* case are presented. It can be observed that the stress after deposition hole excavation reaches about 110 MPa (point 1c), which is 10 MPa higher than in the Forsmark model. Thus, the stress is higher in *Lax 2* than in *Fors 1* even though the in situ stress magnitudes are lower in *Lax 2.* This can be explained by the orientation of the in situ stresses. In *Fors 1,* the major stress is sub parallel to the tunnel axis, whereas in *Lax 2* there is a 63° angle between the major stress and the tunnel axis. The stress orientation in *Lax 2* gives higher stress concentrations around the tunnel. It can also be observed that during the heating phase, the stress reaches about 165 MPa in *Lax 2.*

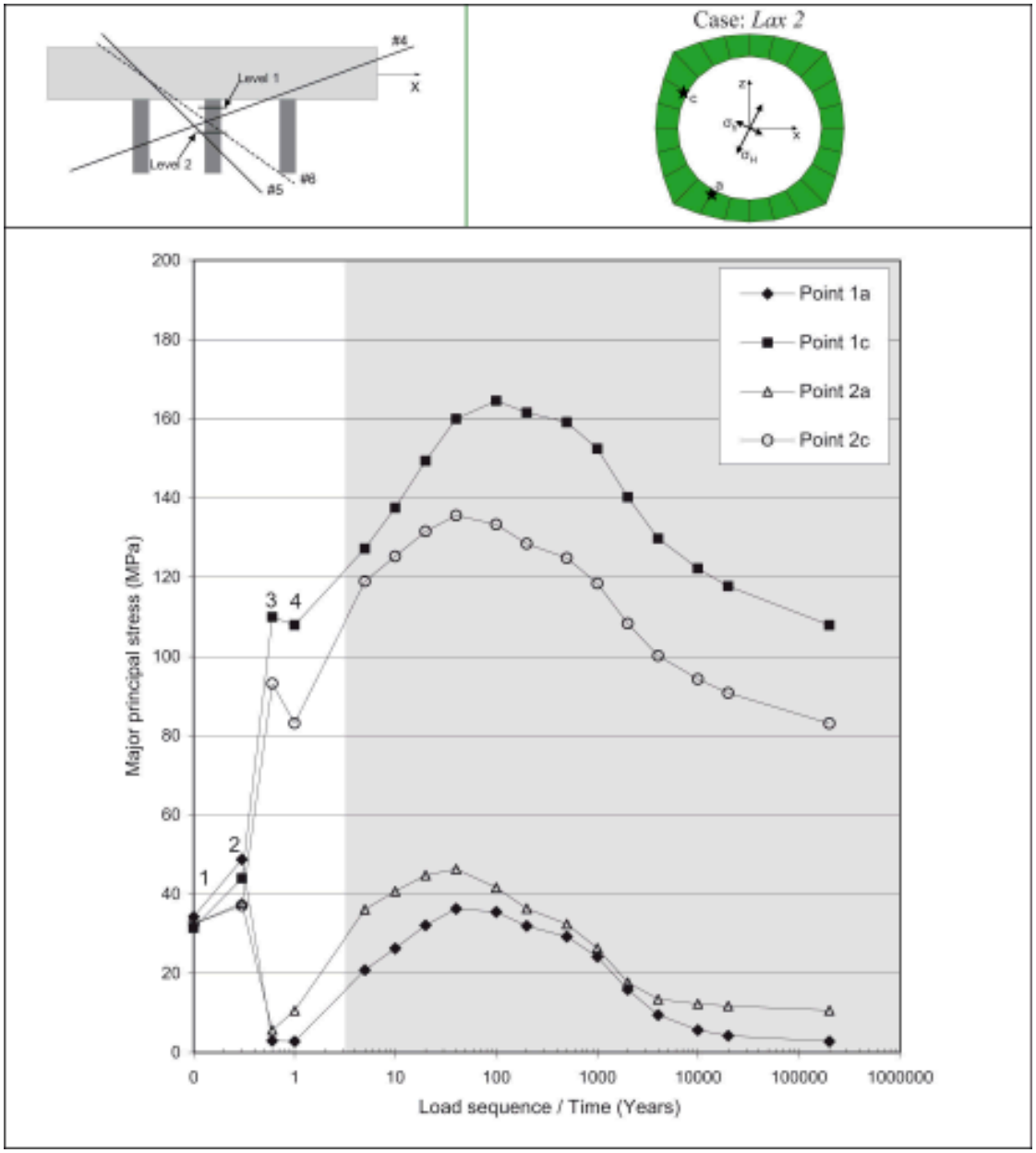

Figure 6-31. *Time histories of major principal stress at four points close to the central deposition hole wall in case Lax 2. The points are located at two levels (upper left): Level 1: 1 m below floor, Level 2: 4 m below floor. Upper right picture shows the two different azimuths at which the points are located and the directions of the horizontal in situ principal stresses. The y-scale is set equal to that of Figure 6-29 to facilitate comparison with the results in that figure. The labels in the diagrams denote the following equilibrium states: 1: Primary equilibrium; 2: Tunnel excavated; 3: Deposition holes excavated; 4: Swelling pressure in deposition hole.*

6.3.3 Sensitivity to fracture strength, pore pressure and thermal expansion

In the previous section, results from elastic models (no fractures) were presented. Stress histories for six history points close to the central deposition hole were considered. In this section, results of the same type are presented but now from models with fractures included. In some of these cases, a 5 MPa pore pressure was applied in all fractures, in the deposition tunnel and in the deposition holes. For comparison, results from the elastic cases are also shown. The results are presented in Figure 6-32 to Figure 6-35.

In Table 6-5, the ratio between peak stresses in different cases are presented. The peak stress during the heated phase in case with fracture and pore pressure is related to the peak stress in corresponding elastic case without fractures. The stress ratios are given in percent, and a value above 100 means higher stress in the case with fractures. Regarding the results from the Forsmark and Simpevarp models, the following can be observed:

- At three of the points, the fractures tend to give reduction of the stress levels compared to the stresses in the elastic case (point 1a, 2a and 2b). The stress ratio varies between 66% and 100%. The stress reduction tends to be larger the lower the fracture strength. The ratio is 66% in point 2b when 27° friction angle is applied whereas the corresponding ratio for the 45° case is 89%.
- At point 1b, the effect of the fractures differs from what is found at the other points. Here, the presence of the fractures results in a significant stress increase. The ratio varies between 105% and 153%. The lowest fractures shear strength gives the highest ratio, i.e. the largest stress increase.

In the Laxemar model, the influence of the fractures is less pronounced and differs from what is found in the other models. The stress ratio is less than 10% at all points considered. The difference between the Laxemar model and the other models is due to the difference in the orientation of the in situ stresses.

Figure 6-33 shows results from the Simpevarp model considering in situ stresses according to stress domain 1. In one case (*Simp 4*), a higher value ($7.7 \cdot 10^{-6}\,K^{-1}$) of the rock's thermal expansion coefficient was used. This value is the same as in the Forsmark model. The 24% increase of the rock thermal expansion gives an increase of the peak stress at point 2a of at most 13 MPa (i.e. 12%) compared to *Simp 1*. At point 1b, the stress increase amounts to about 23 MPa (19%).

The influence of the fractures on the stresses is related to the high intensity of large fractures in the models (All fractures in the models have extensions corresponding to radii in the interval 20–25 m). If the near-field volume (8 x 8 x 8 m^3 box surrounding central deposition hole) is considered, the specific fracture area per unit rock volume is of the order of 1 m^2/m^3. This value should be compared with the corresponding value that can be calculated based on the statistical fracture network models given in the site model descriptions. Considering fractures with radii in the interval 20–25 m, the statistical fracture network model for Forsmark gives a specific fracture area of the order of 0.01 m^2/m^3 /SKB 2005b/. If small fractures with radii in the interval 0.2–1 m are considered, the site model yields a specific area of about 3 m^2/m^3, i.e. higher than in the *3DEC* models. However, the shear displacements in such small fractures are small and consequently their influence also is small compared to that of the larger fractures. The large fractures have no edges in the near-field close to the central deposition hole that limit their shear displacements. Thus, due to the high intensity of large fractures in the *3DEC* models, the impact of the fractures that is observed here is likely to be overestimated.

Table 6-5. Peak major principal stress ratio (%). Stress in case with fractures and pore pressure versus stress in corresponding elastic case. A value above 100 means higher stress in case with fractures. Results at different locations are presented.

Fracture friction angle	Forsmark (basic stress state)						Forsmark (alternative stress state)		Simpevarp stress domain 1		Simpevarp stress domain 2		Laxemar	
	27°		34°		45°		34°		34°		34°		34°	
Point	a	b	a	b	a	b	a	b	a	b	a	b	a	c
Level 1	81	153	85	135	93	108	80	122	83	127	100	105	106	93
Level 2	92	66	95	82	100	89	100	89	92	76	95	88	102	98

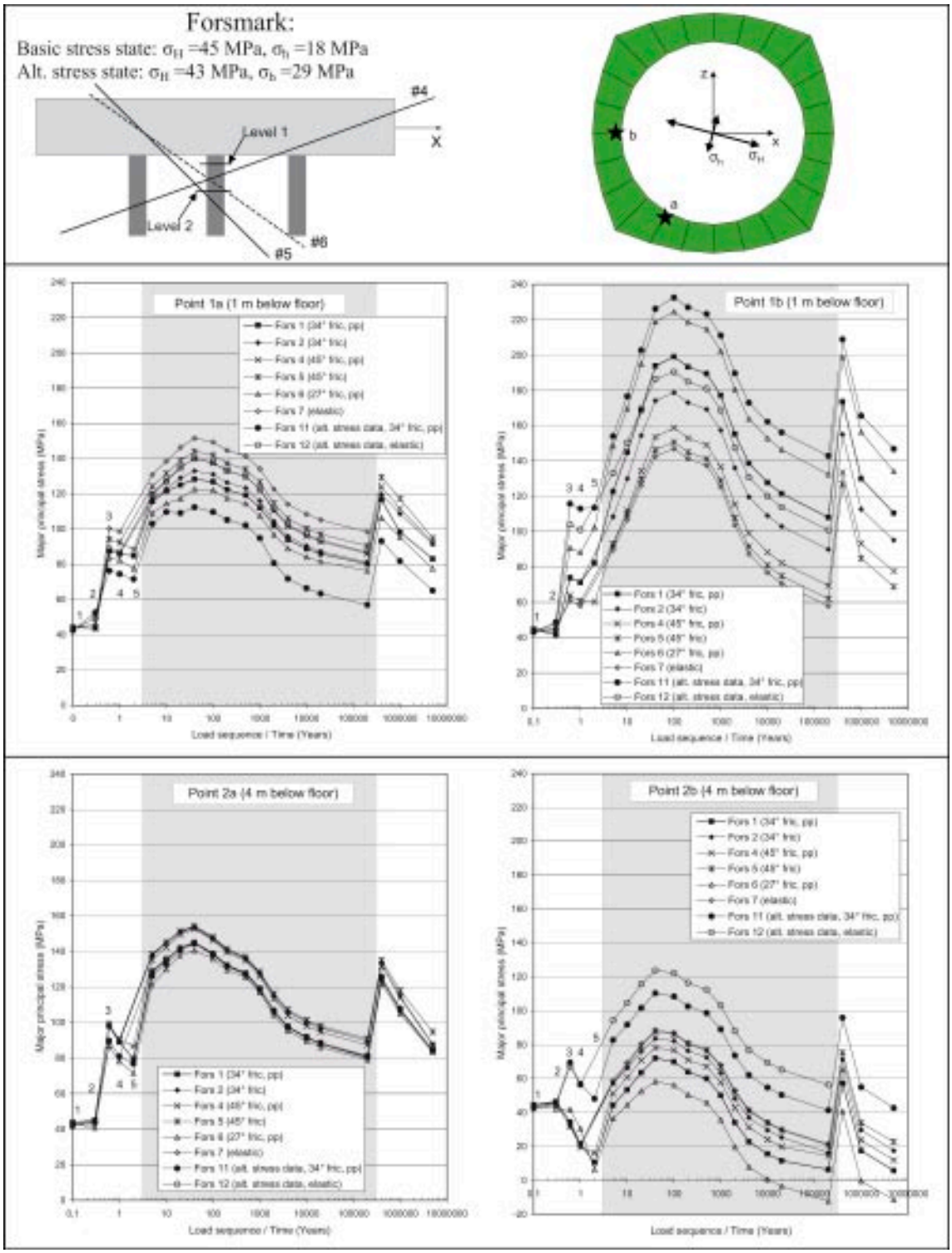

Figure 6-32. *Upper: Time histories of the major principal stress at four points located at two levels and at two azimuths. Level 1: 1 m below floor, Level 2: 4 m below floor. Upper right picture also shows the directions of the horizontal in situ principal stresses. Results from case Fors 1, Fors 2, Fors 4, Fors 5, Fors 6, Fors 7, Fors 11 and Fors 12 are presented. The labels denote the following equilibrium states: 1: Primary equilibrium; 2: Tunnel excavated; 3: Deposition holes excavated; 4: Swelling pressure in deposition hole; 5: Pore pressure.*

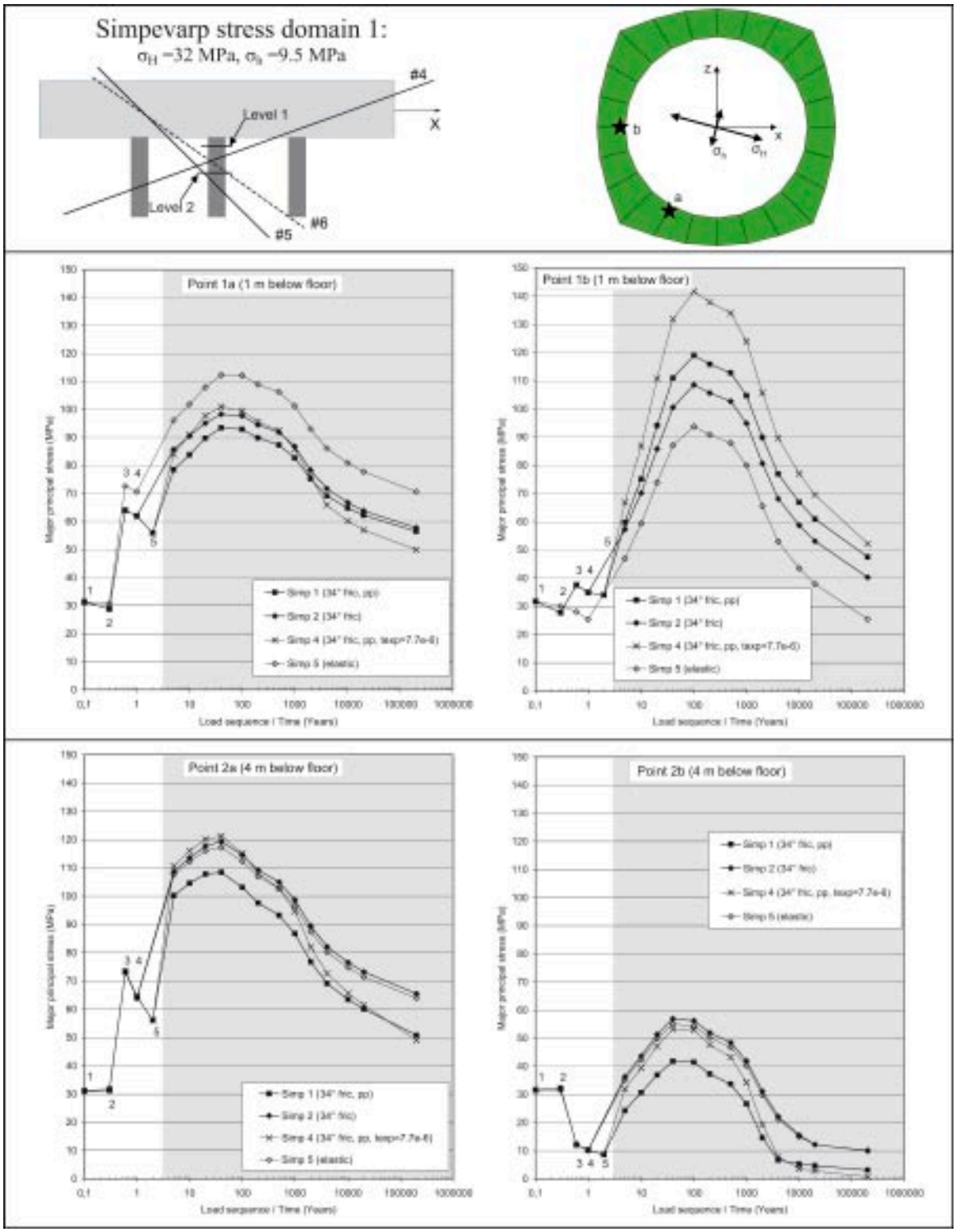

Figure 6-33. *Upper: Time histories of the major principal stress at four points located at two levels and at two azimuths. Level 1: 1 m below floor, Level 2: 4 m below floor. Upper right picture also shows the directions of the horizontal in situ principal stresses. Results from case Simp 1, Simp 2, Simp 4 and Simp 5 are presented. The labels denote the following equilibrium states: 1: Primary equilibrium; 2: Tunnel excavated; 3: Deposition holes excavated; 4: Swelling pressure in deposition hole; 5: Pore pressure.*

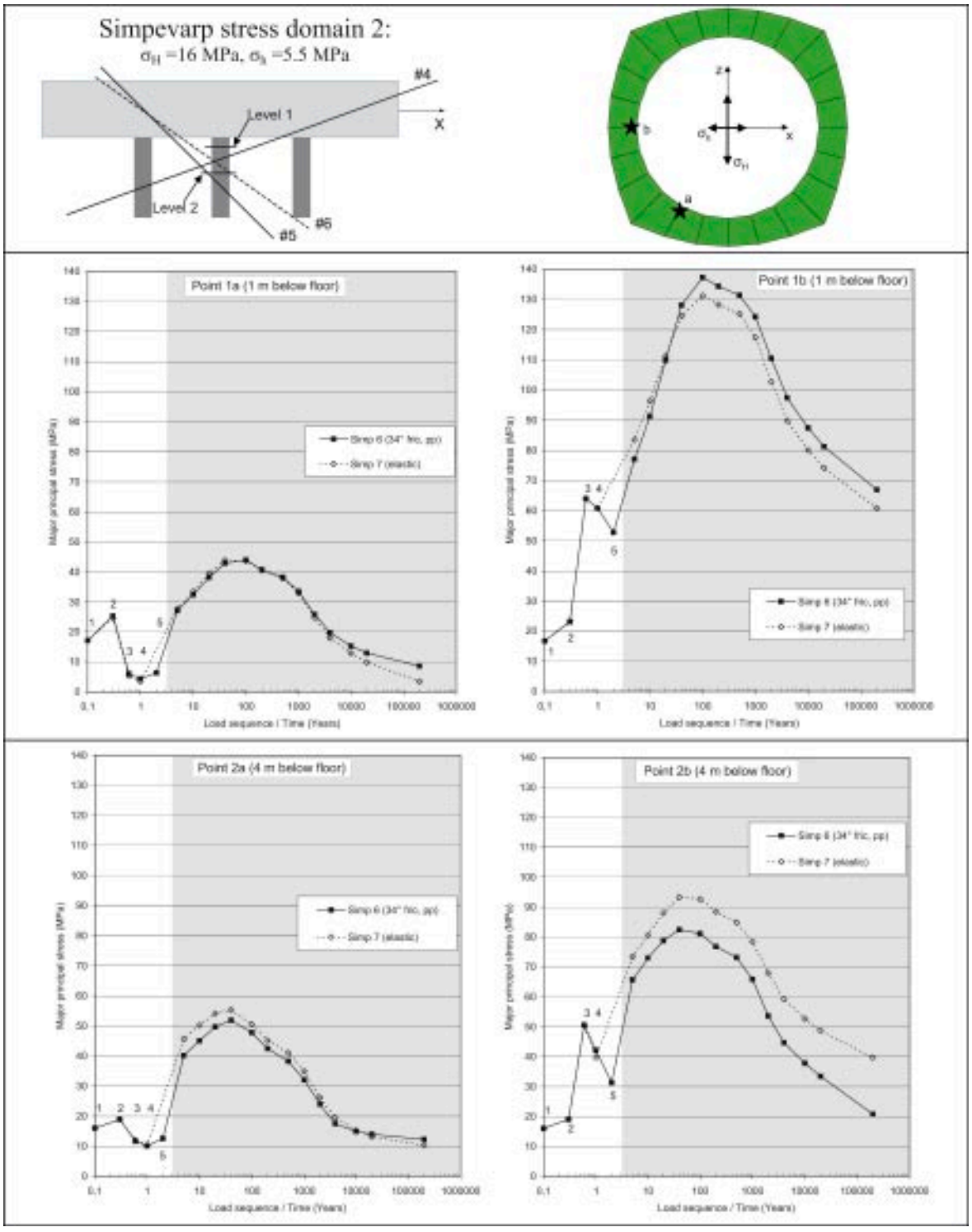

Figure 6-34. *Upper: Time histories of the major principal stress at four points located at two levels and at two azimuths. Level 1: 1 m below floor, Level 2: 4 m below floor. Upper right picture also shows the directions of the horizontal in situ principal stresses. Results from case Simp 6 and Simp 7 are presented. The labels denote the following equilibrium states: 1: Primary equilibrium; 2: Tunnel excavated; 3: Deposition holes excavated; 4: Swelling pressure in deposition hole; 5: Pore pressure.*

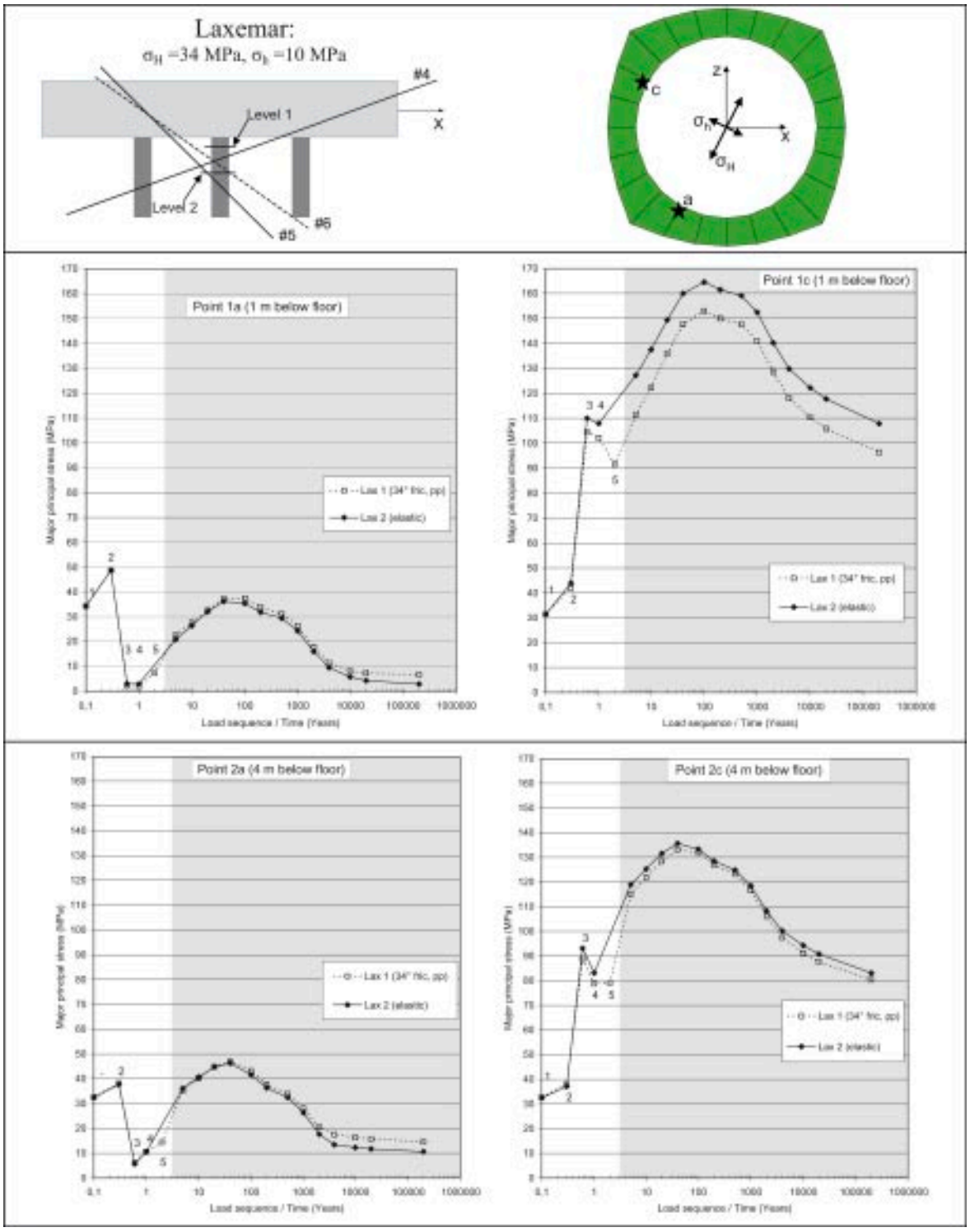

Figure 6-35. *Upper: Time histories of the major principal stress at four points located at two levels and at two azimuths. Level 1: 1 m below floor, Level 2: 4 m below floor. Upper right picture also shows the directions of the horizontal in situ principal stresses. Results from case Lax 1 and Lax 2 are presented. The labels denote the following equilibrium states: 1: Primary equilibrium; 2: Tunnel excavated; 3: Deposition holes excavated; 4: Swelling pressure in deposition hole; 5: Pore pressure.*

6.4 Intact rock failure

6.4.1 General

The combination of high initial stresses and following thermal load may generate stress-induced spalling in the walls of the deposition holes. The spalling process in general and its implications for the stability of KBS-3 type deposition holes in particular have been discussed by, for instance, /Martin et al. 1999/ and /Martin et al. 2001/. The extent and scope of spalling in full-scale KBS-3 deposition holes have been examined experimentally within the Äspö Pillar Stability Experiment (APSE) in the Äspö HRL /Andersson and Eng 2005/. APSE was also aimed at improving the understanding of the details of the spalling process, for instance the importance of small support pressures for suppressing initiation of spalling and, for unsupported walls, values of the spalling strength. The present view is that the spalling strength of the rock in APSE is about 55% of the laboratory-determined uniaxial compressive strength.

If the initial, pre-mining, stresses are sufficiently high, spalling may take place during the operational phase as a response to the stress redistribution caused by excavation, in particular if the deposition tunnels are oriented normally to the major initial stress (see e.g. /Hökmark 2003/). In cases where the initial rock stresses are not sufficient to produce spalling, there is still the possibility that spalling may occur later because of the following thermal load. Estimates of the volumes of rock around a deposition hole in which the spalling strength may be exceeded were made based on results from the elastic cases *Fors 10, Simp 5, Simp 7* and *Lax 2*.

6.4.2 Forsmark

The *Fors 10* case was used to examine the stresses in the vicinity of the central deposition hole. In this case, no swelling pressure was applied. The model was specifically densely meshed in the immediate vicinity of the central deposition hole and the boundary condition scheme shown in Figure 4-5 was applied.

The Forsmark model assumes the rock type to be granite-to-granodiorite with a uniaxial compressive strength (UCS) of 225 MPa. The major horizontal in situ stress is about 45 MPa, the minor horizontal stress 18 MPa and the vertical stress 13 MPa. The tunnels are inclined 15° with respect to the major stress.

Figure 6-36 shows principal stresses in a horizontal section 4 m below the tunnel floor and in a vertical section along the deposition hole axis. Only rock within about 0.3 m distance from the walls is visible. The arrows show the tunnel axis orientation and the dashed lines indicate the locations of the two sections. The stress plots represent three states: After excavation, the state after 5 years and after 40 years, respectively. The stress tensor symbols scale with the projection of the principal stresses onto the viewing plane, whereas the colour code (separate for each set) regards the magnitude of the major principal stress.

The contour lines indicate areas where the major stress exceeds the spalling threshold, which here is assumed to be 124 MPa. This does not mean that spalling will occur everywhere within the contours. The stresses are calculated assuming linear elasticity whereas in reality the stress field will change as soon as the failure process begins. The following can be observed:

- The spalling threshold was not exceeded anywhere after completed excavation.
- After 5 years, the spalling strength was exceeded along two 1 m sections of the periphery to a maximum depth of about 0.1 m.
- After 40 years, the spalling strength was exceeded along two 1.5 m sections of the periphery to a maximum depth of about 0.15 m.

In Table 6-6, the maximum tangential stresses found at the deposition hole wall at the three stages are presented.

Table 6-6. Maximum tangential stress at deposition hole wall in the *Fors 10* case.

Stage	Maximum tangential stress	
After excavation	114 MPa	1.2 m below floor
After 5 years	165 MPa	4.8 m below floor
After 40 years	175 MPa	2.6 m below floor

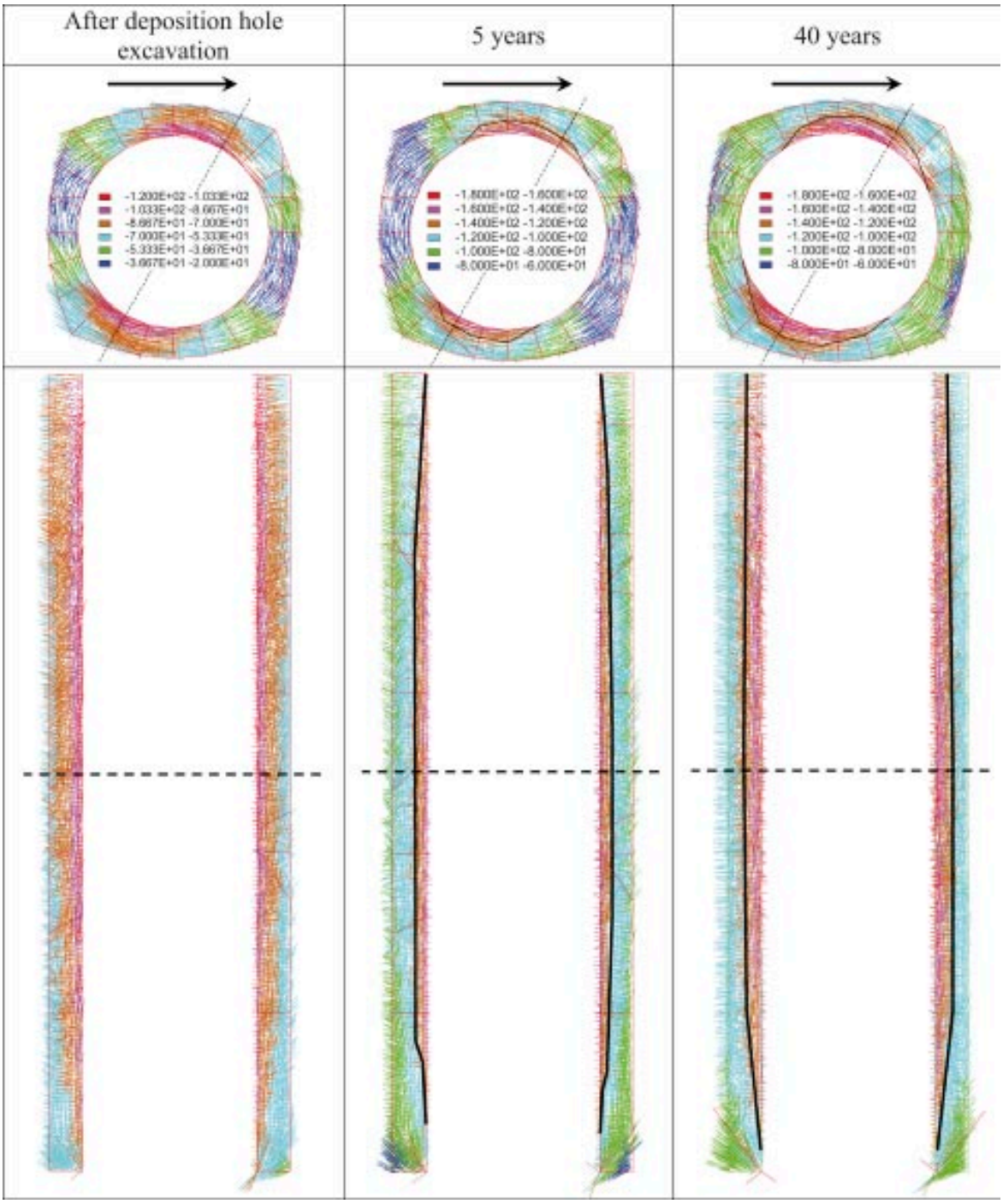

Figure 6-36. *The figure shows principal stress vectors around the central deposition hole at different stages/times. The upper pictures are horizontal sections located 4 meters below the tunnel floor. The lower pictures are vertical sections through the center of the hole. The arrows show the tunnel axis orientation and the dashed lines indicate the locations of the two sections. The solid lines indicate the estimate of the extension of spalling around the hole assuming the spalling strength to be 120 MPa.*

Figure 6-37 (lower) shows the stress path of four points at different distances from the deposition hole wall. All points are located at 4 m depth below the tunnel floor. Here, the damage initiation envelope is based on the assumption that the spalling strength is about 55% of the 225 MPa uniaxial compressive strength. The vertical and horizontal axes represent the major and minor principal stresses respectively, both normalized to the uniaxial compressive strength. The concepts of the plot are those used by /Martin et al. 2001/ (Figure 6-37, upper). The figure indicates that if the stress ratio had been about 40% rather than 55%, then the rock at those points would have been at the limit of failure already during the operational phase.

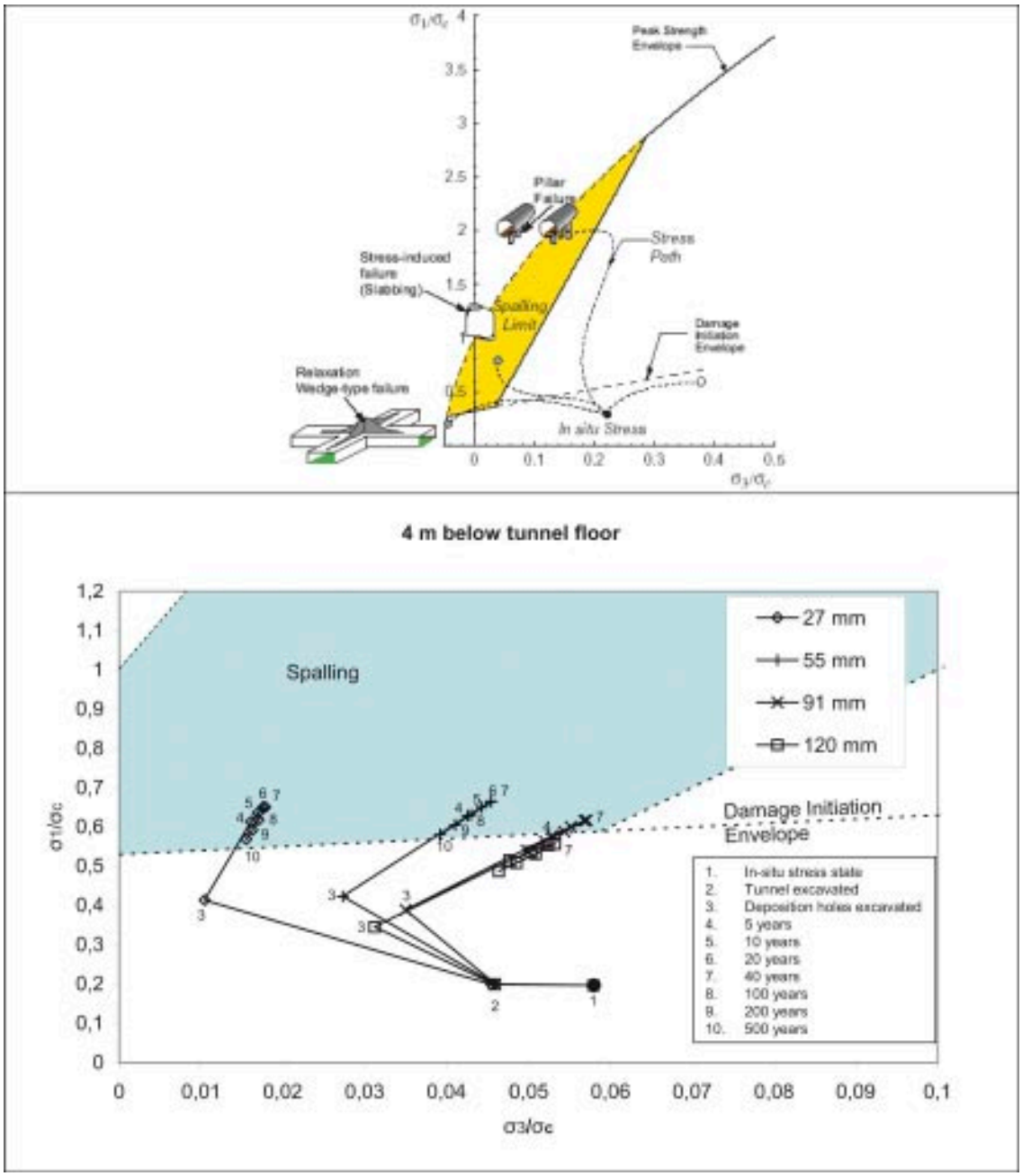

Figure 6-37. *The upper picture shows stress paths and different modes of failure. The shaded area indicates in which stress state spalling is likely to occur (from /Martin et al. 2001/. The concept of the lower picture is that of the upper. It shows calculated stress paths of four points located at different distances from the rock wall at deposition hole mid-height (4 m depth) in the Fors 10 case.*

6.4.3 Simpevarp

The Simpevarp models were analyzed assuming the rock type to be Ävrö granite with a uniaxial compressive strength (UCS) of 165 MPa. Assuming that the spalling limit is 55 % of UCS gives a spalling strength of about 90 MPa for this rock type. For Simpevarp, there is no high resolution model with moving boundaries, such as the *Fors 10* case model. However, there is a case where the rock is considered elastic and with swelling pressure applied (*Simp 5*). In this case, in situ stresses according to stress domain 1 were applied. In stress domain 1, the major horizontal in situ stress is 32 MPa, the minor horizontal stress 9.5 MPa and the vertical stress 14 MPa. The tunnels are inclined 15° with respect to the major stress.

There is also an elastic Simpevarp case where stress domain 2 in situ stresses were applied (*Simp 7*). In this case, the major horizontal stress is 16 MPa and normal to the tunnel axis. The minor horizontal stress is 5.5 MPa and the vertical stress is 9 MPa.

The maximum calculated tangential stresses at the deposition hole wall for the two Simpevarp cases are presented in Table 6-7. Results are presented for the same three stages as for the Forsmark model, i.e. after completed excavation, after 5 years and after 40 years.

Figure 6-38 and Figure 6-39 show principal stresses in a horizontal section 4 m below the tunnel floor and in a vertical section along the deposition hole axis. Figure 6-38 shows results from the *Simp 5* case (stress domain 1) and Figure 6-39 from the *Simp 7* case (stress domain 2). Only rock within about 0.3 m distance from the walls is visible. The arrows show the tunnel axis orientation and the dashed lines indicate the locations of the two sections. The three sets of stress plots represent the state after excavation, the state after 5 years and after 40 years, respectively. The stress tensor symbols scale with the projection of the principal stresses onto the viewing plane, while the colour code (separate for each set) regards the magnitude of the major principal stress.

The contour lines indicate areas where the major stress exceeds the spalling threshold, which here is assumed to be about 90 MPa. This does not mean that spalling will occur everywhere within the contours. The stresses are calculated assuming linear elasticity while in reality the stress field will change as soon as the failure process begins.

The following can be observed for the stress domain 1 case (Figure 6-38):

- The excavation induced a maximum tangential stress of about 82 MPa, i.e. below the spalling threshold.
- After 5 years of heating, the maximum tangential stress amounted to about 125 MPa, i.e. above the spalling threshold. The spalling strength was exceeded along two 1 m sections of the periphery to a maximum depth of about 0.1 m. The development, with deposition holes walls being stable during the operational phase and then entering a state where spalling is likely to occur is very much similar to the situation in the Forsmark model (cf. Section 6.4.2).
- After 40 years of heating, the maximum tangential stress amounted to about 142 MPa. The spalling strength was exceeded along two 1 m sections of the periphery to a maximum depth of about 0.15 m. The region where the spalling strength was exceeded now reached from top to bottom of the deposition hole.

The following can be observed for the stress domain 2 case (Figure 6-39):

- The excavation induced a maximum tangential stress of about 64 MPa at borehole mid-height, i.e. below the spalling threshold.
- After 5 years of heating, the maximum tangential stress amounted to 87 MPa, which is below the spalling threshold. However, there was a 10 MPa swelling pressure applied in the deposition hole. The maximum stress as calculated without assuming any swelling pressure would probably exceed the spalling threshold of 90 MPa.
- After 40 years of heating, a maximum tangential stress of 114 MPa was reached. The spalling strength was exceeded along two 0.7 m sections along the periphery at canister mid-height to a maximum depth of 0.1 m. The region where the spalling strength was exceeded reached from top to about mid-height of the deposition hole.

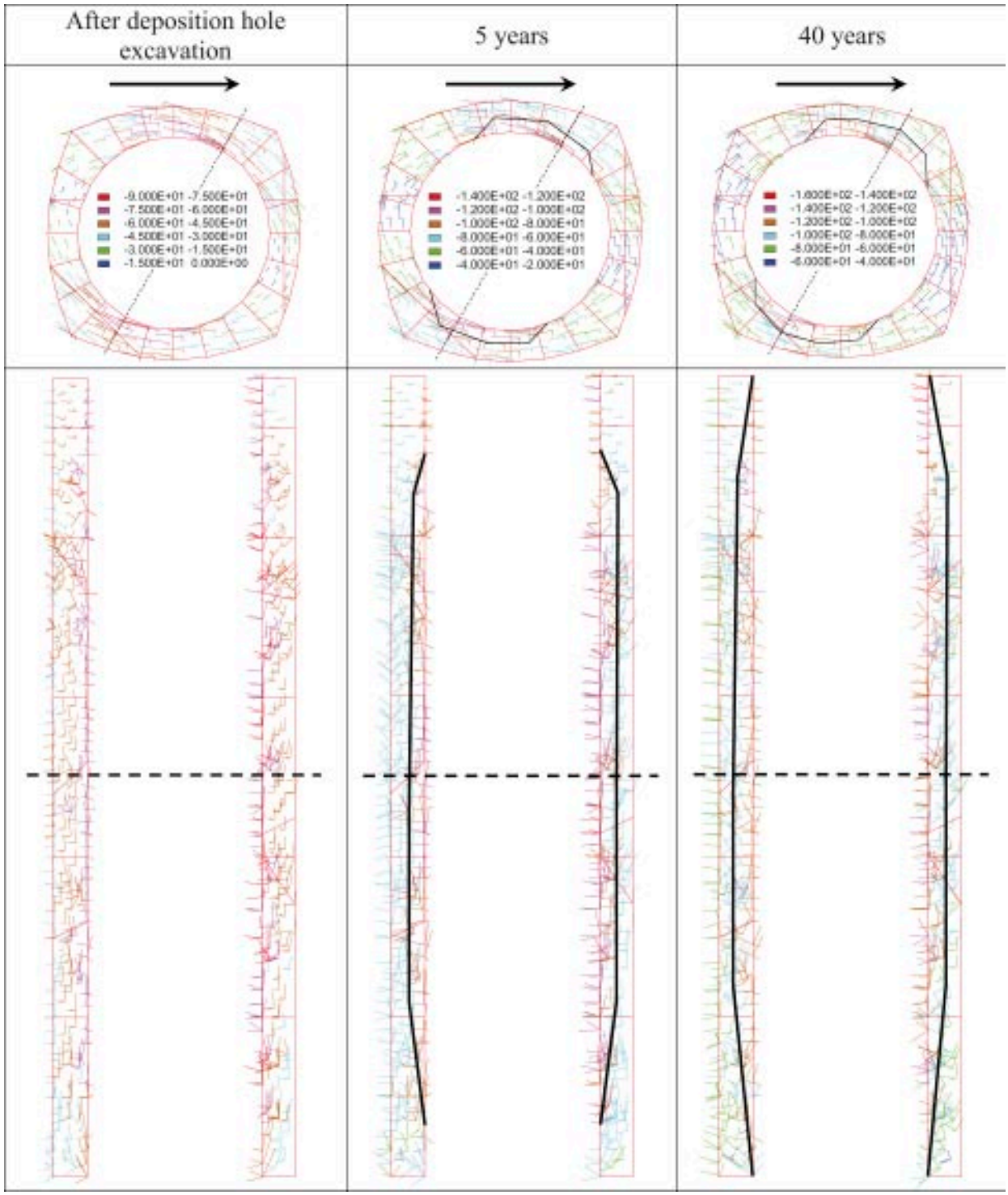

Figure 6-38. *The figure shows principal stress vectors around the central deposition hole at different times in the Simp 5 case (stress domain 1). The upper pictures are horizontal sections located 4 meters below the tunnel floor. The lower pictures are vertical sections through the center of the hole. The arrows show the tunnel axis orientation and the dashed lines indicate the locations of the two sections. The solid lines indicate an estimate of the extension of spalling around the hole assuming the spalling strength to be about 90 MPa.*

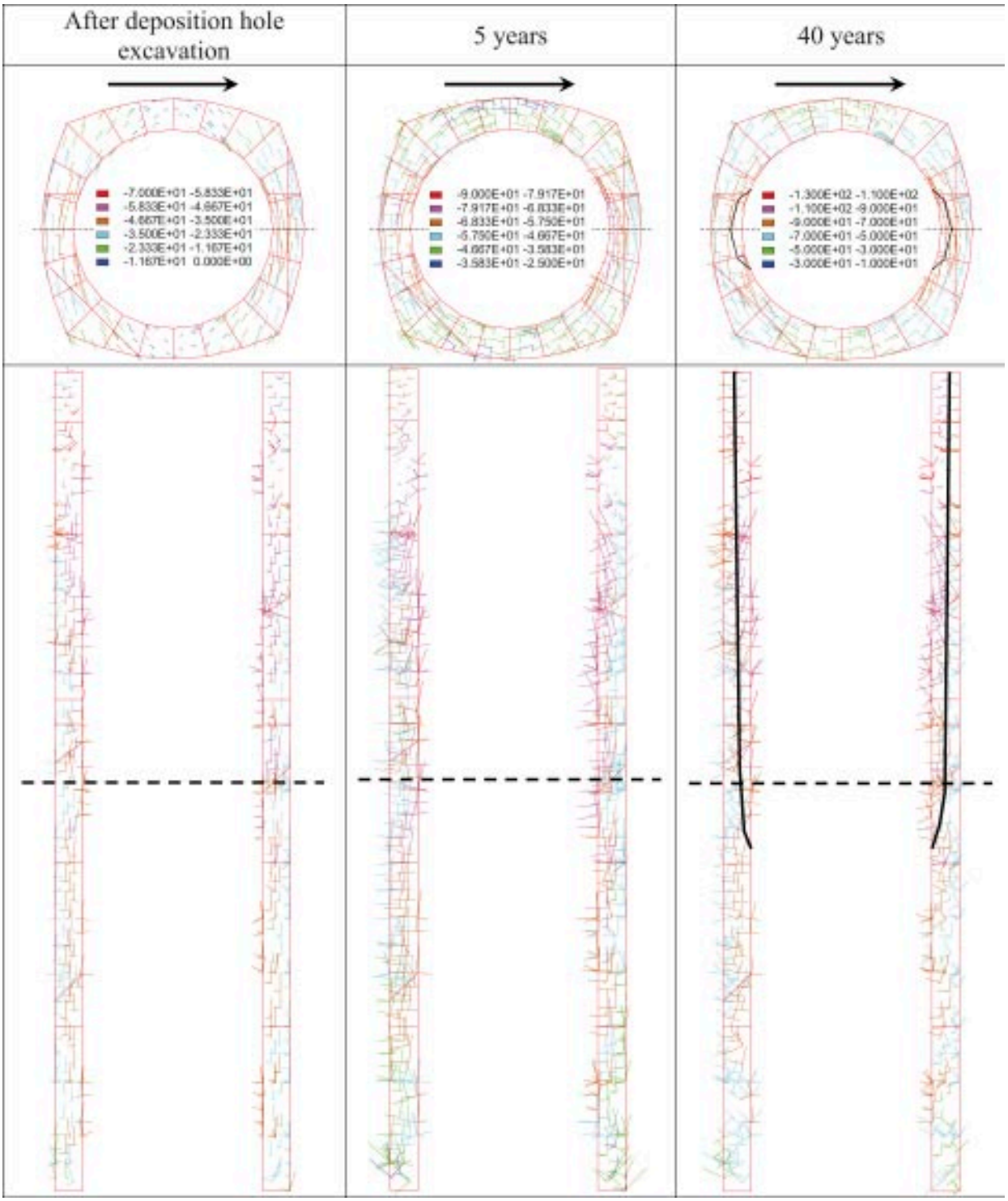

Figure 6-39. *The figure shows principal stress vectors around the central deposition hole at different times in the Simp 7 case (stress domain 2). The upper pictures are horizontal sections located 4 meters below the tunnel floor. The lower pictures are vertical sections through the center of the hole. The arrows show the tunnel axis orientation and the dashed lines indicate the locations of the two sections. The solid lines indicate an estimate of the extension of spalling around the hole assuming the spalling strength to be about 90 MPa.*

Table 6-7. Maximum tangential stress at deposition hole wall.

Stage	Simp 5 (Stress domain 1)		Simp 7 (Stress domain 2)	
After excavation	82 MPa	2 m below floor	64 MPa	1 m below floor
After 5 years	125 MPa	5 m below floor	87 MPa	3.5 m below floor
After 40 years	142 MPa	Near floor	114 MPa	Near floor

6.4.4 Laxemar

The Laxemar model was analyzed assuming the rock type to be a variant of Ävrö granite with the uniaxial compressive strength 195 MPa /SKB 2006a/. Assuming that the spalling limit is 55% of UCS gives a spalling strength of about 107 MPa for this rock type. The model used here (*Lax 2*) is no high resolution model with moving boundaries, such as the *Fors 10* case model. *Lax 2* is a case where the rock is considered elastic and with swelling pressure applied in the deposition holes. The major horizontal in situ stress is 34 MPa, the minor horizontal stress 10 MPa and the vertical stress 13.5 MPa. The tunnel is inclined 63° with respect to the major stress.

The maximum calculated tangential stresses at the deposition hole wall in *Lax 2* are presented in Table 6-8. Results are presented for the same three stages as for the Forsmark and Simpevarp models, i.e. after completed excavation, after 5 years and after 40 years.

Figure 6-40 shows principal stresses in a horizontal section 4 m below the tunnel floor and in a vertical section along the deposition hole axis in *Lax 2*. The concepts of the plots are the same as used in Figure 6-36, Figure 6-38 and Figure 6-39 above. The contour lines indicate regions where the major stress exceeds the spalling threshold, which here is assumed to be about 107 MPa. The following can be observed:

- The spalling threshold was exceeded in the upper parts of the deposition hole. The regions where the threshold was exceeded extended about 7 cm from the hole wall.
- After 5 years of heating, the maximum tangential stress amounted to about 144 MPa, i.e. above the spalling threshold. The spalling strength was exceeded along two 0.7 m sections of the periphery to a maximum depth of about 0.1 m.
- After 40 years of heating, the maximum stress was 187 MPa. The spalling limit was exceeded along two 0.8 m sections of the periphery at a maximum depth of about 0.15 m.

The stresses in *Lax 2* are in general higher than in the corresponding Simpevarp model (*Simp 5*). The *Lax 2* model indicates that spalling will be induced already during the operational phase. This does not mean that spalling after excavation is generally more likely in the Laxemar subarea than in the Simpevarp subarea. The main reason for the higher stresses in *Lax 2* is that the tunnel orientation assumed in that model was the most unfavourable one of those given in /Janson et al. 2006/, i.e. with the major in situ stress nearly normal to the tunnel axis. In Laxemar, there are several deposition areas with other tunnel orientations than the one assumed here. If the tunnels were oriented as assumed in the Simpevarp stress domain 1 model, i.e. with the major in situ stress sub parallel with the tunnel axis, the Laxemar deposition holes would be more stable because of the higher uniaxial compressive strength.

Table 6-8. Maximum tangential stress at deposition hole wall.

Stage	Maximum tangential stress	
After excavation	122 MPa	0.5 m below floor
After 5 years	144 MPa	1 m below floor
After 40 years	187 MPa	0.5 m below floor

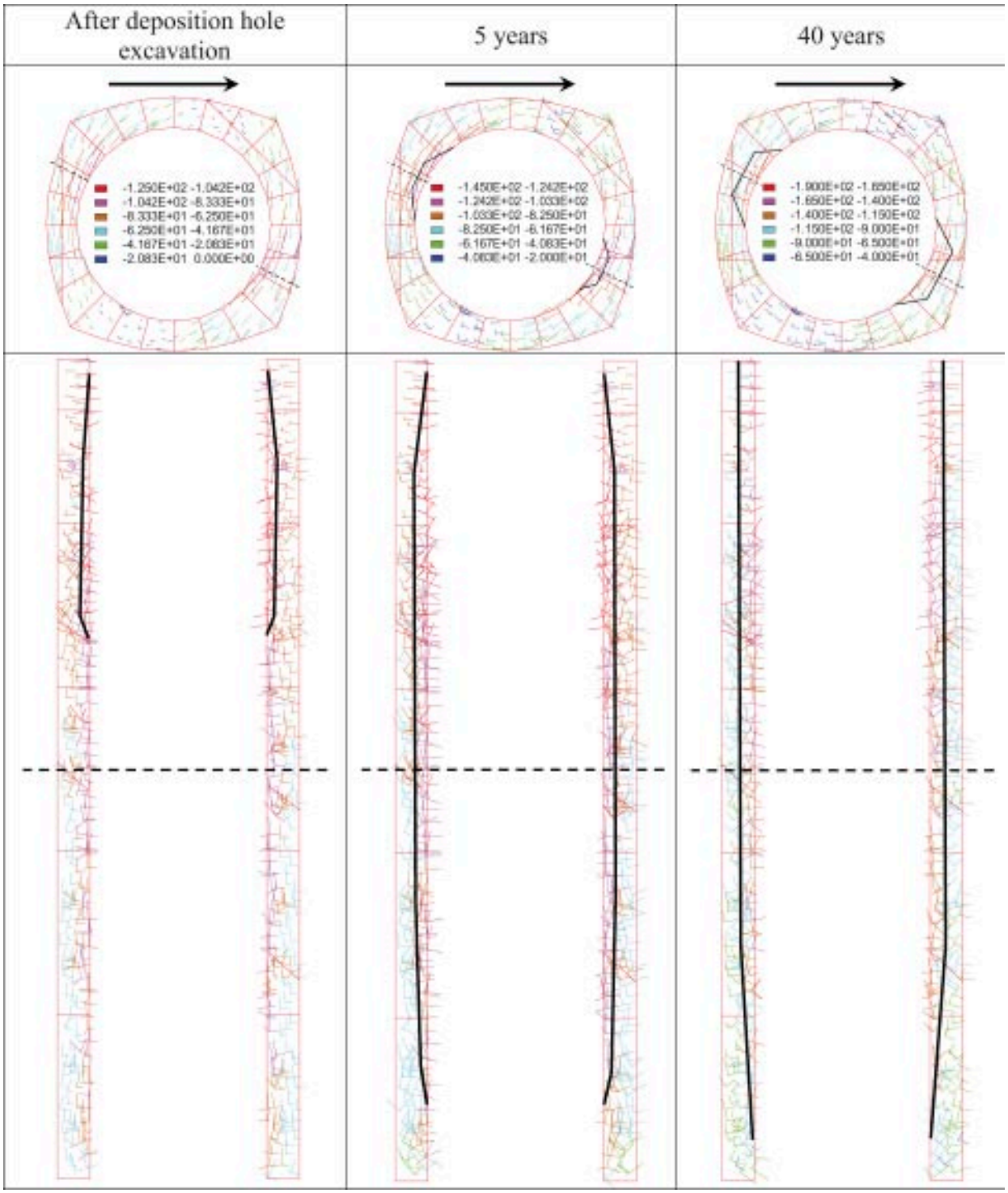

Figure 6-40. *The figure shows principal stress vectors around the central deposition hole at different times in the Lax 2 case. The upper pictures are horizontal sections located 4 meters below the tunnel floor. The lower pictures are vertical sections through the center of the hole. The arrows show the tunnel axis orientation and the dashed lines indicate the locations of the two sections. The solid lines indicate an estimate of the extension of spalling around the hole assuming the spalling strength to be about 107 MPa.*

6.5 Results from large-scale model

The large-scale thermo-mechanical model described in Section 4.6 was used to

- Provide time-dependent boundary conditions to near-field models. The boundary conditions were used to check the validity of the near-field mechanical boundary conditions. They were also applied in a version of the Forsmark model, which was used for the estimation of rock volumes where the spalling strength may be exceeded (cf. Section 6.4.2).
- Explore the thermal stress development in the rock mass around the repository.

The results from the model are presented below.

6.5.1 Time dependent boundary conditions used in near-field models

A box was defined (Figure 6-41). The box had the same dimensions as half of the near-field model (X × Y × Z = 50 m × 50 m × 20 m). The z- and x-displacements of the box vertical boundaries as well as the vertical stress on its top boundary were recorded.

The time histories recorded at the near-field box boundaries are shown in Figure 6-42. As can be seen in the figure, the shapes of the displacement curves in the x- and z-directions are not equal. The x-direction curve has two peaks. The first peak after 100 years corresponds to the thermo-mechanical effects from the local deposition area. The second peak is due to the thermo-mechanical effects from the neighbouring deposition areas. The time at which these effects reach the monitoring point coincides with the time when the thermal pulse from these areas has its maximum at that point (cf Figure 6-2). After a thousand years of thermal development, the temperatures at the repository depth have been evened out and the x- and z-displacement curves become more equal.

The maximum vertical stress is found after 1,000 years and amounts to about 2.8 MPa. The magnitude of the vertical stresses is of the same order of magnitude as those that were calculated earlier with an analytical thermo-mechanical solution by /Probert and Claesson 1997/.

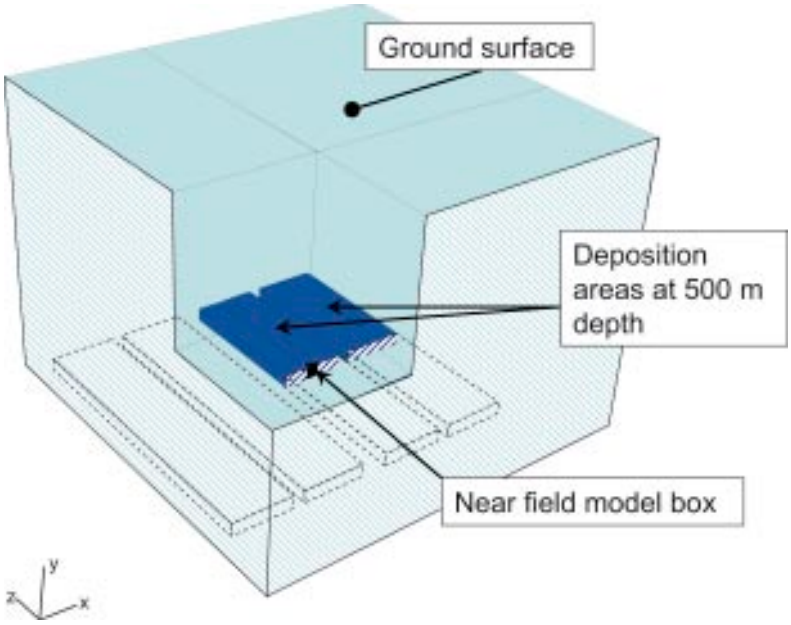

Figure 6-41. *The figure shows an overview of the large-scale model with the box representing half the near-field model volume indicated.*

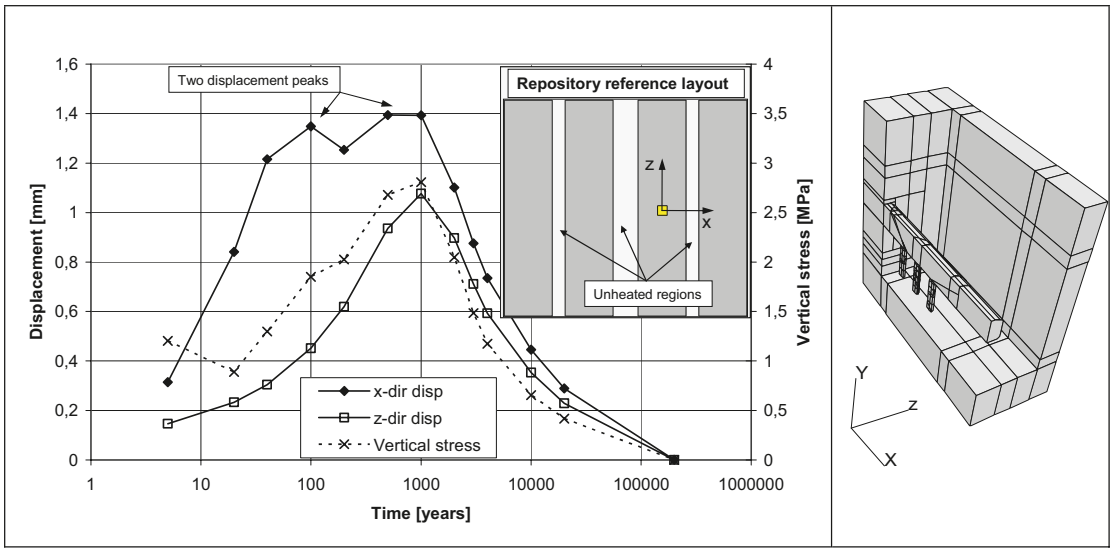

Figure 6-42. *The figure shows the displacements of vertical boundaries of the near-field box and the vertical stress at the top of the box. These results were used as boundary conditions in some of the near-field models. Note the double x-displacement peaks due to the repository layout with unheated regions between the local and the neighbouring deposition areas.*

6.5.2 Thermal stresses between the repository and the ground surface

During the heating period, the rock mass at the repository level will expand and cause thermally induced compressive stresses at this depth. The expanding rock mass will generate tensions at levels above and below the repository. These thermally induced tensions will give reductions of the in situ compressive stresses in the rock between the repository level and the ground surface. A concern is that these stress reductions will give transmissivity changes in vertical or steeply dipping fracture zones. The large-scale *3DEC* thermo-mechanical model was used to examine the thermal stress development around the repository as a function of time.

The horizontal thermal stresses along the two vertical scan-lines shown in Figure 6-43 were considered. Scan-line A intersects the near-field model box close to the central part of the repository. Scan-line B is located close to the corner of the repository. Only thermal stresses where calculated (i.e. no initial stresses considered). In Figure 6-44, the thermal stresses in the x- and z-directions along the two scan-lines are shown. Compressive stresses are negative. The following observations can be done:

- The stresses are higher (both compressive and tensile) in the central parts of repository (along scan-line A). The maximum compressive stress of about 22 MPa is found at the repository depth after 40 years (upper right).
- The maximum tensile stress of about 5 MPa is found close to the ground surface at scan-line A after 500 years. After 10,000 years, the tensile stress at the ground surface is reduced to about 0.5 MPa (upper right).

It can also be concluded that, qualitatively, the thermal stresses agree well with stresses calculated analytically by /Probert and Claesson 1997/ for a generic, square-shaped repository at 500 m depth.

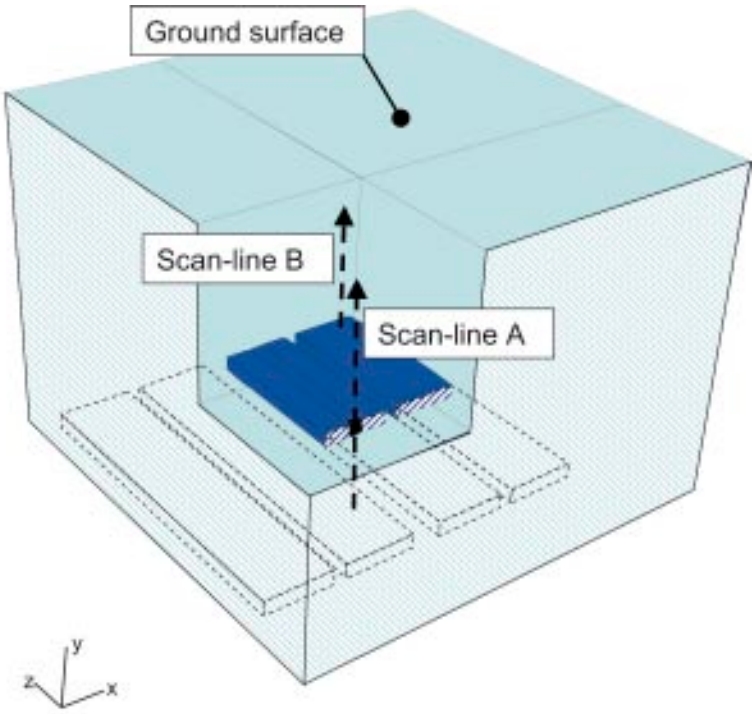

Figure 6-43. *The vertical scan lines for evaluation of thermal stresses. Scan-line A goes through the near-field model box, i.e. close to the central part of the repository while scan-line B is located close to the corner of the deposition areas.*

As noted above, the stress results presented in Figure 6-44 are only thermal stresses. This means that they shall be superpositioned on horizontal in situ stresses to give the resulting stress states at different times. Figure 6-45 shows an example of superposition of stresses. The diagram shows the resulting stresses from superposition of the Sxx-stresses along scan-line A (Figure 6-44, upper left) on the major horizontal in situ stress according to the Forsmark site model /SKB 2005b/. The grey-shaded region denotes the depth of possible tension. In reality, the horizontal stress will be approximately zero (rather than tensile) in these near-surface parts because of rock fractures with low or zero tensile strength. The stresses between the repository and the ground surface are discussed further in /Hökmark et al. 2006/. The thermal stress results presented here are used in that study.

It shall be noted that the results presented here were calculated assuming thermo-mechanical material property parameter values according to the Forsmark site model. The repository layout (canister spacing assumed in *3DEC* thermal model) was set according to the Forsmark model. If parameter values and repository layout according to the Simpevarp or Laxemar subareas had been used instead, the results would be different.

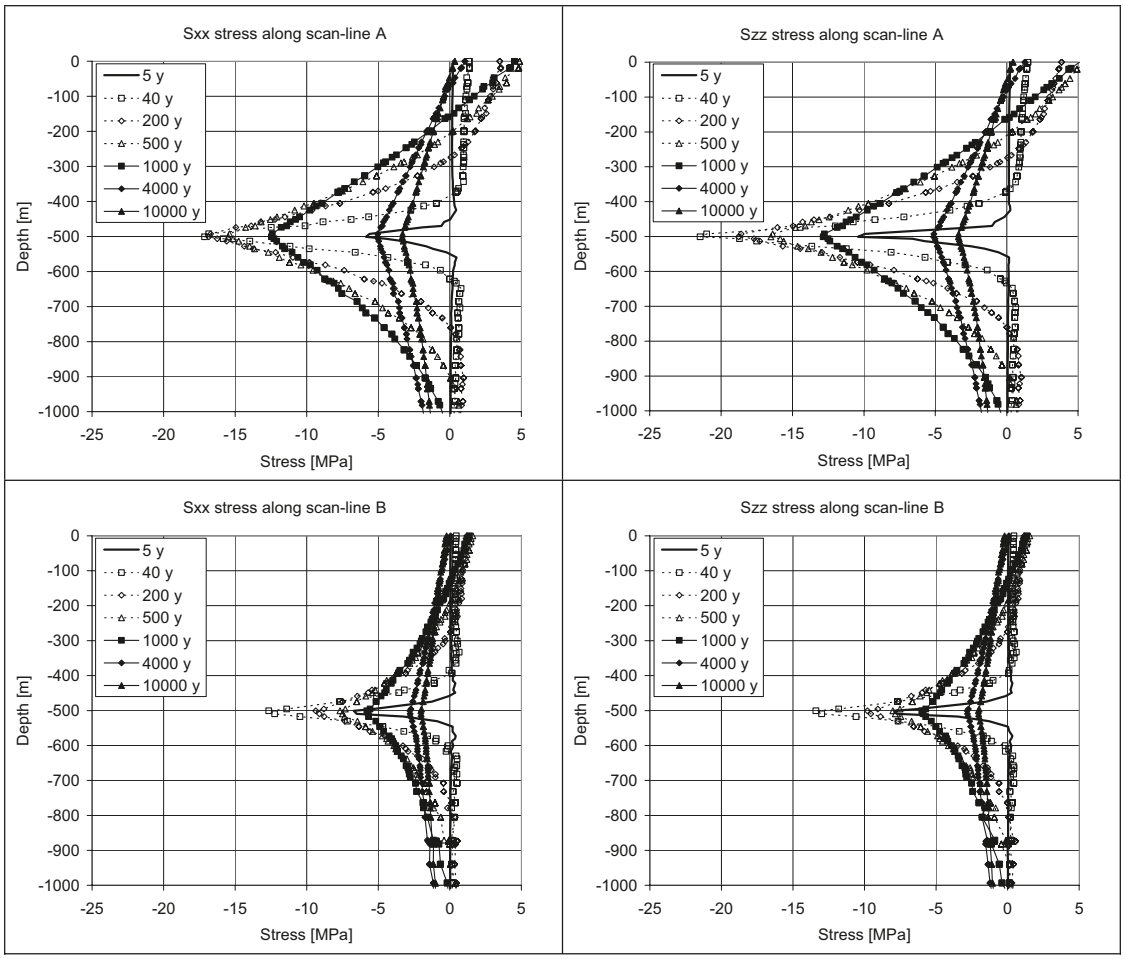

Figure 6-44. *Horizontal thermal stresses versus depth at different times along scan-line A (upper) and scan-line B (lower).*

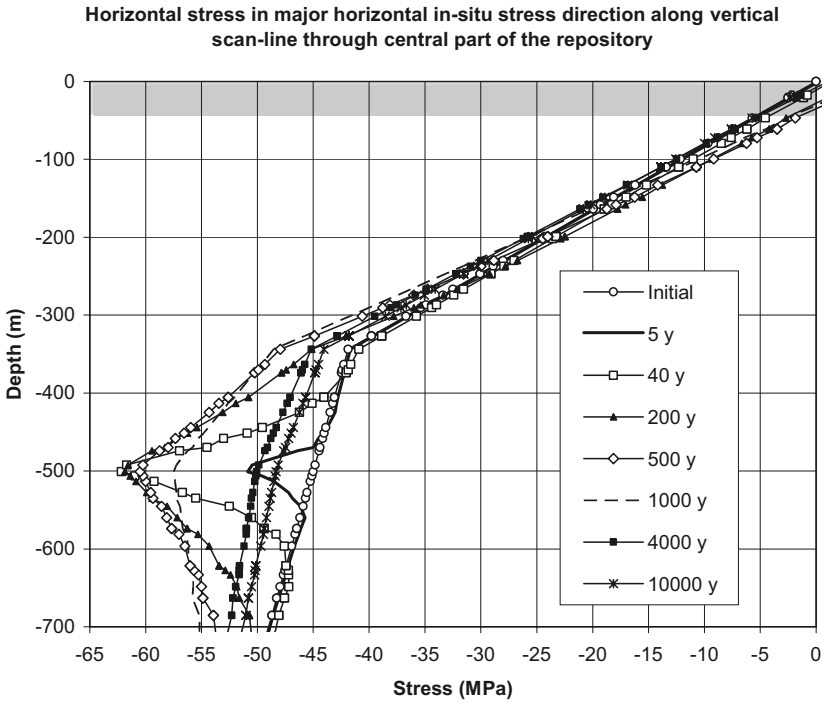

Figure 6-45. *Major horizontal stress at different times. Initial stresses according to /SKB 2005b/ (from /Hökmark et al. 2006/).*

7 Conclusions and discussion

7.1 General

Within the present work, a number of thermo-mechanical models have been analyzed by use of the distinct element code *3DEC*. The models were based on preliminary data from on-going site-investigations at the Forsmark, Simpevarp and Laxemar sites /SKB, 2005ab, 2006a/, on SKB's proposal for the design of a KBS-3 deep repository, Layout E /SKB 2002/ and on the current repository design premises /SKB 2004/.The main body of the work regarded near-field models, which considered the mechanical and thermo-mechanical development around deposition tunnels and deposition holes. In addition to the near-field models, a large-scale thermo-mechanical model including a quarter of the repository was analyzed.

In order to save computer time when numerous similar models were analyzed, a technique for storing and reuse of calculated temperature results was developed. This was done by use of the built-in programming language *FISH*.

7.2 Relevance and validity

7.2.1 Data

Both the near-field and the large-scale models presented and analyzed here are based on data from on-going site investigations. The data used here correspond to the knowledge and the views expressed in preliminary draft versions of the site descriptive models /SKB 2005ab, 2006a/. The site model data has been supplemented by information from the projecting teams. Geometry data has also been obtained from the current repository design premises /SKB 2004/. Effects of spatial variations, anisotropy etc have not been considered. Instead, mean values have been used throughout. However, the models analyzed here are not site models in any strict sense. The objectives of the modelling work were partly generic in nature.

7.2.2 Thermal model

The thermal results from *3DEC* used here for calculation of thermal stresses agree well with results obtained from other validated analytical solutions (cf Figure 6-2, Figure 6-3 and Figure 6-4). In the *3DEC* thermal model, the effect of the ground surface was neglected. This will only have minor influence on the results after thousands of years /Hökmark 1996/, a time long after the temperature maximum has passed.

7.2.3 Fracture system

In the near-field model, six fracture planes with different orientations and locations were defined. One of them was parallel to the tunnel wall, two of them intersected the tunnel only and three of them intersected both the tunnel and the central deposition hole. The ambition was not to create the most realistic fracture system. Instead, a small number of fractures intersecting the near field at different angles and at different positions in relation to the central part of the model were defined. This gave the possibility to draw general conclusions about the mechanical response of differently located and orientated fractures.

7.2.4 Boundary conditions

In the near-field models, the basic assumption was that all boundaries except the model top boundary were prevented to displace in the normal direction. The vertical stresses applied at the top of the models were assumed to be equal to the vertical in situ stress and constant through the analyses. These boundary condition settings do not account for the expansion of the surrounding rock mass due to the heating. Thus they yield some thermal stress overprediction. The amount of stress overprediction was studied by comparison of results from models where only thermal stresses were calculated (cf Section 4.4.2). From the comparison, it could be concluded that the stress overestimations made using the basic boundary condition settings where within reasonable bounds. After 100 years, at the time of maximum stress, the thermal stress was overestimated by about 5 MPa (i.e. about 7%). In addition to the stress overestimation, the stress anisotropy was also overestimated using the basic boundary conditions. Overestimation of the stress levels as well as of the stress anisotropy is conservative.

7.3 Near-field model results

The near-field models included a portion of rock, a part of a deposition tunnel, three deposition holes and six fracture planes. The main issues addressed were fracture shear displacements, fracture normal stresses and rock stresses.

7.3.1 Fracture shear displacements and normal stresses

Fracture shear displacement and fracture normal stress changes due to different load steps were studied. In order to study the sensitivity to variations of fracture strength, thermal expansion coefficient and in situ stress conditions, a number of cases were analyzed. The importance of pore water pressure was also studied. The sensitivity to the different parameters was evaluated by a study of fracture shear displacements and normal stresses at certain points in the fractures. The following conclusions can be drawn regarding the residual fracture shear displacements (after 200,000 years).

- The largest fracture shear displacement found in the models amounted to about 6 mm.
- The largest residual displacements were found in the dipping fractures. However, the shear displacements along these fractures were significant only locally, close to the excavations. The regions where the shear displacements exceeded 3 mm do not extend more than about 1 m from the openings. The only exception from this is fracture #4 in the Forsmark model. In that particular fracture, the regions where the residual shear displacements exceeded 3 mm extend about 5 m from the openings (Figure 6-8, right).
- The displacements along the vertical fractures were insignificant in comparison to the displacements in the dipping fractures.

Regarding fracture normal stresses the following can be concluded:

- The fractures are in approximately the same state of compression after the heated phase and the glaciation phase as before the heating initiation. This indicates that the inelastic fracture shear displacements that take place during the period of the heat load and during the glacial cycle have little importance for the end state of fracture normal stresses.
- There is some sensitivity to variations in fracture strength. At two of the four monitoring points (Figure 6-25), significant influence of the fracture strength could be observed. The largest difference in fracture normal stress was about 50% and was found at the end of the heating period.

7.3.2 Rock stresses

Rock stress results were recorded at points located close to the central deposition hole wall. Results both from elastic models and from models with fractures were studied.

Elastic conditions

The following can be concluded from the results recorded in the elastic models:

- The maximum stress after deposition hole excavation amounts to about 110 MPa. This stress level is found in the Laxemar model. The corresponding results for the Forsmark and Simpevarp models are about 100 MPa and 75 MPa, respectively.
- The peak stresses during the heating phase amount typically to 120–160 MPa and are found 100 years after heating start. The highest peak stress is 190 MPa and is found in the alternative Forsmark in situ stress model.

Sensitivity to fractures and thermal expansion coefficient

The stress history results recorded in the elastic models were compared with corresponding results recorded in the models where fractures were included. The following conclusions can be drawn:

- The fractures give redistributions of the stresses. Stress reductions at some monitored points were accompanied by stress increase at other locations. The observed reductions of the maximum stress in the base case models (34° friction angle + pore pressure) with respect to the elastic models ranges between 2–24%. In the same models, the stress increase ranges between 22–35%.
- At the location with the highest stresses, an increase of the thermal expansion coefficient value from $6.2 \cdot 10^{-6}$ K^{-1} to $7.7 \cdot 10^{-6}$ K^{-1} (i.e. 24%) gives a 19% increase of the maximum stress.

The influence of the fractures on the stresses is related to the high intensity of large fractures in the models (All fractures in the models have extensions corresponding to radii in the interval 20–25 m). If the near-field volume (8 x 8 x 8 m^3 box surrounding central deposition hole) is considered, the specific fracture area per unit rock volume is of the order of 1 m^2/m^3. This value should be compared with the corresponding value that can be calculated based on the statistical fracture network models given in the site model descriptions. Considering fractures with radii in the interval 20–25 m, the statistical fracture network model for Forsmark gives a specific fracture area of the order of 0.01 m^2/m^3 /SKB 2005b/. If small fractures with radii in the interval 0.2–1 m are considered, the site model yields a specific area of about 3 m^2/m^3, i.e. higher than in the *3DEC* models. However, the shear displacements in such small fractures are small and consequently their influence also is small compared to that of the larger fractures. The large fractures have no edges in the near-field close to the central deposition hole that limit their shear displacements. Thus, due to the high intensity of large fractures in the *3DEC* models, the impact of the fractures that is observed here is likely to be overestimated.

Even though the fractures included here result in stress redistributions around the deposition holes, the elastic models give a good approximation of the stresses in most cases. If a more typical and realistic fracture geometry had been used, the approximation would have been even better.

7.3.3 Intact rock failure

Estimates of the volumes of rock around a deposition hole, in which the spalling strength may be exceeded, were made assuming the spalling strength to be 55% of the uniaxial compressive strength. Results from elastic models were used. According to the results, it is unlikely that spalling will occur in Forsmark and in the Simpevarp subarea during the operational phase, but will be induced at a later stage due to the thermal stresses.

According to the results from the Laxemar model, spalling will be induced already during the operational phase. This does not mean that spalling after excavation is generally more likely in the Laxemar subarea than in the Simpevarp subarea. The main reason for the high stresses in the Laxemar model is that the tunnel orientation assumed in that model was the most unfavourable one of those given in /Janson et al. 2006/, i.e. with the major in situ stress nearly normal to the

tunnel axis. In Laxemar there are several deposition areas with other tunnel orientations than the one assumed here. If the tunnels were oriented as assumed in the Simpevarp stress domain 1 model, i.e. with the major in situ stress sub parallel with the tunnel axis, the Laxemar deposition holes would be more stable because of the higher uniaxial compressive strength.

The models used here were fully elastic whereas the spalling process is a non-linear process. The estimates made here of volumes involved in the spalling process can be regarded as an upper bound for the extent of spalling around a deposition hole. The regions indicated here to be involved in the spalling process extend along sections that are of the order of 1 m along the hole periphery. Further, the extensions along the periphery and the depth from the wall grew as the thermal stresses were increased. However, the APSE experience indicates that the failures will be notch-shaped and that the v-shaped notch will self-stabilize at some depth that depends on the stress that prevailed at the time of the failure. Once a stable notch has formed, subsequent increase in stress will not significantly increase the width and depth of the failure, but instead increase its vertical extension /Andersson and Eng 2005/.

7.4 Large-scale model results

The objective for analyzing the large-scale model was to:

- Provide the near-field models with time dependent boundary conditions.
- Explore the way the thermal stresses vary over time around the repository.

The Forsmark thermal model was used (i.e. the Forsmark repository geometry was assumed) and the Forsmark rock mass thermo-mechanical properties were assumed.

Regarding the time dependent near-field model boundary conditions, it can be concluded that these (horizontal displacements and vertical stress) are in agreement with results from previous studies /see e.g. Hökmark 1996, Probert and Claesson 1997/.

When the horizontal thermal stresses are studied (Figure 6-44) it can be concluded that there will be thermal tensile stresses (i.e. reduction of in situ stresses) close to the ground surface. The maximum thermal tensile stress amounts to about 5 MPa after 500 years. After 10,000 years the stress has been reduced to less than 0.5 MPa.

In /Hökmark et al. 2006/ the thermal stress results are used to study the variation of the horizontal stresses between the repository horizon and the ground surface. The thermal stresses calculated here are superpositioned on horizontal in situ stresses according to the Forsmark site model /SKB 2005b/ to obtain the resulting stress states at different times. The results indicate that the stresses are compressive below 100 m depth at all times. /Hökmark et al. 2006/ also use the resulting stresses to make estimates of transmissivity changes in steeply oriented fracture zones.

7.5 FISH routine for handling of temperature results

The technique for storing and reuse of calculated temperature results was developed as a part of the regular work with the near-field models. The work involved the analysis of numerous cases where exactly the same geometry (and consequently the same discretization of the continuum) was used. Thus, the same thermal solution could be used for many analyses. From the work with the *FISH* routine, the following can be concluded:

- The use of the routine lead to significant savings of calculation time. Only about 50% of the computer time was needed. This corresponds to an amount of saved clock time per model of about 10 hours.
- The routine is designed to be general, i.e. it is directly applicable to any other *3DEC* model. Thus it is available for future modelling work.

References

Andersson J C, Eng A, 2005. Äspö Pillar Stability Experiment. Final experiment design, Monitored data and observations. SKB R-05-02, Svensk Kärnbränslehantering AB.

Brady B H G, Brown E T, 1994. Rock mechanics for underground mining. Second edition. Chapman & Hall, London.

Börgesson L, Hernelind J, 1999. Coupled thermo-hydro-mechanical calculations of the water saturation phase of a KBS-3 deposition hole. Influence of hydraulic rock properties on the water saturation phase. SKB TR-99-41, Svensk Kärnbränslehantering AB.

Claesson J, Probert T, 1996. Temperature field due to time-dependent heat sources in a large rectangular grid – Derivation of analytical solution. SKB TR-96-12, Svensk Kärnbränslehantering AB.

Hökmark H, 1996. Canister positioning. Stage 1 near-field rock analysis. SKB AR D-96-014, Svensk Kärnbränslehantering AB.

Hökmark H, 2003. Canister positioning. Influence of fracture system on deposition hole stability. SKB R-03-19, Svensk Kärnbränslehantering AB.

Hökmark H, Fälth B, 2003. Thermal dimensioning of the deep repository. SKB TR-03-09, Svensk Kärnbränslehantering AB.

Hökmark H, Fälth B, Wallroth T, 2006. T-H-M couplings in rock. Overview of results of importance to the SR-Can safety assessment. SKB R-06-88, Svensk Kärnbränslehantering AB.

Itasca, 2003. *3DEC* – 3-Dimensional Distinct Element Code, User's Guide. Itasca Consulting Group, Inc., Minneapolis.

Janson T, Magnusson J, Bergvall M, Olsson R, Cuisiat F, Skurtveit E, Grimstad E, 2006. Final Repository for Spent Nuclear Fuel. Underground design Laxemar, Layout D1. SKB R-06-36. Svensk Kärnbränslehantering AB.

Jaquet O, Siegel P, 2004. Local-scale modelling of density driven flow using CONNECTFLOW. SKB R-04-46, Svensk Kärnbränslehantering AB.

Lund B, 2005. Effects of deglaciation on the crustal stress field and implications for endglacial faulting: A parametric study of simple Earth and ice models. SKB TR-05-04, Svensk Kärnbränslehantering AB.

Lund B, 2006. Stress variations during a glacial cycle at 500 m depth in Forsmark and Oskarshamn: Earth model effects. SKB R-06-95, Svensk Kärnbränslehantering AB

Martin D, Kaiser P, McCreath D, 1999. Hoek-Brown parameters for predicting the depth of brittle failure around tunnels. Can. Geotechnical Journal, 36(1):136–151.

Martin D, Christiansson R, Söderhäll J, 2001. Rock stability considerations for siting and constructing a KBS-3 repository. Based on experiences from Äspö HRL, AECL's URL, tunnelling and mining. SKB TR-01-38, Svensk Kärnbränslehantering AB.

Olsson R, 1998. Mechanical and Hydromechanical Behavior of Hard Rock Joints. A laboratory study. PhD thesis, Dept of Geotechnical Engineering, Chalmers University of Technology, Göteborg.

Probert T, Claesson J, 1997. Thermoelastic stress due to a rectangular heat source in a semi-infinite medium. Application for the KBS-3 repository. SKB TR-97-26, Svensk Kärnbränslehantering AB.

SKB, 2002. Deep repository for spent nuclear fuel. Facility description – Layout E. Spiral ramp with one operational area. SKB R-02-23, Svensk Kärnbränslehantering AB.

SKB, 2004. Deep repository. Underground design premises. Edition D1/1. SKB R-04-60, Svensk Kärnbränslehantering AB.

SKB, 2005a. Preliminary site description. Simpevarp subarea – version 1.2. SKB R-05-08, Svensk Kärnbränslehantering AB.

SKB, 2005b. Preliminary site description. Forsmark area – version 1.2. SKB R-05-18, Svensk Kärnbränslehantering AB.

SKB, 2006a. Preliminary site description. Laxemar subarea – version 1.2. SKB R-06-10, Svensk Kärnbränslehantering AB.

SKB, 2006b. Climate and climate-related issues for the safety assessment SR-Can. SKB TR-06-23, Svensk Kärnbränslehantering AB.

SKB, 2006c. Data report for the safety assessment SR-Can. SKB TR-06-25, Svensk Kärnbränslehantering AB.

Sundberg J, Back P-E, Bengtsson A, Ländell M, 2005a. Thermal modelling. Preliminary site description Simpevarp subarea – version 1.2. SKB R-05-24, Svensk Kärnbränslehantering AB.

Sundberg J, Back P-E, Bengtsson A, Ländell M, 2005b. Thermal modelling. Preliminary site description Forsmark area – version 1.2. SKB R-05-31, Svensk Kärnbränslehantering AB.